

Dr. Qiang Wang
Topical Editor
Geoscientific Model Development
October 28th 2018

Manuscript reference No. GMD-2018-91

Dear Dr. Qiang Wang,

Please find attached a revised version of the manuscript, **The Brazilian Earth System Model version 2.5: Evaluation of its CMIP5 historical simulation**, which we would like to submit for publication in Geoscientific Model Development

We appreciate the opportunity to improve the manuscript.

In the following pages are our point-by-point revisions.

- Page 2, Line 6

“*validated*” has been replaced by “*evaluated*”

- Page 4, Line 1

It has been included the following text: “*(as read-in fields)*”

- Page 4, Line 2

It has been included the following text: “*Currently, work has been done on activate the biogeochemical model (TOPAZ) within the MOM5 in order to simulate biogeochemical cycles in future simulations.*”

- Page 4, Line 5

“*BESM was*” has been replaced by “*The previous version of BESM (BESM-OA2.3) was*”

- Page 4, Line 15

It has been deleted the following text: “*One of primary conceptual aim in developing and improving BESM’s parameterizations is to serve as a model to be used from numerical weather prediction to seasonal forecast up to the projection of climate change scenarios in a seamless framework as proposed by Palmer et al. (2008).*”

- Page 4, Line 19

“*BESM*” has been replaced by “*BESM-OA2.3*”

- Page 4, Line 19

It has been included the following text: “*(10-30 days)*”

- Page 4, Line 20

It has been included the following text: “*(three months)*”

- Page 5, Line 21

“*to 2 W m⁻²*” has been replaced by “*to -4 W m⁻²*”

- Page 8, Line 2

“*for 700 years*” has been replaced by “*for 1140 years*”

- Page 8, Line 4

“*460*” has been replaced by “*for 1000 years*”

- Page 8, Line 16

It has been included the following text: “*The ocean stand-alone runs for 71 years (13 years period of ocean model spin-up forced by climatological atmospheric fields plus 58 years period forced by interannually varying atmospheric fields). Then a spin-up of the fully coupled model is done for 100 years. The ocean and atmosphere states at the end of this 100 years long integration are used as the initial condition for the piControl simulation. The piControl simulation shows stable conditions after a fast adjustment over the first 13 years of simulation (figure not shown). The analysis of the piControl and 4×CO₂ simulations are described in Capistrano et al. (2018) and Nobre et al. (2018, in preparation). Capistrano et al. (2018) estimates that BESM-OA2.5 has an equilibrium climate sensitivity of 2.96 °C for the abrupt 4×CO₂ experiment. This value is within the range from 2.07 to 4.74 °C that has been*”

computed for 25 CMIP5 models and close to the ensemble averaged value (3.30 °C).”

- Page 9, Line 13

It has been included the following text: *“and from the CPC Merged Analysis of Precipitation (CMAP; Xie and Arkin, 1997) with global horizontal resolution of 2.5° × 2.5° (<https://www.esrl.noaa.gov/psd/data/gridded/data.cmap.html>);”*

- Page 12, Line 4

It has been deleted the following text: *“The reason for absence of this warming tendency in the last decades of the 20th century is not clear.”*

- Page 16, Line 21

It has been included the following text: *“The net radiation at the top of atmosphere (TOA) has a negative bias and net of the ocean/atmosphere heat flux has a positive bias (Fig. 3). The net radiation at TOA has a mean value of -4.20 W m^{-2} and the net ocean/atmosphere heat flux has a mean value of 1.16 W m^{-2} in the first 50 years. Throughout the simulation the net radiation at TOA becomes less negative due to the increasing CO_2 on the atmosphere and consequential increasing atmospheric heat content. Part of this heat is transferred into the ocean as positive net of the ocean/atmosphere heat flux increasing indicates. The negative net radiation at TOA and the positive ocean/atmosphere heat flux are likely the reason for the weak warming observed in the Historical simulation (Fig. 2), since the atmosphere is losing heat to the outer space and into ocean during the simulation.”*

- Page 13, Line 1

“3” has been replaced by “4”

- Page 13, Line 1

It has been included the following text: “for (a) BESM-OA2.5, (b) GPCP dataset, and the spatial distribution of annual mean precipitation”

- Page 13, Line 3

“*biases*” has been replaced by “*bias*”

- Page 13, Line 3

It has been included the following text: “(c)”

- Page 13, Line 3

It has been included the following text: “*relative to the GPCP dataset and (d) for BESM-OA2.5 relative to the CMAP dataset. The spatial annual mean precipitation are*”

- Page 13, Line 4

It has been deleted the following text: “*The bias is obtained*”

- Page 13, Line 5

It has been deleted the following text: “*through the difference with GPCP dataset, in which the*”

- Page 13, Line 5

It has been deleted the following text: “*are computed*”

- Page 13, Line 7

It has been included the following text: “*and CMAP datasets*”

- Page 13, Line 7

It has been included the following text: “*The global model’s mean biases are similar for GPCP (0.3 mm day⁻¹) and CMAP (0.4 mm day⁻¹). In the case of the global model’s rmse biases, they are also similar for GPCP (1.4 mm day⁻¹) and CMAP (1.5 mm day⁻¹).*”

- Page 13, Line 19

It has been included the following text: “*This is a particular concern since an important aim is related to the model for future climate projections in the region. Based on the progress observed from BESM-OA2.3 to BESM-OA2.5, work on cloud parametrizations that can improve the precipitation over the Amazon is still carried out. Nevertheless, some state-of-the-art models show deficiencies in generating precipitation over the Amazon region. This is the case of the IITM-ESM (Fig. 5; Swapna et al., 2018), although the bias is more confined to the north of the Amazon and NESM that has a more distributed bias over the region (Fig. 9; Cao et al., 2018).*”

- Page 14, Line 4

It has been included the following text: “*Such strong positive bias over the Indian ocean (near the African coast) is also identified in different versions of CCSM model (Fig. 5; Gent et al., 2011).*”

- Page 14, Line 10

“4” has been replaced by “5”

- Page 14, Line 12

“4” has been replaced by “5”

- Page 14, Line 13

“4” has been replaced by “5”

- Page 14, Line 15

“4” has been replaced by “5”

- Page 14, Line 18

“4” has been replaced by “5”

- Page 14, Line 19

“4” has been replaced by “5”

- Page 14, Line 20

“5” has been replaced by “6”

- Page 15, Line 13

“6” has been replaced by “7”

- Page 15, Line 14

“6” has been replaced by “7”

- Page 15, Line 14

“6” has been replaced by “7”

- Page 15, Line 21

“6” has been replaced by “7”

- Page 15, Line 23

“6” has been replaced by “7”

- Page 16, Line 3

“7” has been replaced by “8”

- Page 16, Line 7

“7” has been replaced by “8”

- Page 16, Line 11

It has been included the following text: “*Such a bias is a matter of concern since other models, despite present strong bias in the Polar Regions, does not show such a strong bias. BNU-ESM presents positive biases up to 10 °C in the austral hemisphere during the season JJA (Fig. 3a; Ji et al., 2014) and NorESM1-M presents negative biases (~ -10 °C) during the seasons DJF and JJA (Fig. 9; Bentsen et al., 2013).*”

- Page 17, Line 1

“8” has been replaced by “9”

- Page 17, Line 1

It has been included the following text: “*This bias is out of the range (-10 m s⁻¹ to 10 m s⁻¹) that some models presents, as NorESM1-M (Fig. 10; Bentsen et al., 2013) or NESMv3 (Fig. 10d; Cao et al., 2018).*”

- Page 17, Line 7

It has been deleted the following text: “*Mean Sea Surface Temperature*”

- Page 17, Line 7

It has been included the following text: “*Ocean Mean State*”

- Page 17, Line 9

“9” has been replaced by “10”

- Page 17, Line 10

It has been included the following text: “*for (a) BESM-OA2.5, (b) ERSSTv4 and (c) the*”

- Page 17, Line 14

It has been included the following text: “*However, the extreme values found in the south of Greenland and in the North Pacific, where it reaches ~6 °C, is well within the range of biases reported by other models, as NorESM1-M (Fig. 12b; Bentsen et al., 2013) or IITM-ESM (Fig. 3; Swapna et al., 2018).*”

- Page 17, Line 17

It has been included the following text: “*warm*”

- Page 17, Line 17

It has been deleted the following text: “*a*”

- Page 18, Line 8

“10” has been replaced by “11”

- Page 18, Line 14

“10” has been replaced by “11”

- Page 18, Line 18

“10” has been replaced by “11”

- Page 19, Line 1

“11” has been replaced by “12”

- Page 19, Line 4

“11” has been replaced by “12”

- Page 19, Line 8

“11” has been replaced by “12”

- Page 19, Line 10

It has been included the following text: “*To evaluate how the global ocean profile evolves throughout the simulation, it is computed the depth-time Hovmöller diagrams of global mean ocean temperature and salinity departures from their respective initial conditions (Fig. 13). Here initial*”

conditional means the value of the first year of simulation, in this case, the year 1850. The prominent warming occurs from the surface up to 400 m depth (Fig. 13a). This warming is more significant at the end of the simulation (~0.6 °C comparing with initial conditions) and is likely to be related to the global warming of the planet and consequential increasing heat flux from the atmosphere into the ocean. In deeper waters, from 1500 m up to the ocean floor, there is a weaker warming, indicating that the ocean is gaining heat mainly in the upper layers. Between 500-1500 m depth, it is observed a cooling tendency respective to initial conditions. The ocean salinity slightly increases below 1000 m depth and from 1935 the increase reaches 0.04 PSU between 1500 and 3000 m depth compared with the initial values (Fig. 13b). Above 1000 m depth there is a significant freshening of the ocean waters, with the surface waters salinity decreasing up to 0.18 PSU at the end of the simulation. Such tendency can mean that the ocean is still drifting from its initial conditions in the Historical simulation.”

- Page 20, Line 3

It has been deleted the following text: “*4.1.5 Atlantic Meridional Ocean Circulation*”

- Page 20, Line 10

“*12*” has been replaced by “*14*”

- Page 20, Line 12

“*12*” has been replaced by “*14*”

- Page 20, Line 17

“12” has been replaced by “14”

- Page 20, Line 18

“*The same figure also plots*” has been replaced by “*For comparison, Figure 14c plots*”

- Page 21, Line 19

“13” has been replaced by “15”

- Page 22, Line 4

“13” has been replaced by “15”

- Page 22, Line 5

“13” has been replaced by “15”

- Page 22, Line 6

“13” has been replaced by “15”

- Page 22, Line 8

“14” has been replaced by “16”

- Page 22, Line 18

“14” has been replaced by “16”

- Page 23, Line 13

“15” has been replaced by “17”

- Page 23, Line 18

“15” has been replaced by “17”

- Page 23, Line 22

“15” has been replaced by “17”

- Page 24, Line 22

“16” has been replaced by “18”

- Page 25, Line 7

“16” has been replaced by “18”

- Page 25, Line 8

“16” has been replaced by “18”

- Page 25, Line 9

It has been included the following text: “4.2.1.4 *Madden-Julian Oscillation*”

- Page 25, Line 10

It has been included the following text: “*The Madden-Julian Oscillation (MJO) is the prominent intraseasonal variability (30-90 days) over the eastern Indian and western Pacific tropical regions and consists on events of deep convection coupled to atmospheric circulation that packed propagate together through the equatorial region eastward (Madden and Julian, 1971, Madden and Julian, 1972; Zhang, 2005). The influence of MJO events with large-scale phenomena has been reported, as in the case of the evolution of ENSO (e.g. Takayabu et al., 1999), formation of tropical cyclones (e.g. Liebmann et al., 1994) or in the North Atlantic Oscillation (e.g. Lin et al., 2009). To evaluate*

the MJO simulated by the model it is performed the wavenumber-frequency power spectrum analysis for tropical (10 °S–10 °N) averaged daily outgoing long-wave radiation (OLR) and daily zonal wind component at 850 hPa pressure level (U850), for the boreal winter (Nov-Apr) over the period 1971–2000. To compute and plot the wavenumber-frequency power spectrum it is used the MJO Simulation Diagnostic package (details in Waliser et al., 2009). Fig. 19a and Fig. 19b show the wavenumber-frequency power spectrum for OLR for BESM-OA2.5 and 20CRv2, respectively. Although BESM-OA2.5 presents an eastward propagating disturbance with wavenumber 1, it is characterized by lower frequency (> 80 days) compared to the maxima peak within 30–80 days frequency band shown by the 20CRv2, despite it spreads over lower frequencies than 80 days. This observed peak has more energy for wavenumber 2. A westward propagating disturbance (negative frequencies) with weaker energy than the eastward propagating counterpart appears in 20CRv2, with a peak for wavenumber 2. Similarly, BESM-OA2.5 also shows a westward propagating disturbance with weaker energy for wavenumber 1–3. The wavenumber-frequency power spectrum for U850 in 20CRv2 shows an eastward propagating disturbance which peaks at the 30–80 days frequency band with wavenumber 1 (Fig. 19d). In the case of BESM-OA2.5 there is an eastward propagation with a periodicity slightly higher than 80 days for wavenumber 1 but this disturbance spreads over different frequencies out of the 30–80 days frequency band (Fig. 19c). It also presents a westward propagating disturbance that is absent in the Reanalysis. BESM-OA2.5 poorly simulates the MJO and underestimates its amplitude. However, MJO has been highlighted as a phenomenon that climate models struggle to simulate in a proper way, especially by underestimate OLR and representing a coherent eastward propagation (Kim et al., 2009; Ahn et al., 2017).”

- Page 27, Line 12

“17” has been replaced by “20”

- Page 27, Line 13

“17” has been replaced by “20”

- Page 27, Line 16

“17” has been replaced by “20”

- Page 28, Line 19

“18” has been replaced by “21”

- Page 28, Line 20

“18” has been replaced by “21”

- Page 28, Line 22

“18” has been replaced by “21”

- Page 29, Line 3

“*Ghil and Mo, 1991*” has been replaced by “*Mo and Peagle, 2001*”. Mo and Peagle (2001) is the correct reference for PSA.

- Page 29, Line 8

“19” has been replaced by “22”

- Page 29, Line 8

“19” has been replaced by “22”

- Page 29, Line 15

“19” has been replaced by “22”

- Page 29, Line 15

“*do*” has been replaced by “*does*”

- Page 29, Line 16

“*19*” has been replaced by “*22*”

- Page 30, Line 10

“*20*” has been replaced by “*23*”

- Page 30, Line 22

“*positive*” has been replaced by “*negative*”

- Page 30, Line 23

“*negative*” has been replaced by “*positive*”

- Page 31, Line 12

“*21*” has been replaced by “*24*”

- Page 31, Line 15

“*21b*” has been replaced by “*24a*”

- Page 31, Line 22

“*22*” has been replaced by “*25*”

- Page 32, Line 2

“*22*” has been replaced by “*25*”

- Page 32, Line 7

“*Earth Systems*” has been replaced by “*Earth System*”

- Page 33, Line 20

“ 2 W m^{-2} ” has been replaced by “ -4 W m^{-2} ”

- Page 35, Line 5

It has been included the following text: “*Assuming that BESM-OA2.5 should respond consistently with CMIP5 models, it would underestimate the warming observed in the last decades. However, models can respond in different ways to external forcing, therefore, in the near future, the aim is to carry out a numerical experiment in which the model is forced with observed estimate of aerosol concentration (as read-in field) in order to address to what extension BESM is impacted.*”

- Page 38, Line 10

The following reference has been included: “*Ahn, M. S., Kim, D., Sperber, K. R., Kang, I. S., Maloney, E., Waliser, D. and Hendon, H.: MJO simulation in CMIP5 climate models: MJO skill metrics and process-oriented diagnosis, Clim. Dyn., 49(11–12), 4023–4045, doi:10.1007/s00382-017-3558-4, 2017.*”

- Page 38, Line 17

The following reference has been included: “*Bentsen, M., Bethke, I., Debernard, J. B., Iversen, T., Kirkevåg, A., Seland, Ø., Drange, H., Roelandt, C., Seierstad, I. A., Hoose, C. and Kristjánsson, J. E.: The Norwegian Earth System Model, NorESM1-M – Part 1: Description and basic evaluation of the physical climate, Geosci. Model Dev., 6(3), 687–720, doi:10.5194/gmd-6-687-2013, 2013.*”

- Page 39, Line 1

The following reference has been included: “*Cao, J., Wang, B., Yang, Y.-M., Ma, L., Li, J., Sun, B., Bao, Y., He, J., Zhou, X. and Wu, L.: The NUIST Earth System Model (NESM) version3: description and preliminary evaluation, Geosci. Model Dev., 11(7), 2975–2993, doi:10.5194/gmd-11-2975-2018, 2018.*”

- Page 39 Line 6

The following reference “*Capistrano, V., Nobre, P., Tedeschi, R., Silva, J., Bottino, M., Baptista Jr., M., Menezes Neto, O., Figueroa, S. N., Bonatti, J.P., Kubota, P., Fernandez J., Giarolla, E., Vial, J., Nobre, C. A.: Overview of climate change in the BESM-OA2.5 climate model. (Submitted to Journal of Climate).*” has been replaced by “*Capistrano, V. B., Nobre, P., Tedeschi, R., Silva, J., Bottino, M., da Silva Jr., M. B., Menezes Neto, O. L., Figueroa, S. N., Bonatti, J. P., Kubota, P. Y., Reyes Fernandez, J. P., Giarolla, E., Vial, J., and Nobre, C. A.: Overview of climate change in the BESM-OA2.5 climate model, Geosci. Model Dev. Discuss., <https://doi.org/10.5194/gmd-2018-209>, in review, 2018.*”

- Page 41, Line 28

The following reference has been included: “*Gent, P. R., Danabasoglu, G., Donner, L. J., Holland, M. M., Hunke, E. C., Jayne, S. R., Lawrence, D. M., Neale, R. B., Rasch, P. J., Vertenstein, M., Worley, P. H., Yang, Z.-L., Zhang, M.: The Community Climate System Model Version 4, J. Clim., 24(19), 4973–4991, doi:10.1175/2011JCLI4083.1, 2011.*”

- Page 42, Line 4

The following reference has been deleted: “*Ghil, M. and Mo, K.: Intraseasonal Oscillations in the Global Atmosphere. Part I: Northern Hemisphere and Tropics, J. Atmos. Sci., 48(5), 752–779, doi:10.1175/1520-0469(1991)048<0752:IOITGA>2.0.CO;2, 1991.*”

- Page 43, Line 18

The following reference has been included: “*Ji, D., Wang, L., Feng, J., Wu, Q., Cheng, H., Zhang, Q., Yang, J., Dong, W., Dai, Y., Gong, D., Zhang, R. H., Wang, X., Liu, J., Moore, J. C., Chen, D. and Zhou, M.: Description and basic evaluation of Beijing Normal University Earth System Model (BNU-ESM) version 1, Geosci. Model Dev., 7(5), 2039–2064, doi:10.5194/gmd-7-2039-2014, 2014.*”

- Page 44, Line 9

The following reference has been included: “*Kim, D., Sperber, K., Stern, W., Waliser, D., Kang, I. S., Maloney, E., Wang, W., Weickmann, K., Benedict, J., Khairoutdinov, M., Lee, M. I., Neale, R., Suarez, M., Thayer-Calder, K. and Zhang, G.: Application of MJO simulation diagnostics to climate models, J. Clim., 22(23), 6413–6436, doi:10.1175/2009JCLI3063.1, 2009.*”

- Page 45, Line 4

The following reference has been included: “*Liebmann, B., Hendon, H. H. and Glick, J. D.: The Relationship Between Tropical Cyclones of the Western Pacific and Indian Oceans and the Madden-Julian Oscillation, J. Meteorol. Soc. Japan. Ser. II, 72(3), 401–412, doi:10.2151/jmsj1965.72.3_401, 1994.*”

- Page 45, Line 8

The following reference has been included: “*Lin, H., Brunet, G. and Derome, J.: An observed connection between the North Atlantic oscillation and the Madden-Julian oscillation, J. Clim., 22(2), 364–380, doi:10.1175/2008JCLI2515.1, 2009.*”

- Page 45, Line 19

The following reference has been included: “*Madden, R. A. and Julian, P. R.: Detection of a 40–50 Day Oscillation in the Zonal Wind in the Tropical Pacific, J. Atmos. Sci., 28(5), 702–708, doi:10.1175/1520-0469(1971)028<0702:DOADOI>2.0.CO;2, 1971.*”

- Page 45, Line 22

The following reference has been included: “*Madden, R. A. and Julian, P. R.: Description of Global-Scale Circulation Cells in the Tropics with a 40–50 Day Period, J. Atmos. Sci., 29(6), 1109–1123, doi:10.1175/1520-0469(1972)029<1109:DOGSCC>2.0.CO;2, 1972.*”

- Page 49, Line 3

The following reference has been included: “*Swapna, P., Krishnan, R., Sandeep, N., Prajeesh, A. G., Ayantika, D. C., Manmeet, S. and Vellore, R.: Long-Term Climate Simulations Using the IITM Earth System Model (IITM-ESMv2) With Focus on the South Asian Monsoon, J. Adv. Model. Earth Syst., 10(5), 1127–1149, doi:10.1029/2017MS001262, 2018.*”

- Page 49, Line 7

The following reference has been included: “*Takayabu, Y. N., Iguchi, T., Kachi, M., Shibata, A. and Kanzawa, H.: Abrupt termination of the 1997-98 El Nino in response to a Madden-Julian oscillation, Nature, 402(6759), 279–282, doi:10.1038/46254, 1999.*”

- Page 49, Line 26

The following reference has been included: “*Waliser, D., Sperber, K., Hendon, H., Kim, D., Maloney, E., Wheeler, M., Weickmann, K., Zhang, C., Donner, L., Gottschalck, J., Higgins, W., Kang, I. S., Legler, D., Moncrieff, M., Schubert, S., Stern, W., Vitart, F., Wang, B., Wang, W. and Woolnough, S.: MJO simulation diagnostics, J. Clim., 22(11), 3006–3030, doi:10.1175/2008JCLI2731.1, 2009.*”

- Page 50, Line 4

The following reference has been included: “*Xie, P., and P.A. Arkin, 1997: Global precipitation: A 17-year monthly analysis based on gauge observations, satellite estimates, and numerical model outputs. Bull. Amer. Meteor. Soc., 78, 2539 - 2558.*”

- Page 50, Line 20

The following reference has been included: “*Zhang, C.: Madden-Julian Oscillation, Rev. Geophys., 43(2), 1–36, doi:10.1029/2004RG000158, 2005.*”

- Page 53

Figure 1 has been improved.

- Page 54

The quality of the Figure 2 has been improved.

- Page 55

A new figure has been included (Figure 3). It has been suggested by reviewer #2.

- Pages 56

Previous Figure 3 has been improved and completed with more figures, as suggested by reviewer #1. It has been renamed as Figure 4.

- Page 57, Line 1

“Spatial map of annual mean precipitation bias of BESM-OA2.5 relative to GPCP. The averages values are computed over the periods 1971–2000 and 1979–2008, for BESM-OA2.5 and GPCP, respectively. Units are in mm day⁻¹.” has been replaced by *“Spatial map of annual mean precipitation for (a) BESM-OA2.5, for (b) GPCP, (c) the bias of BESM-OA2.5 relative to GPCP and (d) the bias of BESM-OA2.5 relative to CMAP. The averages values are computed over the periods 1971–2000 (for BESM-OA2.5) and 1979–2008 (for GPCP and CMAP). Units are in mm day⁻¹.”*

- Page 58

The quality of previous Figure 4 has been improved and it has been renamed as Figure 5.

- Page 60

The quality of previous Figure 5 has been improved and it has been renamed as Figure 6.

- Page 61

The quality of previous Figure 6 has been improved and it has been renamed as Figure 7.

- Page 62

The quality of previous Figure 7 has been improved and it has been renamed as Figure 8.

- Page 63

The quality of previous Figure 8 has been improved and it has been renamed as Figure 9.

- Page 64

Figure 9 has been improved and completed with more figures, as suggested by reviewer #1. It has been renamed as Figure 10.

Page 65, Line 1

“*surface bias*” has been replaced “*surface temperature for (a) BESM-OA2.5, (b) ERSSTv4 and (c) the bias*”

- Page 66

The quality of previous Figure 10 has been improved and it has been renamed as Figure 11.

- Page 68

The quality of previous Figure 11 has been improved and it has been renamed as Figure 14.

- Page 70

A new figure has been included (Figure 13). It has been suggested by reviewer #2.

- Page 71

The quality of previous Figure 12 has been improved and it has been renamed as Figure 14.

- Page 73

The quality of previous Figure 13 has been improved and it has been renamed as Figure 15.

- Page 75

The quality of previous Figure 14 has been improved and it has been renamed as Figure 16.

- Page 76

The quality of previous Figure 15 has been improved and it has been renamed as Figure 17.

- Page 78

The quality of previous Figure 16 has been improved and it has been renamed as Figure 18.

- Page 80

A new figure has been included (Figure 19). It has been suggested by reviewer #1.

- Page 82

The quality of previous Figure 17 has been improved and it has been renamed as Figure 20.

- Page 84

The quality of previous Figure 18 has been improved and it has been renamed as Figure 21.

- Page 85

The quality of previous Figure 19 has been improved and it has been renamed as Figure 22.

- Page 86

The quality of previous Figure 20 has been improved and it has been renamed as Figure 23.

- Page 87

The quality of previous Figure 21 has been improved and it has been renamed as Figure 24.

- Page 88

The quality of previous Figure 22 has been improved and it has been renamed as Figure 25.

1 **The Brazilian Earth System Model version 2.5: Evaluation of**
2 **its CMIP5 historical simulation**

3
4
5 **Sandro F. Veiga¹, Paulo Nobre², Emanuel Giarolla³, Vinicius Capistrano⁴, Manoel**
6 **Baptista Jr.², André L. Marquez², Silvio Nilo Figueroa², José Paulo Bonatti², Paulo**
7 **Kubota², Carlos A. Nobre⁵**

8
9 ¹Earth System Science Center-CCST, National Institute for Space Research (INPE), São
10 José dos Campos 12227-010, São Paulo, Brazil

11 ²Center for Weather Forecasting and Climate Studies-CPTEC, National Institute for
12 Space Research (INPE), Cachoeira Paulista 12630-000, São Paulo, Brazil

13 ³Center for Weather Forecasting and Climate Studies-CPTEC, National Institute for
14 Space Research (INPE), São José dos Campos 12227-010, São Paulo, Brazil

15 ⁴Amazonas State University (UEA), Manaus 69005-010, Amazonas, Brazil

16 ⁵CN Research, São José dos Campos 12544-590, São Paulo, Brazil

17
18 *Correspondence to:* Sandro F. Veiga (sandro.veiga@inpe.br)

1 **Abstract**

2

3 The performance of the coupled ocean-atmosphere component of the Brazilian Earth
4 System Model version 2.5 (BESM-OA2.5) simulating the historical period 1850-2005 is
5 evaluated. Following climate model validation procedure, in which the atmospheric and
6 oceanic main variabilities are ~~validated~~evaluated against observation and Reanalysis
7 datasets, the evaluation particularly focuses the mean climate state and the most
8 important large-scale climate variability patterns simulated in the historical run, which
9 is forced by observed greenhouse gas concentration. The most significant upgrades in
10 the model's components are also presented briefly. BESM-OA2.5 is able to reproduce
11 the most important large-scale variabilities, particularly over the Atlantic (e.g. the North
12 Atlantic Oscillation, the Atlantic Meridional Mode and the Atlantic Meridional
13 Overturning Circulation) and the extratropical modes that occur in both hemispheres.
14 The model's ability in simulating large-scale variabilities indicates its usefulness for
15 seasonal climate prediction and climate change studies.

16

1 **1. Introduction**

2 Climate Models and their recent extension to become Earth System Models, by
3 the inclusion of biogeochemical cycles, are key tools to investigate climate phenomena
4 which greatly influence human societies (e.g. von Storch, 2010; Flato, 2011). Since
5 2008 the Brazilian climate community has been engaged in setting up the Brazilian
6 Earth System Model (BESM; Nobre et al., 2013; Giarolla et al., 2015); a major
7 scientific task which has been carried out by Brazilian scientific institutions invoking
8 the critical need to address reliable future climate projections and their potential
9 impacts, particularly over South America. The primary objective encompassed in this
10 effort is to build up the scientific expertise capable to develop and maintain a state-of-
11 the-art Earth System Model. Such an achievement would represent a significant step
12 forward in establishing a scientific tool which can be used in different arrays of research
13 activities. The importance of such undertaking lies in the understanding of the physics
14 of the Earth system to produce and confer credibility to studies of impacts of climate
15 change in different areas of great importance; such as food and water security, tropical
16 ecosystems, natural disasters, and so on. One of the primordial aims of the BESM
17 project is to participate in the Coupled Model Intercomparison Project's sixth phase
18 (CMIP6; Meehl et al., 2014).

19 The Brazilian Earth System Model (BESM) has been set up at the Brazilian
20 National Institute for Space Research (INPE). At present, it consists of a land-ocean-
21 atmosphere coupled model, in which the coupling is done through the Flexible
22 Modeling System (FMS) coupler, developed at the Geophysical Fluid Dynamics
23 Laboratory (GFDL) of the National Oceanic and Atmospheric Administration (NOAA).

1 The inclusion of aerosols (as read-in fields) and atmospheric chemistry components are
2 in the phase of implementation and tests. Currently, work has been done on activate the
3 biogeochemical model (TOPAZ) within the MOM5 in order to simulate biogeochemical
4 cycles in future simulations.

5 The previous version of BESM (BESM-OA2.3) was firstly evaluated in Nobre et
6 al. (2013). This version showed a significant bias on precipitation in the tropical region,
7 with a deficient representation of precipitation in the Amazon region. In order to
8 improve these aspects, studies were conducted to ameliorate cloud parameterizations
9 over the tropics, which improved the precipitation over the same region and the
10 representation of Convergence Zones over both the Atlantic and Pacific Ocean basins
11 (Bottino and Nobre, 2018). Main changes of the current version relate to BESM's
12 atmospheric model, with modifications in the surface wind field and its
13 parameterizations, described in Capistrano et al. (2018). The updated version presented
14 in this manuscript is BESM-OA2.5.

15 ~~One of primary conceptual future aim in developing and improving BESM's~~
16 ~~parameterizations is to serve as a model to be used from numerical weather prediction to~~
17 ~~seasonal forecast up to the projection of climate change scenarios in a seamless~~
18 ~~framework as proposed by Palmer et al. (2008).~~ From the operational point of view,
19 BESM-OA2.3 is already being used for extended weather forecast (10-30 days) to
20 seasonal climate prediction (three months), as well as for producing global climate
21 change scenarios (Nobre et al., 2013) and to provide atmospheric and oceanic boundary
22 conditions to regional climate models for dynamical downscaling of climate change
23 scenarios (Chou et al., 2014).

1 This overview paper describes the most important developments and
2 improvements in the model components, presenting the simulation of recent past mean
3 climate conditions and major large-scale climate phenomena. In section 2 the BESM-
4 OA2.5 components and experimental design are briefly described; section 3 presents the
5 methodology and the observed data used to evaluate the model; section 4 presents the
6 evaluation of the historical simulation, in which are evaluated the most important
7 atmospheric and oceanic variables regarding to their climatological fields and the
8 prominent large-scale phenomena of the climate system; finally, section 5 presents the
9 summary.

10 **2 Model Description and Simulation Experiment Design**

11 **2.1 BESM-OA2.5**

12 The atmospheric component of BESM-OA2.5 is the Brazilian Global
13 Atmospheric Model (BAM; Figueroa et al., 2016) developed at Center for Weather
14 Forecasting and Climate Studies (CPTEC/INPE). It is a primitive equation model with
15 spectral representation with triangular truncation at the wave number 62, corresponding
16 to a grid resolution of approximately $1.875^\circ \times 1.875^\circ$, and 28 sigma levels in the
17 vertical, with uneven increment between the levels, i.e. T62L28 resolution. As
18 mentioned before, it is in the atmospheric component which resides the main
19 differences between BESM-OA2.5 and BESM-OA2.3 (Nobre et al., 2013). The new
20 version shows a key improvement in the energy balance at the top of the atmosphere, by
21 | reducing the mean global bias from -20 W_m^{-2} in version BESM-OA2.3 to -42 W_m^{-2} in
22 | the current version (Capistrano et al. 2018). Version 2.5 of BESM incorporates the

1 formulation presented in Jiménez et al. (2012) for the representation of the wind,
2 humidity and temperature in the surface layer. The model runs without flux correction
3 or adjustment. The physics parameterizations for the continental processes are based on
4 the Simplified Simple Biosphere Model (SSiB) land surface model (Xue et al., 1991), in
5 shortwave radiation Clirad scheme (Tarasova et al. 2007; Chou and Suarez 1999), in
6 longwave radiation Harshvardhan scheme (Harshvardhan et al., 1987), in Cloud
7 microphysics Ferrier scheme (Ferrier et al. 2002), in the turbulence level 2 module
8 (Mellor and Yamada, 1982), in the gravity wave module (Anthes, 1977), in the deep
9 convection module (Arakawa and Schubert, 1974; Grell and Dévényi, 2002), and in the
10 shallow convection module (Tiedtke, 1983). More details can be found in Figueroa et
11 al. (2016) and in Capistrano et al. (2018).

12 The oceanic component of BESM-OA2.5 is the Modular Ocean Model version
13 4p1 (MOM4p1; Griffies, 2009) developed at GFDL, which includes the Sea Ice
14 Simulator (SIS) built-in ice model (Winton, 2000). There are no changes in the physics
15 parameterizations from those used in BESM-OA2.3. The horizontal grid resolution in
16 the zonal direction is 1° and in the meridional direction it varies uniformly from $1/4^\circ$
17 between 10° S and 10° N to 1° of resolution at 45° and to 2° of resolution at 90° , in both
18 hemispheres. The vertical resolution has 50 levels with approximately 10 m resolution
19 in the upper 220 m, increasing gradually to about 370 m resolution at deeper levels. The
20 oceanic model spin-up was done in a manner similar to that of Nobre et al. (2013) and
21 | Giarolla et al. (2015), in which is begin the spin_{up} run from rest, and the T-S structure
22 | of the oceans of Levitus (1982). The initial stage of the ocean model spin_{up} was done
23 | over a 13 years period, forced by climatological atmospheric fields (winds, solar

1 radiation, air temperature and humidity, and precipitation). It was then integrated by an
2 additional 58 years period, forced by interannually varying atmospheric fields from
3 Large and Yeager (2009), while the river discharges and the sea ice variables were kept
4 at their respective monthly mean climatological values. The forced ocean model run
5 was used to save the oceanic dynamical and thermodynamical structures in order to be
6 used in the initialization of future coupled model experiments.

7 The atmospheric and oceanic models are coupled via the Flexible Modeling
8 System (FMS) coupler, which was also developed at GFDL and incorporated in
9 MOM4p1. The atmospheric model receives SST and ocean albedo from the ocean and
10 sea ice models at hourly time steps. On the other hand, the oceanic model receives
11 information about freshwater (liquid and solid precipitation), momentum fluxes (winds
12 at 10 m), specific humidity, heat, vertical diffusion of velocity components and surface
13 pressure, all also at hourly time steps. Wind stress fields are computed within MOM4p1
14 using Monin-Obukhov scheme (Obukhov, 1971). In coupled simulations, the ocean
15 temperature and salinity restoration options are turned off.

16 **2.2 Experiments design**

17 A set of numerical experiments were carried out with the coupled ocean-
18 atmosphere version of BESM-OA2.5, following the CMIP5 experiment design protocol
19 (Taylor et al., 2012), and shown schematically in Figure 1. Out of those experiments
20 listed below, only the Historical simulation is evaluated in this paper:

- 21 • Historical: the simulation runs over the period 1850–2005 (156 years), forced by
22 atmospheric equivalent CO₂ observed historical concentration (greenhouse gas

only) over this period, based on CMIP5 protocol.

- piControl: it runs for ~~114700~~ years, forced by invariant pre-industrial atmospheric CO₂ concentration level (280 ppmv).
- Abrupt 4×CO₂: it runs for ~~1000460~~ years, consisting of an abrupt quadruplication of the atmospheric CO₂ concentration level from the piControl simulation.
- RCP4.5: it runs over the period 2006–2105 (100 years), forced by the time series of greenhouse gases level projected by the Representative Concentration Pathways 4.5 (RCP4.5), based on CMIP5 protocol. This simulation continues the historical simulation throughout the 21th century, reaching the radiative atmospheric forcing of 4.5 W_m⁻² in 2100.
- RCP8.5: same as the RCP4.5 simulation, but forced by the time series of greenhouse gases level projected by the Representative Concentration Pathways 8.5 (RCP8.5), based on CMIP5 protocol; i.e., reaching the radiative atmospheric forcing of 8.5 W_m⁻² in 2100.

The ocean stand-alone runs for 71 years (13 years period of ocean model spin-up forced by climatological atmospheric fields plus 58 years period forced by interannually varying atmospheric fields). Then a spin-up of the fully coupled model is done for 100 years. The ocean and atmosphere states at the end of this 100 years long integration are used as the initial condition for the piControl simulation. The piControl simulation shows stable conditions after a fast adjustment over the first 13 years of simulation (figure not shown). The analysis of the piControl and 4×CO₂ simulations are described in Capistrano et al. (2018) and Nobre et al. (2018, in preparation). Capistrano et al. (2018) estimates that BESM-OA2.5 has an equilibrium climate sensitivity of 2.96 °C for

1 the abrupt 4×CO₂ experiment. This value is within the range from 2.07 to 4.74 °C that
2 has been computed for 25 CMIP5 models and close to the ensemble averaged value
3 (3.30 °C).

4 **3. Methods and Data**

5 To evaluate the outputs of the BESM-OA2.5 historical simulation, comparisons
6 are done against observed datasets and Reanalysis products. The atmospheric fields are
7 from the Twentieth-Century Reanalysis dataset version 2 (20CRv2; Compo et al., 2011)
8 with a global horizontal resolution of 2° × 2° and 24 vertical levels
9 (https://www.esrl.noaa.gov/psd/data/gridded/data.20thC_ReanV2.html); the
10 precipitation dataset is obtained from Global Precipitation Climatology Project version
11 2.2 Combined Precipitation Dataset (GPCP; Adler et al., 2003; Huffman et al., 2009)
12 with global horizontal resolution of 2.5° × 2.5°
13 (<http://rda.ucar.edu/datasets/ds728.2/#!/description>) and from the CPC Merged Analysis
14 of Precipitation (CMAP; Xie and Arkin, 1997) with global horizontal resolution of 2.5°
15 × 2.5° (<https://www.esrl.noaa.gov/psd/data/gridded/data.cmap.html>); for comparison of
16 the global average air surface temperature, it is used the Hadley Centre-Climate
17 Research Unit Temperature Anomalies version 4 (HadCRUT4, Morice et al., 2012),
18 globally averaged air temperature anomaly at 2 meters time series
19 (<https://crudata.uea.ac.uk/cru/data/temperature/>); the cloud cover is compared to data
20 from The International Satellite Cloud Climatology Project (ISCCP D2; Rossow and
21 Schiffer, 1999) with global horizontal resolution of 2.5° × 2.5°
22 (<https://isccp.giss.nasa.gov/products/onlineData.html>); finally, for Sea Surface
23 Temperature (SST) comparisons it is used the Extended Reconstructed Sea Surface

1 Temperature version 4 (ERSSTv4, Huang et al., 2015) available on a $2^\circ \times 2^\circ$ grids
2 resolution (<https://www.esrl.noaa.gov/psd/data/gridded/data.noaa.ersst.v4.html>).

3 To identify the main modes of climate variability, all analyses presented in the
4 paper are done using detrended data sets anomalies. Detrended data sets are obtained by
5 removing the linear trend based on a least squares regression. Analysis using monthly
6 data sets, the annual cycle was removed by subtracting climatological monthly means
7 from the respective individual month. Prior to performing the analysis, the model's data
8 sets were interpolated to the grid resolution of the respective observation or Reanalysis
9 data sets used for comparison.

10 The Empirical Orthogonal Function analysis (EOF; Hannachi et al., 2007) is
11 used to analyze the capacity of the model in simulating major modes of climate
12 variability and compare them with observations. Prior to performing the EOF
13 calculations, the data were weighted by the square root of the cosine of latitude. The
14 results of the EOF maps are shown as the original data anomalies regressed onto the
15 normalized Principal Component (PC) time series, i.e. by the standard deviation.

16 In this paper, in order to evaluate the periodicity of the phenomena, it is applied
17 the power spectrum technique based on Fourier Analysis on the normalized time series,
18 in which the normalization is done by their long-term monthly standard deviation.

19 To have a better insight of BESM-OA2.5 performance of the global average
20 near-surface air temperature and on the average SST along both equatorial Pacific and
21 Atlantic, a comparison with 11 CMIP5 models is carried out. Since BESM-OA2.5
22 historical simulation is forced only by observed CO₂ equivalent concentration, for the

1 comparison it is chosen the historical simulation forced only by greenhouse gas
2 (historical GHG) shown in Table 1.

3 **4. Results**

4 **4.24.1 Mean Climate State**

5 In this section, the most important atmospheric and oceanic variables are
6 evaluated regarding their climatological fields, either globally or over regions in which
7 their representation are key elements of the climate system.

8 **4.1.1 Mean Surface Air Temperature**

9 The evolution of global surface air temperature throughout the industrial era is a
10 key element to analyze the long-term model behavior while being forced by the
11 observed conditions. The HadCRUT4 observation and BESM-OA2.5 time series of the
12 globally averaged air temperature anomaly at 2 meters are shown in Figure 2. The time
13 series are annual mean anomalies relative to the period 1850–1879. BESM-OA2.5
14 simulation of the global average surface air temperature evolution follows closely the
15 observed time series. However, since BESM-OA2.5 does not have the representation of
16 aerosols and consequently its cooling effects, the rate surface air warming should be
17 higher similarly to the remaining models (the grey shadow in Figure 2). In order to
18 compare BESM-OA2.5 with the selected CMIP5 models, the grey shadow represents
19 the spread of the minimum and the maximum values of anomalies at each year among
20 the 11 models (Table 1). In this comparison, it is used the historical GHG simulation, in
21 which the models are only forced by well-mixed greenhouse gases (mainly carbon
22 dioxide, methane, and nitrous oxides), without the cooling resulting from the direct and

1 indirect effects of aerosols, volcanos and effects of the land use change. Thus, the
2 CMIP5 models show a warmer tendency compared with the observations (see Jones et
3 al., 2013 for more details). Although BESM-OA2.5 has the same forcing conditions it
4 does not show the warming tendency of remaining models. ~~The reason for the absence
5 of this warming tendency in the last decades of the 20th century is not clear.~~ With
6 exception of GFDL-ESM2M (1861–2005) and HadGEM2-ES (1860–2005), all the
7 remaining CMIP5 models span their simulations throughout the period 1850–2005 and
8 their respective anomalies are from the period 1850–1879. For GFDL-ESM2M and
9 HadGEM2-ES, the anomalies are computed relative to the periods 1861–1890 and
10 1860–1889, respectively.

11 The net radiation at the top of atmosphere (TOA) has a negative bias and net of
12 the ocean/atmosphere heat flux has a positive bias (Fig. 3). The net radiation at TOA
13 has a mean value of -4.20 W m^{-2} and the net ocean/atmosphere heat flux has a mean
14 value of 1.16 W m^{-2} in the first 50 years. Throughout the simulation the net radiation at
15 TOA becomes less negative due to the increasing CO_2 on the atmosphere and
16 consequential increasing atmospheric heat content. Part of this heat is transferred into
17 the ocean as positive net of the ocean/atmosphere heat flux increasing indicates. The
18 negative net radiation at TOA and the positive ocean/atmosphere heat flux are likely the
19 reason for the weak warming observed in the Historical simulation (Fig. 2), since the
20 atmosphere is losing heat to the outer space and into ocean during the simulation.

21 **4.1.2 Mean Precipitation**

22 One of the key points in evaluating a Climate Model is to gauge its ability to
23 simulate the hydrological cycle due to its importance to the energy balance of the

1 climate system. Figure 43 shows the spatial distribution of annual mean precipitation for
2 (a) BESM-OA2.5, (b) GPCP dataset, and the spatial distribution of annual mean
3 precipitation biases (c) for BESM-OA2.5 relative to the GPCP dataset and (d) for
4 BESM-OA2.5 relative to the CMAP dataset. ~~The bias is obtained~~ The spatial annual
5 mean precipitation are ~~through the difference with GPCP dataset, in which the~~ averaged
6 values ~~are computed~~ over the periods 1971–2000 and 1979–2008, for BESM-OA2.5,
7 and GPCP and CMAP datasets, respectively. The global model's mean biases are
8 similar for GPCP (0.3 mm day^{-1}) and CMAP (0.4 mm day^{-1}). In the case of the global
9 model's rmse biases, they are also similar for GPCP (1.4 mm day^{-1}) and CMAP (1.5
10 mm day^{-1}). BESM-OA2.5 is able to reproduce global observed patterns of precipitation
11 and indicates a slight improvement in the global mean precipitation simulation
12 compared with the previous version (BESM-OA2.3). The spatial average biases are 0.3
13 mm day^{-1} and 0.5 mm day^{-1} , and the rmse are 1.4 mm day^{-1} and 1.7 mm day^{-1} for
14 BESM-OA2.5 and BESM-OA2.3, respectively. The improvements are particularly seen
15 in the Pacific and Atlantic Ocean areas, where BESM-OA2.5 reduces the positive bias
16 that extends to subtropical southeast Pacific and both north and south Atlantic
17 subtropics observed in BESM-OA2.3 (see Fig. 6a of Nobre et al., 2013). Despite these
18 improvements, BESM-OA2.5 still generates a strong negative bias over the Amazon
19 region. This is a particular concern since an important aim is related to the model for
20 future climate projections in the region. Based on the progress observed from BESM-
21 OA2.3 to BESM-OA2.5, work on cloud parametrizations that can improve the
22 precipitation over the Amazon is still carried out. Nevertheless, some state-of-the-art
23 models show deficiencies in generating precipitation over the Amazon region. This is
24 the case of the IITM-ESM (Fig. 5; Swapna et al., 2018), although the bias is more

1 | confined to the north of the Amazon and NESM that has a more distributed bias over
2 | the region (Fig. 9; Cao et al., 2018). The Indian subcontinent region also has a
3 | significant negative bias and strong positive bias appears over the Indian Ocean and in
4 | the South Pacific Convergence Zone (SPCZ). Such strong positive bias over the Indian
5 | ocean (near the African coast) is also identified in different versions of CCSM model
6 | (Fig. 5; Gent et al., 2011).

7 | In order to draw an associated global atmospheric circulation associated with the
8 | deficient precipitation over both the Amazon and Indian regions, it is computed the
9 | global anomalies of the velocity potential and the divergence of the wind at 200 hPa
10 | pressure level, and shown in Figure 54. The velocity potential and divergent wind
11 | anomalies are averaged over the period 1971–2000 for BESM-OA2.5 outputs (Fig.
12 | 54a), Reanalysis (Fig. 54b) and the difference BESM-OA2.5 minus Reanalysis (Fig.
13 | 54c, 54d and 54e). Figure 54c shows anomalous convergence over the Amazonian and
14 | Indian regions, resulting of the model's deficient capacity for creating convection and
15 | consequently in generating precipitation. Figures 54d and 54e show the velocity
16 | potential and wind divergence separated by seasons. For the Amazonian rainfall season,
17 | which occurs during MAM, it is possible to observe anomalous convergence at high
18 | levels of the atmosphere (Fig 54d). The equivalent result is observed for the Indian
19 | region for the JJA season (Fig. 54e).

20 | Figure 65 shows zonally averaged precipitation during the four seasons. For this
21 | comparison, results of BESM-OA2.3 used in Nobre et al. (2013) are also shown. Both
22 | versions are able to reproduce the maximum peaks of precipitation in both tropical and
23 | subtropical regions. BESM-OA2.5 shows a negative bias from around 40° latitude

1 poleward in both hemispheres. In the seasons DJF, JJA and SON, BESM-OA2.5 has a
2 positive bias on the peak of maximum precipitation corresponding to the ITCZ. In
3 MAM season the model still fails to perform the interhemispheric transition of the
4 ITCZ. However, the JJA season shows that BESM-OA2.5 is able to do the transition
5 completely, whilst BESM-OA2.3 shows a double ITCZ in JJA and SON seasons. The
6 double ITCZ problem is one of the most significant biases that persist in climate models
7 (e.g. Hwang and Frierson, 2013; Li and Xie, 2014; Tian, 2015). With the exception of
8 the MAM season, BESM-OA2.5 shows identical zonal precipitation to the observations,
9 although with a generally positive bias. It should be noted that BESM-OA2.5 has a
10 rapid precipitation decline at high latitudes. The model shows peaks of precipitation at
11 the mid-latitudes related to the storm tracks and less precipitation at the subtropics
12 compared to the GPCP dataset.

13 | Figure 76 shows the general characteristics of cloudiness over the globe
14 | simulated by the model. In particular, Figure 76a shows that the model underestimates
15 | cloudiness in most part of the globe, with significant exceptions of the high latitudes in
16 | the boreal hemisphere and in the southern subequatorial regions of the Pacific and
17 | Atlantic oceans when compared to observations. Globally, BESM-OA2.5 has a
18 | cloudiness negative bias of -13.9% with a root-mean-square-error of 19.9% . The
19 | periods used are 1971–2000 and 1984–2009 for BESM-OA2.5 and ISCCP,
20 | respectively. The model fails to generate clouds in the high latitudes of the austral
21 | hemisphere, as can be observed in Figure 76b, where the percentage of cloud cover is
22 | negligible. The reason for such lack of simulated cloudiness in this region is not clear
23 | yet. However, through the Figure 76b it is possible to see the meridional variation of

1 cloud cover simulated by the model is similar to the observation.

2 **4.1.3 Zonal Atmospheric Mean State**

3 | Figures 87 and 98 present the analysis of the zonally averaged vertical profiles
4 | of air temperature and zonal wind for all seasons simulated by BESM-OA2.5 and the
5 | respective bias relative to the 20CRv2 Reanalysis dataset, in which all data are time
6 | averaged over the period 1971–2000. BESM-OA2.5 has a large positive air temperature
7 | bias that appears above 250 hPa height (Fig. 87) in subpolar and polar regions in all
8 | seasons. This result indicates that the model warms abnormally in the tropopause and
9 | the lower stratosphere in polar regions. The warm bias is stronger in DJF and MAM
10 | seasons over the northern polar region, reaching a maximum bias of 20 °C in the DJF
11 | season. Such a bias is a matter of concern since other models, despite present strong
12 | bias in the Polar Regions, does not show such a strong bias. BNU-ESM presents
13 | positive biases up to 10 °C in the austral hemisphere during the season JJA (Fig. 3a; Ji et
14 | al., 2014) and NorESM1-M presents negative biases (~ -10 °C) during the seasons DJF
15 | and JJA (Fig. 9; Bentsen et al., 2013). In the lower and middle troposphere, the model
16 | shows a negative temperature bias, which is stronger in the lower troposphere over the
17 | polar region in the respective winter-spring seasons in both hemispheres, i.e. DJF and
18 | MAM over the North Pole, and JJA and SON over the South Pole. This negative bias
19 | reaches its maximum of –10 °C over the South Pole in SON. This negative bias over the
20 | troposphere has already been reported to occur in many CMIP5 models (see Charlton-
21 | Perez et al., 2013; Tian et al., 2013).

22 Concerning to the zonal wind, BESM-OA2.5 simulates a much weaker wind
23 | speed at the tropopause and stratosphere over the boreal hemisphere, mainly in the DJF

1 | season, which has a maximum negative bias of -26 m s^{-1} at 50–30 hPa (Fig. 98a). This
2 | bias is out of the range (-10 m s^{-1} to 10 m s^{-1}) that some models presents, as NorESM1-
3 | M (Fig. 10; Bentsen et al., 2013) or NESMv3 (Fig. 10d; Cao et al., 2018). The
4 | tropospheric jets and their seasonal migration are reasonably well simulated, although
5 | the eastward wind is stronger at subtropics with the maximum positive bias of 12 m s^{-1}
6 | occurring at 300–100 hPa in the MAM season.

7 | **4.1.4 Ocean Mean State~~Mean Sea Surface Temperature~~**

8 | The global distribution and the range values of the sea surface temperature
9 | (SST) are important characteristics of the mean climate state. Figure 109 shows the
10 | spatial map of the annual mean SST for (a) BESM-OA2.5, (b) ERSSTv4 and (c) the
11 | bias for BESM-OA2.5 relative to the ERSSTv4 dataset. BESM-OA2.5 has a warm SST
12 | bias which spreads throughout all oceans, contrasting with the negative biases which
13 | most of the CMIP5 models show over the North Pacific and North Atlantic oceans (see
14 | Wang et al., 2014). However, the extreme values found in the south of Greenland and in
15 | the North Pacific, where it reaches $\sim 6 \text{ }^\circ\text{C}$, is well within the range of biases reported by
16 | other models, as NorESM1-M (Fig. 12b; Bentsen et al., 2013) or IITM-ESM (Fig. 3;
17 | Swapna et al., 2018). Such warma bias does not appear in the tropical and subtropical
18 | regions in the BESM-OA2.3 simulation (Fig. 5a of Nobre et al., 2013), where there are
19 | cold SST biases. The spatial average biases are $1.5 \text{ }^\circ\text{C}$ and $0.9 \text{ }^\circ\text{C}$, and the rmse are 1.9
20 | $^\circ\text{C}$ and $2.1 \text{ }^\circ\text{C}$ for BESM-OA2.5 and BESM-OA2.3, respectively. A notable feature of
21 | BESM-OA2.5 is its strong warm SST bias in the North Pacific and in the Californian
22 | coast, and south of Greenland. The model still overestimates SSTs in the major eastern
23 | coastal upwelling regions. Such a feature is a systematic error observed in different

1 state-of-the-art models, in which the causes can be related to a simulation of a weaker
2 than observed alongshore winds which leads to an underrepresentation of upwelling and
3 alongshore currents (e.g. Humboldt, California and Benguela Currents), and/or the
4 under predicted effects of shortwave radiation due to deficient simulation of
5 stratocumulus clouds over cold waters (see Richter, 2015). Nevertheless, the bias is
6 negligible over the north equatorial Pacific and in large parts of tropical western
7 Atlantic.

8 | Figure [11+0a](#) shows the mean SST along equatorial Pacific for BESM-OA2.5
9 | and ERSSTv4, averaged over the period 1971–2000. The equatorial region is defined
10 | over the region between the latitudes 2° S and 2° N. The model simulates a warmer
11 | mean SST over the western and extreme eastern parts of the equatorial Pacific Ocean.
12 | This positive bias is most notable in the western part, where it is about 1.5–2 °C warmer
13 | than observations and is warmer than the CMIP5 models (shown by the shaded grey
14 | area in Figure [11+0a](#)). But for the extreme eastern part of the basin, the model has a
15 | lower bias compared with the CMIP5 models. For most of the central Pacific Ocean, the
16 | model has a very good representation of the SST, with a RMSE of 0.14 °C between
17 | 160 °E and 120 °W. The annual cycle of the equatorial Pacific SST anomalies for
18 | BESM-OA2.5 and ERSSTv4 are shown in figure [11+0b](#) and c, respectively. BESM-
19 | OA2.5 simulates reasonably well the marked annual cycle which occurs on the eastern
20 | Pacific, although the negative SST anomalies between July and December are up to 1
21 | °C colder than observations. The propagation of the SST anomaly patterns from the
22 | eastern to the western part of the Pacific Ocean that occurs throughout the year is not
23 | well captured by the model. BESM-OA2.5 shows an annual cycle in the western part of
24 | the Pacific Ocean, where observations show a semiannual pattern of SST anomalies.

1 | The same methodology is used for the tropical Atlantic. Figure [12H1a](#) shows that in the
2 | Atlantic basin there is a significant bias of ~ 3 °C in the eastern part of the basin. This
3 | bias starts in the central Atlantic and it is higher than the CMIP5 models (shown by the
4 | shaded grey area in Figure [12H1a](#)). However, it should be noted that the CMIP5 models
5 | also have a warm bias in the eastern part of the tropical Atlantic, which is a problem
6 | discussed in previous studies (e.g. Richter et al., 2014 and references therein). Although
7 | this warm bias, the tropical Atlantic seasonal SST variation is well simulated by BESM-
8 | OA2.5 in particular on the eastern side of the basin, as it can be seen in Figures [12H1b](#)
9 | and c.

10 | To evaluate how the global ocean profile evolves throughout the simulation, it is
11 | computed the depth-time Hovmöller diagrams of global mean ocean temperature and
12 | salinity departures from their respective initial conditions (Fig. 13). Here initial
13 | conditional means the value of the first year of simulation, in this case, the year 1850.
14 | The prominent warming occurs from the surface up to 400 m depth (Fig. 13a). This
15 | warming is more significant at the end of the simulation (~ 0.6 °C comparing with initial
16 | conditions) and is likely to be related to the global warming of the planet and
17 | consequential increasing heat flux from the atmosphere into the ocean. In deeper waters,
18 | from 1500 m up to the ocean floor, there is a weaker warming, indicating that the ocean
19 | is gaining heat mainly in the upper layers. Between 500-1500 m depth, it is observed a
20 | cooling tendency respective to initial conditions. The ocean salinity slightly increases
21 | below 1000 m depth and from 1935 the increase reaches 0.04 PSU between 1500 and
22 | 3000 m depth compared with the initial values (Fig. 13b). Above 1000 m depth there is
23 | a significant freshening of the ocean waters, with the surface waters salinity decreasing

1 up to 0.18 PSU at the end of the simulation. Such tendency can mean that the ocean is
2 still drifting from its initial conditions in the Historical simulation.

3 **4.1.5 Atlantic Meridional Ocean Circulation**

4 The meridional overturning circulation (MOC) plays an important role in
5 transporting heat from the tropics to higher latitudes of both hemispheres. This is
6 particularly important in the North Atlantic, where the Atlantic Meridional Overturning
7 Circulation (AMOC) has a profound impact on the climate of the surrounding
8 continents (see Buckley and Marshall, 2015). The AMOC in the BESM-OA2.5
9 historical experiment has the typical structure described in Lumpkin and Speer (2007),
10 with the main layers well depicted in the appropriated depths (Figure ~~14~~12a). The
11 annual mean maximum AMOC strength simulated by BESM-OA2.5 is about 15 Sv (1
12 $\text{Sv} \equiv 10^6 \text{ m}^3 \text{ s}^{-1}$) between 25° N and 30° N at about 850 m depth (see Figure ~~14~~12a). This
13 maximum value is within the 17.2 ± 4.6 Sv mean strength (with a 10 day filtered root
14 mean square variability of 4.6 Sv) observed by the project RAPID at 26.5° N
15 (McCarthy et al., 2015). It is also in the range of maximum volume transport strength
16 simulated by the state-of-the-art models of the CMIP5 (Weaver et al., 2012; Cheng et
17 al., 2013). Figure ~~14~~12b shows the maximum annual mean AMOC strength time series
18 for the historical period at the 30° N. For comparison, The same Ffigure 14c also plots
19 the AMOC maximum volume transport strength measured by the Rapid project over the
20 period April/2004 to October/2015
21 (http://www.rapid.ac.uk/rapidmoc/rapid_data/datadl.php).

22 Averaging the maximum AMOC strength over the first and the last 30 years of
23 the time series, i.e. over the periods 1850–1879 and 1976–2005 respectively, the result

1 shows a decrease of 11.2 %, from 16.9 Sv to 15.1 Sv in each period, respectively.
2 Modeling results indicate that the AMOC has a multidecadal cycle, however the power
3 spectrum of its strength time series do not show a multidecadal oscillation (not shown).
4 The standard deviation of the detrended maximum AMOC strength time series is 1.4
5 Sv.

6 **4.2 Climate Variability**

7 In this section, we evaluate the most prominent global climate variability
8 patterns. This allows us to infer the ability of the model in simulating atmospheric
9 internal and ocean-atmosphere coupled variabilities in the climate system correctly.

10 **4.2.1 Tropical Variability**

11 **4.2.1.1 El Niño-Southern Oscillation**

12 The El Niño-Southern Oscillation (ENSO) in the equatorial Pacific Ocean is one
13 of the most prominent climate variability phenomena at interannual time scales
14 (Dijkstra, 2006), with strong impacts on regions surrounding the Indian and Pacific
15 Oceans and regions that are influenced by its teleconnections (see McPhaden et al.,
16 2006 and references therein). There are many methods to evaluate the ENSO variability.
17 In the present study, it is applied the EOF to detrended monthly SST anomalies over the
18 tropical Pacific ocean (30° S–30° N; 240°–70° W) for the period 1950–2005 for both
19 BESM-OA2.5 simulations and ERSSTv4 data. Figures ~~15~~¹³a and b show the leading
20 EOF patterns associated with the El Niño/La Niña variability. The model simulates the
21 El Niño/La Niña variability deficiently, with lower amplitude of SST variability and the
22 center of maxima variability confined to the eastward part of the basin. The model's

1 leading EOF explains 17.9 % of the total variance, substantially less than the 45 %
2 explained by observations. The lower amplitude of the simulated El Niño/La Niña can
3 be verified in the power spectrum of the leading Principal Component (PC) shown in
4 Figure 1513. Even though the simulation shows two significant peaks between 2–4
5 years cycle (Fig. 1513c), which is within the range of the period cycle given by the
6 leading PC of observations (3–7 years cycle; figure 1513d), the amplitude of the
7 simulated variance is lower than that of observations.

8 Figure 1614 shows the spatial correlation between detrended monthly anomalies
9 of the Niño-3 index (defined inside the black rectangle area, bounded by 5° S–5° N,
10 90°–150° W) and detrended monthly anomalies of global SST computed for BESM-
11 OA2.5 and ERSSTv4 over the period 1900–2005. The model has not a strong
12 correlation at grid points inside the Niño-3 area, which is a signal that the El Niño/La
13 Niña spatial pattern is weakly simulated. The horseshoe pattern of negative correlation
14 observed in the Pacific ocean is also weakly simulated by the model, particularly in the
15 westward equatorial part. The positive correlation of observed SST over the Indian
16 ocean and Niño-3 index is absent in the model’s simulation. It is worth mentioning that
17 the model simulates the observed correlation pattern of SST anomalies over the Atlantic
18 Ocean with Niño-3 index, although it is not so robust (Figure 1614).

19 **4.2.1.2 Atlantic Meridional Mode**

20 The leading modes of coupled ocean-atmosphere variability over the Tropical
21 Atlantic ocean are the zonal mode, also referred as equatorial mode (Zebiak, 1993; Lutz
22 et al., 2015), and the meridional mode, also referred as the interhemispheric mode
23 (Nobre and Shukla, 1996). The first is an ENSO-like phenomenon that emerges in the

1 Gulf of Guinea mainly in the boreal summer and has a strong impact on West African
2 precipitation (Zebiak, 1993; Lutz et al., 2015). The second is characterized by a cross-
3 equatorial SST gradient associated with a meridional wind stress toward the warmer
4 SST anomalies. The maxima amplitude of the meridional mode occurs during the boreal
5 spring, influencing the precipitation in Northeast Brazil and West Africa (Nobre and
6 Shukla, 1996; Chang et al., 1997; Chiang and Vimont, 2004). The Atlantic Meridional
7 Mode (AMM) has an interannual and decadal temporal scale of variability and is a
8 result of a thermodynamic coupling between the wind speed, the sea surface
9 evaporation induced by the wind stress, and the SST, mechanism known as Wind-
10 Evaporation-SST feedback (WES feedback, Xie and Philander, 1994; Chang et al.,
11 1997; Xie, 1999). To evaluate the AMM simulations, a joint EOF of SST and wind
12 stress (Taux and Tauy) fields analysis is computed, as such a variability is the response
13 | of a coupled ocean-atmospheric system. Figure [1715](#) shows the AMM simulated by
14 | BESM-OA2.5, and obtained by observed data. The AMM pattern simulated by the
15 | model is similar to obtained from observations, regardless of the weaker gradient pole at
16 | the South Atlantic. Nevertheless, the explained variance by the model is very close to
17 | the observed one, being respectively, 10.7 % and 11.8 %. The patterns shown in Figure
18 | [1715](#) are defined as a positive phase of the AMM, with the inter-hemisphere cross-
19 | equatorial wind from south to north, and with corresponding negative SST anomalies
20 | over the southern pole and positive SST anomalies over the northern pole (the negative
21 | phase of AMM is the reverse pattern). Over the second half of the 20th century, the
22 | AMM shows a predominant decadal periodicity of 11–13 years. Figures [1715c](#) and [d](#)
23 | show the power spectrum of the PC of the AMM patterns simulated by the model and
24 | from the observation, respectively. It is possible to see that the pattern simulated by

1 BESM-OA2.5 shows, similarly to the observed one, a predominant periodicity at
2 decadal timescales.

3 **4.2.1.3 South Atlantic Convergence Zone**

4 The South Atlantic Convergence Zone (SACZ) is characterized by an intense
5 NW-SE oriented cloud band that extends from the Amazon Basin to the South Atlantic
6 subtropics, mainly during austral summer (Nogués-Paegle and Mo, 1997; Carvalho et
7 al., 2004; de Oliveira Vieira et al., 2013). The formation of the SACZ has a strong
8 influence on the precipitation over southeast South America and is considered, together
9 with the convection activity over the Amazon Basin, the main component of the South
10 American Monsoon System (Jones and Carvalho, 2002). The southern part of the SACZ
11 usually lies over cooler SST (Grimm, 2003; Robertson and Mechoso, 2000). Chaves
12 and Nobre (2004) suggests that the formation of SACZ over the ocean tend to block the
13 solar radiation by clouds, cooling the SST beneath. AGCM are not able to simulate the
14 precipitation over cooler SST caused by SACZ (Marengo et al., 2003; Nobre et al.,
15 2006; Nobre et al., 2012), since such models tend to increase the precipitation over
16 warmer SST, as an hydrostatic response. Nobre et al. (2012) has shown that coupled
17 AOGCMs are able to simulate the SACZ formation over colder SST anomalies, as this
18 class of models englobes the atmosphere-ocean surface thermodynamic coupling.
19 Following Nobre et al. (2012), a correlation between seasonal precipitation and SST
20 anomalies for the austral summer (DJF) over the tropical South Atlantic (40° S–10° N;
21 70° W–20° E) over the period 1979–2010 for observations and for the period
22 | 1971–2002 for the model, so 32 years are used. Figure [1846](#) shows the rainfall-SST
23 anomaly correlation maps for both BESM-OA2.5 and observations. BESM-OA2.5 are

1 able to simulate an inverse correlation between precipitation and SST in the southeast of
2 Brazil (near 20° S), suggesting the capacity of simulating precipitation over cooler SST,
3 a feature related to the formation of SACZ (that tends to cooler the SST). Its noteworthy
4 in Figure 16 that BESM-OA2.5 is capable to generate both positive and negative SSTA-
5 rainfall correlations over the equatorial Atlantic (positive, thermally direct driven
6 circulation over the equatorial region and negative, thermally indirect driven
7 atmospheric circulation over the SW tropical Atlantic, Figure ~~1816~~a), a feature also
8 present in the observation correlation map of Figure ~~1816~~b.

9 **4.2.1.4 Madden-Julian Oscillation**

10 The Madden-Julian Oscillation (MJO) is the prominent intraseasonal variability
11 (30-90 days) over the eastern Indian and western Pacific tropical regions and consists on
12 events of deep convection coupled to atmospheric circulation that packed propagate
13 together through the equatorial region eastward (Madden and Julian, 1971, Madden and
14 Julian, 1972; Zhang, 2005). The influence of MJO events with large-scale phenomena
15 has been reported, as in the case of the evolution of ENSO (e.g. Takayabu et al., 1999),
16 formation of tropical cyclones (e.g. Liebmann et al., 1994) or in the North Atlantic
17 Oscillation (e.g. Lin et al., 2009). To evaluate the MJO simulated by the model it is
18 performed the wavenumber-frequency power spectrum analysis for tropical (10 °S–10
19 °N) averaged daily outgoing long-wave radiation (OLR) and daily zonal wind
20 component at 850 hPa pressure level (U850), for the boreal winter (Nov-Apr) over the
21 period 1971–2000. To compute and plot the wavenumber-frequency power spectrum it
22 is used the MJO Simulation Diagnostic package (details in Waliser et al., 2009).

1 Fig. 19a and Fig. 19b show the wavenumber-frequency power spectrum for
2 OLR for BESM-OA2.5 and 20CRv2, respectively. Although BESM-OA2.5 presents an
3 eastward propagating disturbance with wavenumber 1, it is characterized by lower
4 frequency (> 80 days) compared to the maxima peak within 30–80 days frequency band
5 shown by the 20CRv2, despite it spreads over lower frequencies than 80 days. This
6 observed peak has more energy for wavenumber 2. A westward propagating disturbance
7 (negative frequencies) with weaker energy than the eastward propagating counterpart
8 appears in 20CRv2, with a peak for wavenumber 2. Similarly, BESM-OA2.5 also
9 shows a westward propagating disturbance with weaker energy for wavenumber 1–3.
10 The wavenumber-frequency power spectrum for U850 in 20CRv2 shows an eastward
11 propagating disturbance which peaks at the 30–80 days frequency band with
12 wavenumber 1 (Fig. 19d). In the case of BESM-OA2.5 there is an eastward propagation
13 with a periodicity slightly higher than 80 days for wavenumber 1 but this disturbance
14 spreads over different frequencies out of the 30–80 days frequency band (Fig. 19c). It
15 also presents a westward propagating disturbance that is absent in the Reanalysis.
16 BESM-OA2.5 poorly simulates the MJO and underestimates its amplitude. However,
17 MJO has been highlighted as a phenomenon that climate models struggle to simulate in
18 a proper way, especially by underestimate OLR and representing a coherent eastward
19 propagation (Kim et al., 2009; Ahn et al., 2017).

20 **4.2.2 Extratropical Variability**

21 **4.2.2.1 North Atlantic Oscillation**

22 The North Atlantic Oscillation (NAO) is a major atmospheric variability pattern
23 occurring in the North Atlantic, which is characterized by the oscillation of the

1 difference on the sea level pressure (SLP) between Iceland and Portugal (Wanner et al.,
2 2001; Hurrell et al., 2003). NAO has a great impact in the Euro-Atlantic region (Hurrell
3 et al., 2003; Hurrell and Deser, 2009), with the notable work of Namias (1972) relating
4 droughts over the Northeast Brazil to NAO variations. Recent studies also show its
5 teleconnections to the East Asia (e.g. Yu and Zhou, 2004; Wu et al., 2012). The NAO's
6 influence on a rapid climate change in the Northern Hemisphere has been highlighted in
7 (Delworth et al., 2016), which increases the importance of its correct simulation. Since
8 NAO's largest amplitude of variation occurs mainly during the boreal winter, the
9 analysis here is centered on this season. The period used to perform the analyses is
10 1950–2005. The leading EOF of the SLP averaged for boreal winter season (DJF) in the
11 Euro-Atlantic region shows that the NAO is well simulated by BESM-OA2.5 (Fig.
12 [2017a](#)), simulating the NAO dipole centers and their amplitudes very similar to the
13 observed pattern (Fig. [2017b](#)). The variances explained by the leading EOF are also
14 similar, 50.2 % and 44 % for BESM-OA2.5 and Reanalysis, respectively. The spectral
15 analysis of the leading PCs shows that BESM-OA2.5 captures the ~2.5 years cycle on
16 the time variability but fails to capture the ~8 years cycle (Fig. [2017c](#) and d). It is
17 interesting to note that BESM-OA2.5 simulates a NAO spatial pattern, without
18 capturing its low-frequency variability. By analyzing the NAO variability, we consider
19 that it is not necessary to analyze the Northern Annular Mode (NAM), since both are
20 manifestation of same mode of variability (Hurrell and Deser, 2009).

21 **4.2.1.2 Pacific-North America Pattern**

22 Jointly, the NAO and the Pacific-North American pattern (PNA) are the
23 dominant atmospheric internal modes over the boreal hemisphere. The PNA is

1 characterized by four centers of high pressure anomalies in the North Pacific and North
2 America, respectively; over Hawaii, to the south of the Aleutian Islands, in the
3 intermountain region of North America, and in the Gulf Coast region of the U.S.A.,
4 representing the centers of action of a stationary wave train extending from the tropical
5 Pacific into North America (Wallace and Gutzler, 1981). It exerts a significant influence
6 on surface temperature and precipitation over North America (Leathers et al., 1991).
7 Some studies have shown that, although the PNA is an internal atmospheric variability
8 phenomena, it is influenced by other climate variabilities, as the ENSO and the Pacific
9 Decadal Oscillation (PDO) (see Straus and Shukla, 2002; Yu and Zwiers, 2007).

10 Similar to NAO, the PNA has its largest variation of amplitude during the boreal
11 winter; therefore, the present analysis is performed for this season. Following Wallace
12 and Gutzler (1981), we construct one-point correlation maps for BESM-OA2.5 and
13 20CRv2 Reanalysis in order to evaluate the capacity of the model to reproduce the PNA
14 pattern. The one-point correlation maps correlate 500 hPa geopotential height at the
15 reference point (45° N, 165° W) with all the other grid points of the map domain (0°–80°
16 N; 240°–70° W). The time series used to perform the correlations are averaged boreal
17 winter seasonal (DJF) dataset over the period 1950–2005. The time series are departed
18 from their long-term mean and normalized at each grid point prior the correlation
19 computation. Figure [2148](#) shows the one-point correlation maps for BESM-OA2.5 (Fig.
20 [2148a](#)) and 20CRv2 (Fig. [2148b](#)). In this figure, it is possible to check the four centers
21 of action simulated by the model, which shows a stronger correlation between the four
22 high pressure centers when compared with reanalysis correlation maps in Figure [2148b](#).

23 **4.2.1.2 Pacific-South America Patterns**

1 The second and third EOF of 500 hPa geopotential height over the Southern
2 Hemisphere (20°–90° S) present a notable resemblance to the Pacific-South America
3 | (PSA) teleconnection pattern (~~Ghil and Mo, 1991~~Mo and Peagle, 2001). PSA patterns
4 | are stationary Rossby wave trains extending from central Pacific to Argentina, in which
5 the PSA1 (EOF2) is a response to ENSO and the PSA2 (EOF3) is associated to the
6 quasi-biennial component of ENSO (Karoly, 1989; Mo and Peagle, 2001). These
7 patterns have a significant impact on rainfall anomalies over South America (Mo and
8 | Peagle, 2001). Figure ~~2219~~ shows the PSA patterns both simulated by BESM-OA2.5
9 | and from Reanalysis. As the explained variance of EOF2 and EOF3 are close, the EOFs
10 seem to degenerate for both Reanalysis and model simulation. In order to relax the
11 orthogonality constraint, it is performed a rotated EOF (REOF) retaining the first 10
12 modes. The REOF2 and REOF3 resemble the EOF2 and EOF3 respectively, implying
13 that they are independent modes. The PSA pattern is well simulated by BESM-OA2.5,
14 although the model changes the order of the EOF patterns. BESM-OA2.5 shows an
15 | anomaly south of South Africa (Fig. ~~2219c~~) that does not appear in the Reanalysis (Fig.
16 | ~~2219b~~). PSA patterns have significant interannual and decadal variabilities (Zhang et
17 | al., 2016). PSA patterns simulated by BESM-OA2.5 have only significant variability in
18 the interannual scale, with absent decadal variability (figure not shown).

19 **4.2.1.4 Southern Annular Mode**

20 The Southern Annular Mode (SAM) is the dominant atmospheric variability in
21 the Southern Hemisphere, occurring in the extra-tropics and in the high latitudes
22 (Kidson, 1988). It is also referred to as Antarctic Oscillation (AAO; Gong and Wang,
23 1999). SAM variability is characterized by anomalies variation in the polar low-

1 pressure and in the surrounded zonally high-pressure belt. It can be captured through the
2 first EOF applied to different atmospheric variables, as the sea level pressure, different
3 geopotential height levels or the surface air temperature (Kidson, 1988; Rogers and van
4 Loon, 1982; Thompson and Wallace, 2000). To evaluate the capacity of BESM-OA2.5
5 to simulate this atmospheric mode of variability, EOF analysis is applied to the monthly
6 mean 500 hPa geopotential height field from 20° S to 90° S, over the period 1950–2005,
7 for both model and Reanalysis. The SAM pattern simulated by BESM-OA2.5 resembles
8 very well the observed pattern, with the mid-latitude 500 hPa geopotential height
9 variation centers depicted in the same longitudes as observations, but with differences in
10 the amplitude values (Fig. ~~23~~20). However, the explained variance is higher compared
11 with observation. The explained variances of BESM-OA2.5 and 20CRv2 are 34.1 %
12 and 21.0 %, respectively. The SAM is a quasi-decadal mode of variability (see Yuan
13 and Yonekura, 2011), however the BESM-OA2.5 power spectrum reveals a SAM with
14 a markedly interannual variability, without the peak between 8 and 16 years as obtained
15 in the Reanalysis (figure not shown).

16 **4.2.1.5 Pacific Decadal Oscillation**

17 Observed SST anomalies over the North Pacific have shown an oscillatory
18 pattern in the central and western parts in relation to the tropical part and along the
19 North American west coast. This oscillatory shift of SST anomalies with interdecadal
20 periodicity was termed Pacific Decadal Oscillation (PDO) and it is defined as the
21 leading EOF of the monthly SST anomalies over North Pacific (Mantua et al., 1997).

22 The positive phase of PDO is defined when ~~negative~~positive SST anomalies
23 predominate over the central and western parts of North Pacific, and ~~positive~~negative

1 SST anomalies predominate over the Tropical Pacific and along the North American
2 west coast; being the negative phase the reverse pattern. Many studies have connected
3 the PDO with variations on precipitation regimes in different regions around the world,
4 as South China monsoon (e.g. Wu and Mao, 2016), Indian monsoon (e.g.
5 Krishnamurthy and Krishnamurthy, 2016) and together with ENSO in the precipitation
6 regime in North America (see Hu and Huang, 2009). There are different mechanisms
7 that modulate PDO, in which one of them is the response of the Northern Pacific SST to
8 the ENSO variability via the “atmospheric bridge” (for a detailed review, see Newman
9 et al., 2016).

10 Following the definition (Mantua et al., 1997), the spatial pattern of PDO is
11 obtained by regressing the SST anomalies onto the leading normalized PC time series,
12 shown in Figure ~~24~~²¹ which in this case is showing the positive phase of the PDO. The
13 EOF is applied to monthly SST anomalies over North Pacific (20°–60° N; 240°–110°
14 W) over the period 1900–2005. BESM-OA2.5 is not capable of reproducing this pattern
15 by the leading EOF. The PDO pattern only appears on the second EOF (Fig. ~~24a~~^{21b}),
16 with the explained variance of 14.0 % against 20.5 % of observations. Although the
17 EOF2 resembles the PDO mode, the tropical part has a weaker variation than the
18 observation. The reason of incapacity of the model in reproducing the PDO as the
19 leading mode of variability is probably due to the model’s simulation of weaker ENSO
20 variability, both in spatial and temporal scales. These deficiencies may impact the
21 mechanisms that reproduce the PDO, mainly via the “atmospheric bridge” as referred
22 earlier. Figures ~~25~~²²a and b show the normalized PC2 and PC1 time series of BESM-
23 OA2.5 and ERSSTv4, respectively. It is possible to note that both time series present a

1 multidecadal periodicity, but in different time scales as it is confirmed by the power
2 spectrum (Fig. [2522c](#) and d). The power spectrum shows that both time series present
3 interannual periodicity (~5-6 years), with BESM-OA2.5 multidecadal variability
4 strongest spectrum around 15 years, a higher frequency compared with observation (~22
5 and ~40-45 years).

6 **5. Summary**

7 The capacity of Earth Systems Models to project a future climate under the
8 conditions given by future scenarios of atmospheric greenhouse gas concentrations can
9 be assessed by how accurate these models are able to reproduce observed climate
10 features. Therefore, the evaluation of how these models perform for the historical period
11 when there are observations to compare with model's calculations represents a key part
12 of the Earth System modelling. In this study, BESM-OA2.5 historical simulation is
13 evaluated for the period 1850–2005 following the CMIP5 protocol (Taylor et al., 2012)
14 with focus on simulations of its mean climate and key large-scale modes of climate
15 variability.

16 BESM-OA2.5 is an updated version of BESM-OA2.3 (Nobre et al. 2013;
17 Giarolla et al. 2015) regarding the atmospheric model, which consists in the new
18 Brazilian Global Atmospheric Model (BAM; Figueroa et al., 2016). This new version
19 allowed to alleviate a mean global bias of energy balance at the top of the atmosphere of
20 -20 W_m^{-2} to -42 W_m^{-2} . Moreover, systematic errors were reduced in wind, humidity
21 and temperature in the surface layer over oceanic regions by the inclusion formulations
22 presented by Jiménez et al. (2012).

1 The analysis of the mean climate shows that the model is able to simulate the
2 general mean climate state. Nevertheless, some significant biases appear at the
3 simulation, as a double ITCZ over the Pacific and Atlantic Oceans, some notable
4 regional biases in the precipitation field (e.g., over the Amazon and Indian regions) and
5 in the SST field (e.g., south of Greenland). Yet, the model has shown an improvement
6 in simulating the ITCZ and a reduction in the global precipitation RMSE compared with
7 BESM-OA version 2.3. BESM-OA2.5 shows an almost globally positive SST bias,
8 which did not occur in version 2.3, however the SST RMSE was slightly reduced in the
9 newer version of the model.

10 The most relevant climate patterns on interannual to decadal time scales
11 simulated by BESM-OA2.5 are compared with the ones obtained from observations and
12 Reanalysis. Over the Pacific, the ENSO is simulated with lower amplitude of variability
13 than the observations and such weak ENSO seems to impact other Pacific variability
14 patterns such as the PDO. Conversely, the major phenomena on the Atlantic basin are
15 well represented in BESM-OA2.5 simulations. This is the case for the Tropical Atlantic
16 mode of interhemispheric variability (AMM) that is very well simulated by the model in
17 term of the spatial pattern and temporal variability. It is worth to note that this mode is
18 considered poorly simulated by the models used in the Intergovernmental Panel on
19 Climate Change (IPCC) fifth assessment report (AR5) (Flato et al., 2013). It is also
20 relevant to highlight BESM-OA2.5 ability to represent the enhanced rainfall over cooler
21 waters over the SW Tropical Atlantic, associated with the South Atlantic Convergence
22 Zone (SACZ). The capacity of the model in simulating the AMM and SACZ is an
23 important result since one of the main aims is the representation of modes that directly

1 impacts the precipitation over South America. The AMOC reproduced by BESM-
2 OA2.5 has the meridional overturning structure comparable with the ensemble AMOC
3 simulated by the CMIP5's models. BESM's maximum AMOC strength average value is
4 slighter lower than the average value that has been observed by the project RAPID, but
5 well within the range of mean square root variability that is observed. Although the
6 averaged maximum strength AMOC simulated by the CMIP5 models is within the
7 mean range square root variability that is observed, most models tend to simulate strong
8 AMOC, with a maximum strength above 20 Sv, and out of the range (Zhang and Wang,
9 2013). The NAO atmospheric variability, which is well simulated by the CMIP5 models
10 (Ning and Bradley, 2016) is also very well simulated by BESM-OA2.5. In the extra-
11 tropics, BESM-OA2.5 is capable to reproduce fairly well majors variabilities in both
12 Hemispheres, as the PNA, PSA, and the SAM teleconnections patterns, comparable to
13 CMIP5 models that reproduce the PNA (Ning and Bradley, 2016) and the SAM (Zheng
14 et al. 2013).

15 Similarly to Nobre et al. (2013), this study aims to evaluate the BESM-OA2.5
16 by comparing the most important features of the climate system simulated by the model
17 with observations and Reanalysis. The next version of the model (BESM-OA2.8) is
18 already under development. In this new version, the MOM4p1 ocean model has been
19 replaced by the MOM5. Regarding the atmospheric model, new developments have
20 been carried out to improve BAM's capacity, being the most important the inclusion of
21 a scheme of humidity in the planetary boundary layer, a new dynamic core and new
22 cloud cover scheme (Figuroa et al., 2016). This new version of BESM carries the
23 challenges of improving the simulation of the precipitation, in particular to alleviate the

1 deficit over the Amazon. The ENSO is the large-scale phenomenon that will receive a
2 scrutiny in order to understand the reasons for a weak variability. The other feature of
3 the model is the weaker warming under the CO₂ equivalent only forcing, relative to
4 other CMIP5 that do not consider the direct and indirect effects of atmospheric aerosols.

5 Assuming that BESM-OA2.5 should respond consistently with CMIP5 models, it would
6 underestimate the warming observed in the last decades. However, models can respond
7 in different ways to external forcing, therefore, in the near future, the aim is to carry out
8 a numerical experiment in which the model is forced with observed estimate of aerosol
9 concentration (as read-in field) in order to address to what extension BESM is impacted.

10 In the future, a study comparing the versions 2.5 and 2.8 of the BESM-OA is aimed in
11 order to fully report the advances of the modeling work developed in the last couple
12 years. Such a study will give a broader perspective of the technical challenges overcome
13 throughout this project and assess the improvements achieved in each version of the
14 model in simulating the climate system.

15

16 **Code and data availability**

17 The BESM-OA2.5 source code is freely available after signature of a license agreement.

18 Please contact Paulo Nobre to obtain the source code and data of BESM-OA2.5.

19

20 **Competing interests**

21 There are no competing interests of which the authors are aware.

1

2 **Acknowledgements**

3 This research was partially funded by FAPESP (2009/50528-6), FAPESP (2008/57719-
4 9) and by the National Institute of S&T for Climate Change (CNPq (573797/2008-0).
5 SFV is supported by a Ph.D. grant funded by CAPES. The authors would like to
6 acknowledge Rede CLIMA, FAPESP and INPE for the use of its supercomputer
7 facility, which made this work possible. Twentieth Century Reanalysis Project data sets
8 (20CRv2) are provided by the U.S. Department of Energy, Office of Science Innovative
9 and Novel Computational Impact on Theory and Experiment (DOE INCITE) program,
10 and Office of Biological and Environmental Research (BER), and by the National
11 Oceanic and Atmospheric Administration Climate Program Office. The GPCP
12 combined precipitation data sets were developed and computed by the NASA/Goddard
13 Space Flight Center's Mesoscale Atmospheric Processes Laboratory. The HadCRUT4
14 data sets are provided by the Met Office Hadley Centre and the University of East
15 Anglia/Climatic Research Unit. The ISCCP D2 data sets are provided through the
16 International Satellite Cloud Climatology Project, maintained by the ISCCP research
17 group at the NASA/Goddard Institute for Space Studies. The Extended Reconstructed
18 Sea Surface Temperature (ERSSTv4) is provided by the NOAA/OAR/ESRL/PSD. Data
19 from the RAPID-WATCH MOC monitoring project are funded by the Natural
20 Environment Research Council. The authors acknowledge the World Climate Research
21 Programme's Working Group on Coupled Modelling, which is responsible for CMIP,
22 and we thank the climate modeling groups (listed in Table 1 of this paper) for producing
23 and making available their model output. For CMIP the U.S. Department of Energy's

1 Program for Climate Model Diagnosis and Intercomparison provides coordinating
2 support and led development of software infrastructure in partnership with the Global
3 Organization for Earth System Science Portals. This work is part of the Ph.D. thesis of
4 SFV under the guidance of CN and PN.

5

1 **References**

- 2 Adler, R. F., Huffman, G. J., Chang, A., Ferraro, R., Xie, P.-P., Janowiak, J., Rudolf, B.,
3 Schneider, U., Curtis, S., Bolvin, D., Gruber, A., Susskind, J., Arkin, P. and
4 Nelkin, E.: The Version-2 Global Precipitation Climatology Project (GPCP)
5 Monthly Precipitation Analysis (1979–Present), *J. Hydrometeorol.*, 4(6), 1147–
6 1167, doi:10.1175/1525-7541(2003)004<1147:TVGPCP>2.0.CO;2, 2003.
- 7 Anthes, R. A.: A Cumulus Parameterization Scheme Utilizing a One-Dimensional
8 Cloud Model, *Mon. Weather Rev.*, 105(3), 270–286, doi:10.1175/1520-
9 0493(1977)105<0270:ACPSUA>2.0.CO;2, 1977.
- 10 [Ahn, M. S., Kim, D., Sperber, K. R., Kang, I. S., Maloney, E., Waliser, D. and Hendon,](#)
11 [H.: MJO simulation in CMIP5 climate models: MJO skill metrics and process-](#)
12 [oriented diagnosis, *Clim. Dyn.*, 49\(11–12\), 4023–4045, doi:10.1007/s00382-](#)
13 [017-3558-4, 2017.](#)
- 14 Arakawa, A. and Schubert, W. H.: Interaction of a Cumulus Cloud Ensemble with the
15 Large-Scale Environment, Part I, *J. Atmos. Sci.*, 31(3), 674–701,
16 doi:10.1175/1520-0469(1974)031<0674:IOACCE>2.0.CO;2, 1974.
- 17 [Bentsen, M., Bethke, I., Debernard, J. B., Iversen, T., Kirkevåg, A., Seland, Ø., Drange,](#)
18 [H., Roelandt, C., Seierstad, I. A., Hoose, C. and Kristjánsson, J. E.: The](#)
19 [Norwegian Earth System Model, *NorESM1-M – Part 1: Description and basic*](#)
20 [evaluation of the physical climate, *Geosci. Model Dev.*, 6\(3\), 687–720,](#)
21 [doi:10.5194/gmd-6-687-2013, 2013.](#)
- 22 Bottino, M. J., and Nobre, P.: Impacts of cloud cover schemes on the Atlantic climate in
23 the Brazilian Earth System Model – BESM-OA2.3. (Submitted to *Climate*
24 *Dynamics*).
- 25 Buckley, M. W. and Marshall, J.: Observations, inferences, and mechanisms of the
26 Atlantic Meridional Overturning Circulation: A review, *Rev. Geophys.*, 54, 5–
27 63, doi:10.1002/2015RG000493.Received, 2015.

1 Cao, J., Wang, B., Yang, Y.-M., Ma, L., Li, J., Sun, B., Bao, Y., He, J., Zhou, X. and
2 Wu, L.: The NUIST Earth System Model (NESM) version3: description and
3 preliminary evaluation, Geosci. Model Dev., 11(7), 2975–2993,
4 doi:10.5194/gmd-11-2975-2018, 2018.

5
6 Capistrano, V. B., Nobre, P., Tedeschi, R., Silva, J., Bottino, M., da Silva Jr., M. B.,
7 Menezes Neto, O. L., Figueroa, S. N., Bonatti, J. P., Kubota, P. Y., Reyes
8 Fernandez, J. P., Giarolla, E., Vial, J., and Nobre, C. A.: Overview of climate
9 change in the BESM-OA2.5 climate model, Geosci. Model Dev. Discuss.,
10 <https://doi.org/10.5194/gmd-2018-209>, in review, 2018.

11 ~~Capistrano, V., Nobre, P., Tedeschi, R., Silva, J., Bottino, M., Baptista Jr., M., Menezes~~
12 ~~Neto, O., Figueroa, S. N., Bonatti, J.P., Kubota, P., Fernandez J., Giarolla, E.,~~
13 ~~Vial, J., Nobre, C. A.: Overview of climate change in the BESM-OA2.5 climate~~
14 ~~model. (Submitted to Journal of Climate).~~

15 Carvalho, L. M. V, Jones, C. and Liebmann, B.: The South Atlantic convergence zone:
16 Intensity, form, persistence, and relationships with intraseasonal to interannual
17 activity and extreme rainfall, J. Clim., 17(1), 88–108, doi:10.1175/1520-
18 0442(2004)017<0088:TSACZI>2.0.CO;2, 2004.

19 Chang, P., Ki, L. and Li, H.: A decadal climate variation in the tropical Atlantic Ocean
20 from thermodynamic air-sea interactions, Nature, 385(6), 516–518,
21 1997.

22 Charlton-Perez, A. J., Baldwin, M. P., Birner, T., Black, R. X., Butler, A. H., Calvo, N.,
23 Davis, N. A., Gerber, E. P., Gillett, N., Hardiman, S., Kim, J., Krüger, K., Lee,
24 Y. Y., Manzini, E., McDaniel, B. A., Polvani, L., Reichler, T., Shaw, T. A.,
25 Sigmond, M., Son, S. W., Toohey, M., Wilcox, L., Yoden, S., Christiansen, B.,
26 Lott, F., Shindell, D., Yukimoto, S. and Watanabe, S.: On the lack of
27 stratospheric dynamical variability in low-top versions of the CMIP5 models, J.
28 Geophys. Res. Atmos., 118(6), 2494–2505, doi:10.1002/jgrd.50125, 2013.

29

- 1 Chaves, R. R. and Nobre, P.: Interactions between sea surface temperature over the
2 South Atlantic Ocean and the South Atlantic Convergence Zone, *Geophys. Res.
3 Lett.*, 31(3), 1–4, doi:10.1029/2003GL018647, 2004.
- 4 Cheng, W., Chiang, J. C. H. and Zhang, D.: Atlantic meridional overturning circulation
5 (AMOC) in CMIP5 Models: RCP and historical simulations, *J. Clim.*, 26(18),
6 7187–7197, doi:10.1175/JCLI-D-12-00496.1, 2013.
- 7 Chiang, J. C. H. and Vimont, D. J.: Analogous Pacific and Atlantic Meridional Modes
8 of Tropical Atmosphere – Ocean Variability, *J. Clim.*, 17, 4143–4158,
9 doi:10.1175/JCLI4953.1, 2004.
- 10 Chou, M.-D. and Suarez, M. J.: A solar radiation parameterization (CLIRAD-SW) for
11 atmospheric studies. NASA Tech. Memo NASA/TM-1999-104606, 40 pp.,
12 1999.
- 13 Chou, S. C., Lyra, A., Mourão, C., Dereczynski, C., Pilotto, I., Gomes, J., Bustamante,
14 J., Tavares, P., Silva, A., Rodrigues, D., Campos, D., Chagas, D., Sueiro, G.,
15 Siqueira, G., Nobre, P. and Marengo, J.: Evaluation of the Eta Simulations
16 Nested in Three Global Climate Models, *Am. J. Clim. Chang.*, 3(5), 438–454,
17 doi:10.4236/ajcc.2014.35039, 2014.
- 18
- 19 Compo, G. P., Whitaker, J. S., Sardeshmukh, P. D., Matsui, N., Allan, R. J., Yin, X.,
20 Gleason, B. E., Vose, R. S., Rutledge, G., Bessemoulin, P., BroNnimann, S.,
21 Brunet, M., Crouthamel, R. I., Grant, A. N., Groisman, P. Y., Jones, P. D., Kruk,
22 M. C., Kruger, A. C., Marshall, G. J., Maugeri, M., Mok, H. Y., Nordli, O.,
23 Ross, T. F., Trigo, R. M., Wang, X. L., Woodruff, S. D. and Worley, S. J.: The
24 Twentieth Century Reanalysis Project, *Q. J. R. Meteorol. Soc.*, 137(654), 1–28,
25 doi:10.1002/qj.776, 2011.
- 26 Delworth, T. L. and Mann, M. E.: Observed and simulated multidecadal variability in
27 the Northern Hemisphere, *Clim. Dyn.*, 16(9), 661–676,
28 doi:10.1007/s003820000075, 2000.

- 1 Delworth, T. L., Zeng, F., Vecchi, G. A., Yang, X., Zhang, L. and Zhang, R.: The North
2 Atlantic Oscillation as a driver of rapid climate change in the Northern
3 Hemisphere, *Nat. Geosci.*, 9(7), 509–512, doi:10.1038/ngeo2738, 2016.
- 4 Dijkstra, H. A.: The ENSO phenomenon: theory and mechanisms, *Adv. Geosci.*, 6, 3–
5 15, doi:10.5194/adgeo-6-3-2006, 2006.
- 6 Enfield, D. B., Mestas-Nuñez, A. M. and Trimble, P. J.: The Atlantic multidecadal
7 oscillation and its relation to rainfall and river flows in the continental U.S.,
8 *Geophys. Res. Lett.*, 28(10), 2077–2080, doi:10.1029/2000GL012745, 2001.
- 9 Ferrier, B. S., Jin, Y., Lin, Y., Black, T., Rogers, E. and DiMego, G.: Implementation of
10 a 527 new grid-scale cloud and precipitation scheme in the NCEP Eta model.
11 *Amer. Meteor. Soc.*, 280–283, 2002.
- 12 Figueroa, S. N., Bonatti, J. P., Kubota, P. Y., Grell, G. A., Morrison, H., Barros, S. R.
13 M., Fernandez, J. P. R., Ramirez, E., Capistrano, V. B., Alvim, D. S., Enoré, D.
14 P., Diniz, F. L. R., Barbosa, H. M. J., Mendes, C. L. and Panetta, J.: The
15 Brazilian Global Atmospheric Model (BAM): Performance for Tropical Rainfall
16 Forecasting and Sensitivity to Convective Scheme and Horizontal Resolution,
17 *Weather Forecast.*, 31(5), 1547–1572, doi:10.1175/WAF-D-16-0062.1, 2016.
- 18 Flato, G. M.: Earth system models: An overview, *Wiley Interdiscip. Rev. Clim. Chang.*,
19 2(6), 783–800, doi:10.1002/wcc.148, 2011.
- 20 Flato, G., J. Marotzke, B. Abiodun, P. Braconnot, S.C. Chou, W. Collins, P. Cox, F.
21 Driouech, S. Emori, V. Eyring, C. Forest, P. Gleckler, E. Guilyardi, C. Jakob, V.
22 Kattsov, C. Reason and M. Rummukainen, 2013: Evaluation of Climate Models.
23 In: *Climate Change 2013: The Physical Science Basis. Contribution of Working*
24 *Group I to the Fifth Assessment Report of the Intergovernmental Panel on*
25 *Climate Change* [Stocker, T.F., D. Qin, G.-K. Plattner, M. Tignor, S.K. Allen, J.
26 Boschung, A. Nauels, Y. Xia, V. Bex and P.M. Midgley (eds.)]. Cambridge
27 University Press, Cambridge, United Kingdom and New York, NY, USA.
- 28 [Gent, P. R., Danabasoglu, G., Donner, L. J., Holland, M. M., Hunke, E. C., Jayne, S. R.,](#)

- 1 [Lawrence, D. M., Neale, R. B., Rasch, P. J., Vertenstein, M., Worley, P. H.,](#)
2 [Yang, Z.-L., Zhang, M.: The Community Climate System Model Version 4, J.](#)
3 [Clim., 24\(19\), 4973–4991, doi:10.1175/2011JCLI4083.1, 2011.](#)
- 4 ~~Ghil, M. and Mo, K.: Intraseasonal Oscillations in the Global Atmosphere. Part I:~~
5 ~~Northern Hemisphere and Tropics, J. Atmos. Sci., 48(5), 752–779,~~
6 ~~doi:10.1175/1520-0469(1991)048<0752:IOITGA>2.0.CO;2, 1991.~~
- 7 Giarolla, E., Siqueira, L. S. P., Bottino, M. J., Malagutti, M., Capistrano, V. B. and
8 Nobre, P.: Equatorial Atlantic Ocean dynamics in a coupled ocean atmosphere
9 model simulation, *Ocean Dyn.*, 65(6), 831–843, doi:10.1007/s10236-015-0836-
10 8, 2015.
- 11 Gong, D. and Wang, S.: Definition of Antarctic Oscillation Index, *Geophys. Res. Lett.*,
12 26(4), 459–462, doi:10.1029/1999GL900003, 1999. Grell, G. and Dévényi, D.
13 A.: A generalized approach to parameterizing convection combining ensemble
14 and data assimilation techniques, *Geophys. Res. Lett.*, 29(14), 10–13,
15 doi:10.1029/2002GL015311, 2002.
- 16 Griffies, S. M.: Elements of MOM4p1. NOAA/Geophysical Fluid Dynamics Laboratory
17 Ocean Group Tech. Rep. 6, 444 pp., 2009.
- 18 Grimm, A. M.: The El Niño impact on the summer monsoon in Brazil: Regional
19 processes versus remote influences, *J. Clim.*, 16(2), 263–280, doi:10.1175/1520-
20 0442(2003)016<0263:TENIOT>2.0.CO;2, 2003.
- 21 Harshvardhan, Davies, R., Randall, D. A. and Corsetti, T. G.: A fast radiation
22 parameterization for atmospheric circulation models, *J. Geophys. Res.*, 92(D1),
23 1009–1016, doi:10.1029/JD092iD01p01009, 1987.
- 24 Hu, Z. Z. and Huang, B.: Interferential impact of ENSO and PDO on dry and wet
25 conditions in the U.S. great plains, *J. Clim.*, 22(22), 6047–6065,
26 doi:10.1175/2009JCLI2798.1, 2009.
- 27 Huang, B., Banzon, V. F., Freeman, E., Lawrimore, J., Liu, W., Peterson, T. C., Smith,

- 1 T. M., Thorne, P. W., Woodruff, S. D. and Zhang, H. M.: Extended
2 reconstructed sea surface temperature version 4 (ERSST.v4). Part I: Upgrades
3 and intercomparisons, *J. Clim.*, 28(3), 911–930, doi:10.1175/JCLI-D-14-
4 00006.1, 2015.
- 5 Huffman, G. J., Adler, R. F., Bolvin, D. T. and Gu, G.: Improving the global
6 precipitation record: GPCP Version 2.1, *Geophys. Res. Lett.*, 36(17), L17808,
7 doi:10.1029/2009GL040000, 2009.
- 8 Hurrell, J. W. and Deser, C.: North Atlantic climate variability: The role of the North
9 Atlantic Oscillation, *J. Mar. Syst.*, 78(1), 28–41,
10 doi:10.1016/j.jmarsys.2008.11.026, 2009.
- 11 Hurrell, J. W., Kushnir, Y., Otterson, G. and Visbeck, M.: An Overview of the North
12 Atlantic Oscillation, *North Atl. Oscil. Clim. Significance Environ. Impact*, 134,
13 263, doi:10.1029/GM134, 2003.
- 14 Hwang, Y.-T. and Frierson, D. M. W.: Link between the double-Intertropical
15 Convergence Zone problem and cloud biases over the Southern Ocean., *Proc.*
16 *Natl. Acad. Sci. U. S. A.*, 110(13), 4935–40, doi:10.1073/pnas.1213302110,
17 2013.
- 18 Ji, D., Wang, L., Feng, J., Wu, Q., Cheng, H., Zhang, Q., Yang, J., Dong, W., Dai, Y.,
19 Gong, D., Zhang, R. H., Wang, X., Liu, J., Moore, J. C., Chen, D. and Zhou, M.:
20 Description and basic evaluation of Beijing Normal University Earth System
21 Model (BNU-ESM) version 1, *Geosci. Model Dev.*, 7(5), 2039–2064,
22 doi:10.5194/gmd-7-2039-2014, 2014.
- 23
- 24 Jiménez, P. A., Dudhia, J., González-Rouco, J. F., Navarro, J., Montávez, J. P. and
25 García-Bustamante, E.: A Revised Scheme for the WRF Surface Layer
26 Formulation, *Mon. Weather Rev.*, 140(3), 898–918, doi:10.1175/MWR-D-11-
27 00056.1, 2012.

28

- 1 Jones, C. and Carvalho, L. M. V: Active and break phases in the South American
2 monsoon system, *J. Clim.*, 15(8), 905–914, doi:10.1175/1520-
3 0442(2002)015<0905:AABPIT>2.0.CO;2, 2002.
- 4 Karoly, D. J.: Southern Hemisphere Circulation Features Associated with El-Nino-
5 Southern Oscillation Events, *J. Clim.*, 2, 1239–1252, doi: 10.1175/1520-
6 0442(1989)002<1239:SHCFAW>2.0.CO;2., 1989.
- 7 Kidson, J. W.: Interannual Variations in the Southern Hemisphere Circulation, *J. Clim.*,
8 1(12), 939–953, doi:10.1175/1520-0442(1988)001<1177:IVITSH>2.0.CO;2,
9 1988.
- 10 [Kim, D., Sperber, K., Stern, W., Waliser, D., Kang, I. S., Maloney, E., Wang, W.,
11 Weickmann, K., Benedict, J., Khairoutdinov, M., Lee, M. I., Neale, R., Suarez,
12 M., Thayer-Calder, K. and Zhang, G.: Application of MJO simulation
13 diagnostics to climate models, *J. Clim.*, 22\(23\), 6413–6436,
14 doi:10.1175/2009JCLI3063.1, 2009.](#)
- 15 Krishnamurthy, L. and Krishnamurthy, V.: Indian monsoon' s relation with the decadal
16 part of PDO in observations and NCAR CCSM4, *Int. J. Climatol.*,
17 doi:10.1002/joc.4815, 2016.
- 18 Large, W. G. and Yeager, S. G.: The global climatology of an interannually varying air
19 - Sea flux data set, *Clim. Dyn.*, 33(2–3), 341–364, doi:10.1007/s00382-008-
20 0441-3, 2009.
- 21 Leathers, D. J., Yarnal, B., Palecki, M. A., Leathers, D. J., Yarnal, B. and Palecki, M.
22 A.: The Pacific/North American Teleconnection Pattern and United States
23 Climate. Part I: Regional Temperature and Precipitation Associations, *J. Clim.*,
24 4(5), 517–528, doi:10.1175/1520-0442(1991)004<0517:TPATPA>2.0.CO;2,
25 1991.
- 26 Levitus, S.: Climatological Atlas of the World Ocean. NOAA Prof. Paper 13, 173 pp.
27 and 17 microfich, 1982.

- 1 Li, G. and Xie, S. P.: Tropical biases in CMIP5 multimodel ensemble: The excessive
2 equatorial pacific cold tongue and double ITCZ problems, *J. Clim.*, 27(4), 1765–
3 1780, doi:10.1175/JCLI-D-13-00337.1, 2014.
- 4 [Liebmann, B., Hendon, H. H. and Glick, J. D.: The Relationship Between Tropical](#)
5 [Cyclones of the Western Pacific and Indian Oceans and the Madden-Julian](#)
6 [Oscillation, *J. Meteorol. Soc. Japan. Ser. II*, 72\(3\), 401–412,](#)
7 [doi:10.2151/jmsj1965.72.3_401, 1994.](#)
- 8 [Lin, H., Brunet, G. and Derome, J.: An observed connection between the North Atlantic](#)
9 [oscillation and the Madden-Julian oscillation, *J. Clim.*, 22\(2\), 364–380,](#)
10 [doi:10.1175/2008JCLI2515.1, 2009.](#)
- 11 Lu, R., Dong, B. and Ding, H.: Impact of the Atlantic Multidecadal Oscillation on the
12 Asian summer monsoon, *Geophys. Res. Lett.*, 33, L24701, doi(24), 101029/
13 doi:10.1029/2006GL027655, 2006.
- 14 Lumpkin, R. and Speer, K.: Global Ocean Meridional Overturning, *J. Phys. Oceanogr.*,
15 37(10), 2550–2562, doi:10.1175/JPO3130.1, 2007.
- 16 Lutz, K., Jacobeit, J. and Rathmann, J.: Atlantic warm and cold water events and impact
17 on African west coast precipitation, *Int. J. Climatol.*, 35(1), 128–141,
18 doi:10.1002/joc.3969, 2015.
- 19 [Madden, R. A. and Julian, P. R.: Detection of a 40–50 Day Oscillation in the Zonal](#)
20 [Wind in the Tropical Pacific, *J. Atmos. Sci.*, 28\(5\), 702–708, doi:10.1175/1520-](#)
21 [0469\(1971\)028<0702:DOADOI>2.0.CO;2, 1971.](#)
- 22 [Madden, R. A. and Julian, P. R.: Description of Global-Scale Circulation Cells in the](#)
23 [Tropics with a 40–50 Day Period, *J. Atmos. Sci.*, 29\(6\), 1109–1123,](#)
24 [doi:10.1175/1520-0469\(1972\)029<1109:DOGSCC>2.0.CO;2, 1972.](#)
- 25 Mantua, N. J., Hare, S. R., Zhang, Y., Wallace, J. M. and Francis, R. C.: A Pacific
26 Interdecadal Climate Oscillation with Impacts on Salmon Production, *Bull. Am.*
27 *Meteorol. Soc.*, 78(6), 1069–1079, doi:10.1175/1520-

- 1 0477(1997)078<1069:APICOW>2.0.CO;2, 1997.
- 2 Marengo, J. A., Calvalcanti, I. F. A., Satyamurty, P., Trosnikov, I., Nobre, C. A.,
3 Bonatti, J. P., Camargo, H., Sampaio, G., Sanches, M. B., Manzi, A. O., Castro,
4 C. A. C., D’Almeida, C., Pezzi, L. P. and Candido, L.: Assessment of regional
5 seasonal rainfall predictability using the CPTEC/COLA atmospheric GCM,
6 *Clim. Dyn.*, 21(5–6), 459–475, doi:10.1007/s00382-003-0346-0, 2003.
- 7 McCarthy, G. D., Smeed, D. A., Johns, W. E., Frajka-Williams, E., Moat, B. I., Rayner,
8 D., Baringer, M. O., Meinen, C. S., Collins, J. and Bryden, H. L.: Measuring the
9 Atlantic Meridional Overturning Circulation at 26°N, *Prog. Oceanogr.*, 130, 91–
10 111, doi:10.1016/j.pocean.2014.10.006, 2015.
- 11 McPhaden, M. J., Zebiak, S. E. and Glantz, M. H.: ENSO as an integrating concept in
12 earth science, *Science*, 314(5806), 1740–1745, doi:10.1126/science.1132588,
13 2006.
- 14 Meehl, G. A., Moss, R., Taylor, K. E., Eyring, V., Stouffer, R. J., Bony, S. and Stevens,
15 B.: Climate model intercomparisons: Preparing for the next phase, *Eos*, 95(9),
16 77–78, doi:10.1002/2014EO090001, 2014.
- 17 Mellor, G. L. and Yamada, T.: Development of a turbulence closure model for
18 geophysical fluid problems, *Rev. Geophys.*, 20(4), 851–875,
19 doi:10.1029/RG020i004p00851, 1982.
- 20 Mo, K. C. and Peagle, J. N.: The Pacific-South American modes and their downstream
21 effects, *Int. J. Climatol.*, 21(10), 1211–1229, doi:10.1002/joc.685, 2001.
- 22 Morice, C. P., Kennedy, J. J., Rayner, N. A. and Jones, P. D.: Quantifying uncertainties
23 in global and regional temperature change using an ensemble of observational
24 estimates: The HadCRUT4 data set, *J. Geophys. Res. Atmos.*, 117(8), 1–22,
25 doi:10.1029/2011JD017187, 2012.
- 26 Newman, M., Alexander, M. A., Ault, T. R., Cobb, K. M., Deser, C., Di Lorenzo, E.,
27 Mantua, N. J., Miller, A. J., Minobe, S., Nakamura, H., Schneider, N., Vimont,

- 1 D. J., Phillips, A. S., Scott, J. D. and Smith, C. A.: The Pacific decadal
2 oscillation, revisited, *J. Clim.*, 29(12), 4399–4427, doi:10.1175/JCLI-D-15-
3 0508.1, 2016.
- 4 Ning, L. and Bradley, R. S.: NAO and PNA influences on winter temperature and
5 precipitation over the eastern United States in CMIP5 GCMs, *Clim. Dyn.*, 46(3–
6 4), 1257–1276, doi:10.1007/s00382-015-2643-9, 2016.
- 7 Nobre, P., Shukla, J.: Variation of Sea surface Temperature, Wind Stress, and Rainfall
8 over the Tropical Atlantic and South America, *J. Clim.*, 9, 2464–2479,
9 doi:http://dx.doi.org/10.1175/1520-0442(1996)009<2464:VOSSTW>2.0.CO;2,
10 1996.
- 11 Nobre, P., Marengo, J. A., Cavalcanti, I. F. A., Obregon, G., Barros, V., Camilloni, I.,
12 Campos, N. and Ferreira, A. G.: Seasonal-to-decadal predictability and
13 prediction of South American climate, *J. Clim.*, 19(23), 5988–6004,
14 doi:10.1175/JCLI3946.1, 2006.
- 15 Nobre, P., De Almeida, R. A., Malagutti, M. and Giarolla, E.: Coupled ocean-
16 atmosphere variations over the South Atlantic Ocean, *J. Clim.*, 25(18), 6349–
17 6358, doi:10.1175/JCLI-D-11-00444.1, 2012.
- 18 Nobre, P., Siqueira, L. S. P., De Almeida, R. A. F., Malagutti, M., Giarolla, E., Castelã
19 O, G. P., Bottino, M. J., Kubota, P., Figueroa, S. N., Costa, M. C., Baptista, M.,
20 Irber, L. and Marcondes, G. G.: Climate simulation and change in the brazilian
21 climate model, *J. Clim.*, 26(17), 6716–6732, doi:10.1175/JCLI-D-12-00580.1,
22 2013.
- 23 Nogués-Paegle, J. and Mo, K. C.: Alternating Wet and Dry Conditions over South
24 America during Summer, *Mon. Weather Rev.*, 125, 279–291, doi:10.1175/1520-
25 0493(1997)125<0279:AWADCO>2.0.CO;2, 1997.
- 26 Obukhov, A. M.: Turbulence in an atmosphere with a non-uniform temperature,
27 *Boundary-Layer Meteorol.*, 2(1), 7–29, doi:10.1007/BF00718085, 1971.

- 1 de Oliveira Vieira, S., Satyamurty, P. and Andreoli, R. V.: On the South Atlantic
2 Convergence Zone affecting southern Amazonia in austral summer, *Atmos. Sci.*
3 *Lett.*, 14(1), 1–6, doi:10.1002/asl2.401, 2013.
- 4 Palmer, T. N., Doblas-Reyes, F. J., Weisheimer, A. and Rodwell, M. J.: Toward
5 seamless prediction: Calibration of climate change projections using seasonal
6 forecasts, *Bull. Am. Meteorol. Soc.*, 89(4), 459–470, doi:10.1175/BAMS-89-4-
7 459, 2008.
- 8 Richter, I.: Climate model biases in the eastern tropical oceans: Causes, impacts and
9 ways forward, *Wiley Interdiscip. Rev. Clim. Chang.*, 6(3), 345–358,
10 doi:10.1002/wcc.338, 2015.
- 11 Richter, I., Xie, S. P., Behera, S. K., Doi, T. and Masumoto, Y.: Equatorial Atlantic
12 variability and its relation to mean state biases in CMIP5, *Clim. Dyn.*, 42(1–2),
13 171–188, doi:10.1007/s00382-012-1624-5, 2014.
- 14 Robertson, A. and Mechoso, C.: Interannual and interdecadal variability of the South
15 Atlantic Convergence Zone, *Mon. Weather Rev.*, 128(8), 2947–2957,
16 doi:10.1175/1520-0493(2000)128<2947:IAIVOT>2.0.CO;2, 2000.
- 17 Rogers, J. C. and van Loon, H.: Spatial Variability of Sea Level Pressure and 500 mb
18 Height Anomalies over the Southern Hemisphere, *Mon. Weather Rev.*, 110(10),
19 1375–1392, doi:10.1175/1520-0493(1982)110<1375:SVOSLP>2.0.CO;2, 1982.
- 20 Rossow, W. B. and Schiffer, R. a: Advances in Understanding Clouds from ISCCP,
21 *Bull. Amer. Meteor. Soc.*, 80(11), 2261–2287, doi:10.1175/1520-
22 0477(1999)080<2261:AIUCFI>2.0.CO;2, 1999.
- 23 von Storch, H.: Climate models and modeling: an editorial essay, *Wiley Interdiscip.*
24 *Rev. Clim. Chang.*, 1(3), 305–310, doi:10.1002/wcc.12, 2010.
- 25 Straus, D. M. and Shukla, J.: Does ENSO force the PNA?, *J. Clim.*, 15(17), 2340–2358,
26 doi:10.1175/1520-0442(2002)015<2340:DEFTP>2.0.CO;2, 2002.
- 27 Sutton, R. T. and Hodson, D. L. R.: Atlantic Ocean Forcing of North American and

- 1 European Summer Climate, Science, 309(5731), 115–118,
2 doi:10.1126/science.1109496, 2005.
- 3 Swapna, P., Krishnan, R., Sandeep, N., Prajeesh, A. G., Ayantika, D. C., Manmeet, S.
4 and Vellore, R.: Long-Term Climate Simulations Using the IITM Earth System
5 Model (IITM-ESMv2) With Focus on the South Asian Monsoon, J. Adv. Model.
6 Earth Syst., 10(5), 1127–1149, doi:10.1029/2017MS001262, 2018.
- 7 Takayabu, Y. N., Iguchi, T., Kachi, M., Shibata, A. and Kanzawa, H.: Abrupt
8 termination of the 1997-98 El Nino in response to a Madden-Julian oscillation,
9 Nature, 402(6759), 279–282, doi:10.1038/46254, 1999.
- 10 Tarasova, T. A., Barbosa, H. M. J. and Figueroa, S. N.: In- corporation of new solar
11 radiation scheme into CPTECGCM. Instituto Nacional de Pesquisas Espaciais
12 Tech. Rep. INPE- 14052-NTE/371, 44 pp. [Available online at [http://mtc-m15.](http://mtc-m15.sid.inpe.br/col/sid.inpe.br/iris%401915/2006/01.16.10.40/doc/publicacao.pdf)
13 [sid.inpe.br/col/sid.inpe.br/iris%401915/2006/01.16.10.40/doc/publicacao.pdf](http://mtc-m15.sid.inpe.br/col/sid.inpe.br/iris%401915/2006/01.16.10.40/doc/publicacao.pdf),
14 2006.
- 15 Tian, B.: Spread of model climate sensitivity linked to double-Intertropical
16 Convergence Zone bias, Geophys. Res. Lett., 42(10), 4133–4141,
17 doi:10.1002/2015GL064119, 2015.
- 18 Tian, B., Fetzer, E. J., Kahn, B. H., Teixeira, J., Manning, E. and Hearty, T.: Evaluating
19 CMIP5 models using AIRS tropospheric air temperature and specific humidity
20 climatology, J. Geophys. Res. Atmos., 118(1), 114–134,
21 doi:10.1029/2012JD018607, 2013.
- 22 Tiedtke, M.: The sensitivity of the time-mean large-scale flow to cumulus convection in
23 the ECMWF model. Proc. Work-shop on Convection in Large-Scale Models,
24 Reading, United Kingdom, ECMWF, 297–316, 1983.
- 25
- 26 Waliser, D., Sperber, K., Hendon, H., Kim, D., Maloney, E., Wheeler, M., Weickmann,
27 K., Zhang, C., Donner, L., Gottschalck, J., Higgins, W., Kang, I. S., Legler, D.,
28 Moncrieff, M., Schubert, S., Stern, W., Vitart, F., Wang, B., Wang, W. and

- 1 | [Woolnough, S.: MJO simulation diagnostics, *J. Clim.*, 22\(11\), 3006–3030,](#)
2 | [doi:10.1175/2008JCLI2731.1, 2009.](#)
- 3 | Wallace, J. M. and Gutzler, D. S.: Teleconnections in the Geopotential Height Field
4 | during the Northern Hemisphere Winter, *Mon. Weather Rev.*, 109(4), 784–812,
5 | doi:10.1175/1520-0493(1981)109<0784:TITGHF>2.0.CO;2, 1981.
- 6 | Wang, C., Zhang, L. and Lee, S.: A global perspective on CMIP5 climate model biases,
7 | *Nat. Clim. Chang.*, 4(3), 201–205, doi:10.1038/NCLIMATE2118, 2014.
- 8 | Wanner, H., Brönnimann, S., Casty, C., Luterbacher, J., Schmutz, C. and David, B.:
9 | North Atlantic Oscillation – Concepts and Studies, *Surv. Geophys.*, 22(1984),
10 | 321–382, doi:10.1023/A:1014217317898, 2001.
- 11 | Weaver, A. J., Sedláček, J., Eby, M., Alexander, K., Crespin, E., Fichefet, T.,
12 | Philippon-Berthier, G., Joos, F., Kawamiy, M., Matsumoto, K., Steinacher, M.,
13 | Tachiiri, K., Tokos, K., Yoshimori, M. and Zickfeld, K.: Stability of the Atlantic
14 | meridional overturning circulation: A model intercomparison, *Geophys. Res.*
15 | *Lett.*, 39(20), 1–7, doi:10.1029/2012GL053763, 2012.
- 16 | Winton, M.: A reformulated three-layer sea ice model, *J. Atmos. Ocean. Technol.*,
17 | 17(4), 525–531, doi:10.1175/1520-0426(2000)017<0525:ARTLSI>2.0.CO;2,
18 | 2000.
- 19 | Wu, X. and Mao, J.: Interdecadal variability of early summer monsoon rainfall over
20 | South China in association with the Pacific Decadal Oscillation, *Int. J. Climatol.*,
21 | doi:10.1002/joc.4734, 2016.
- 22 | Wu, Z., Li, J., Jiang, Z., He, J. and Zhu, X.: Possible effects of the North Atlantic
23 | Oscillation on the strengthening relationship between the East Asian Summer
24 | monsoon and ENSO, *Int. J. Climatol.*, 32(5), 794–800, doi:10.1002/joc.2309,
25 | 2012.
- 26 | Xie, S.-P.: A Dynamic Ocean – Atmosphere Model of the Tropical Atlantic Decadal
27 | Variability, *J. Clim.*, 12(1), 64–71, 1999.

- 1 | Xie, S. -P. and Philander, S. G. H.: A coupled ocean-atmosphere model of relevance to
2 | the ITCZ in the eastern Pacific, *Tellus A*, 46(4), 340–350, doi:10.1034/j.1600-
3 | 0870.1994.t01-1-00001.x, 1994.
- 4 | [Xie, P., and P.A. Arkin, 1997: Global precipitation: A 17-year monthly analysis based
5 | on gauge observations, satellite estimates, and numerical model outputs. *Bull.*
6 | *Amer. Meteor. Soc.*, 78, 2539 - 2558.](#)
- 7 | Xue, Y., Sellers, P., Kinter, J. and Shukla, J.: A Simplified Biosphere Model for Global
8 | Climate Studies, *J. Clim.*, 4(3), 345–364, doi:10.1175/1520-
9 | 0442(1991)004<0345:ASBMFG>2.0.CO;2, 1991.
- 10 | Yu, B. and Zwiers, F. W.: The impact of combined ENSO and PDO on the PNA
11 | climate: A 1,000-year climate modeling study, *Clim. Dyn.*, 29(7–8), 837–851,
12 | doi:10.1007/s00382-007-0267-4, 2007.
- 13 | Yu, R. and Zhou, T.: Impacts of winter-NAO on March cooling trends over subtropical
14 | Eurasia continent in the recent half century, *Geophys. Res. Lett.*, 31(12), 3–6,
15 | doi:10.1029/2004GL019814, 2004.
- 16 | Yuan, X. and Yonekura, E.: Decadal variability in the Southern Hemisphere, *J.*
17 | *Geophys. Res.*, 116(D19), 1–12, doi:10.1029/2011JD015673, 2011.
- 18 | Zebiak, S. E.: Air–Sea Interaction in the Equatorial Atlantic Region, *J. Clim.*, 6(8),
19 | 1567–1586, doi:10.1175/1520-0442(1993)006<1567:AIITEA>2.0.CO;2, 1993.
- 20 | [Zhang, C.: Madden-Julian Oscillation, *Rev. Geophys.*, 43\(2\), 1–36,
21 | doi:10.1029/2004RG000158, 2005.](#)
- 22 | Zhang, L. and Wang, C.: Multidecadal North Atlantic sea surface temperature and
23 | Atlantic meridional overturning circulation variability in CMIP5 historical
24 | simulations, *J. Geophys. Res. Ocean.*, 118(10), 5772–5791,
25 | doi:10.1002/jgrc.20390, 2013.
- 26 | Zhang, L., Ma, H. and Wu, L.: Dynamics and mechanisms of decadal variability of the
27 | Pacific-South America mode over the 20th century, *Clim. Dyn.*, 46(11–12),

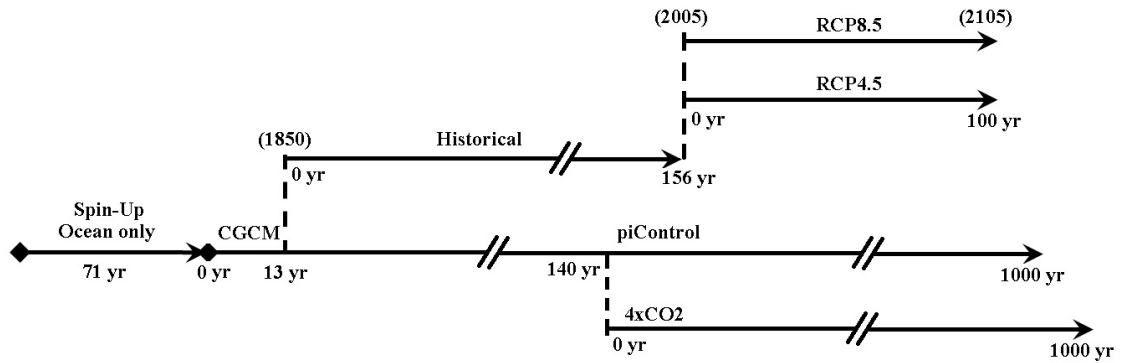
1 3657–3667, doi:10.1007/s00382-015-2794-8, 2016.

2 Zheng, F., Li, J., Clark, R. T. and Nnamchi, H. C.: Simulation and projection of the
3 Southern Hemisphere annular mode in CMIP5 models, *J. Clim.*, 26(24), 9860–
4 9879, doi:10.1175/JCLI-D-13-00204.1, 2013.

5

1 List of Figures

2



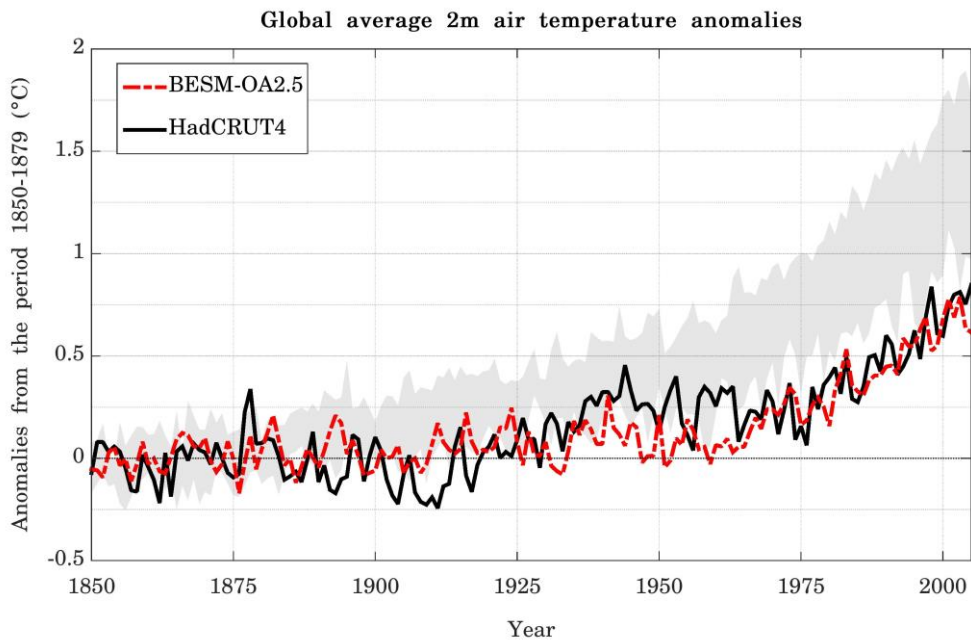
3

4 Figure 1 – The scheme of principal simulations carried out by BESM-OA2.5 using
5 different forcing conditions according to CMIP5 protocols. The date for the Historical
6 and RCPs simulations are from actual calendar years.

7

8

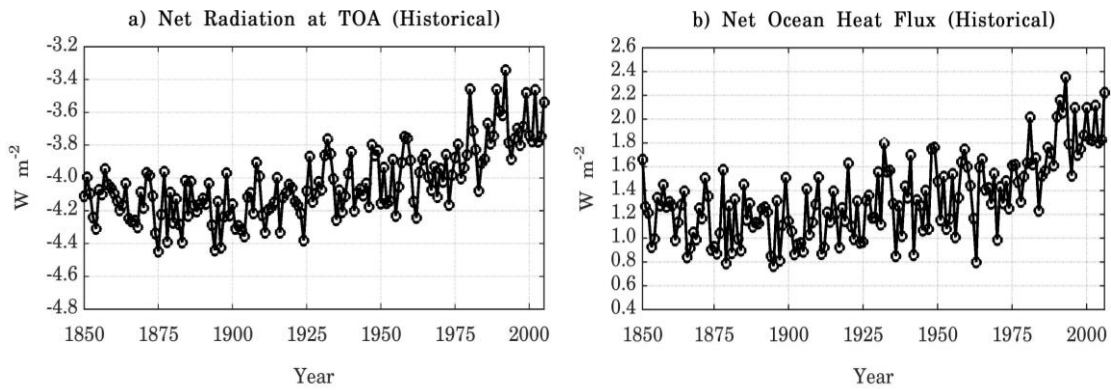
1



2

3 Figure 2 – Global averaged 2-m annual mean air temperature anomalies relative to the
4 period 1850–1879 for BESM-OA2.5 (dashed red line) and observation (solid black
5 line). The grey shadow represents the spread of 11 CMIP5 models (historical GHG
6 simulations). The CMIP5 models anomalies are also computed relative to the period
7 1850–1879, with exception of GFDL-ESM2M and HadGEM2-ES which anomalies are
8 computed relative to the periods 1861–1890 and 1860–1889, respectively. Units are in
9 °C.

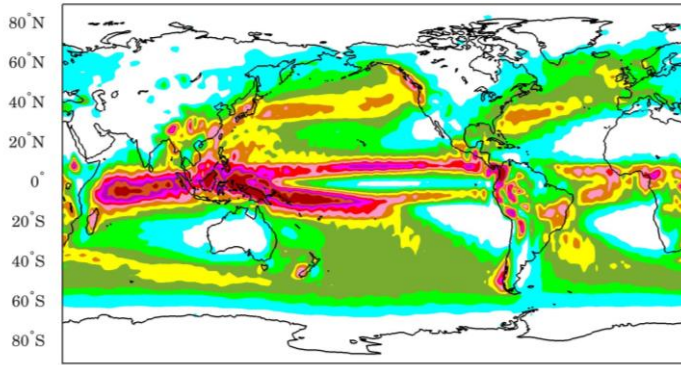
10



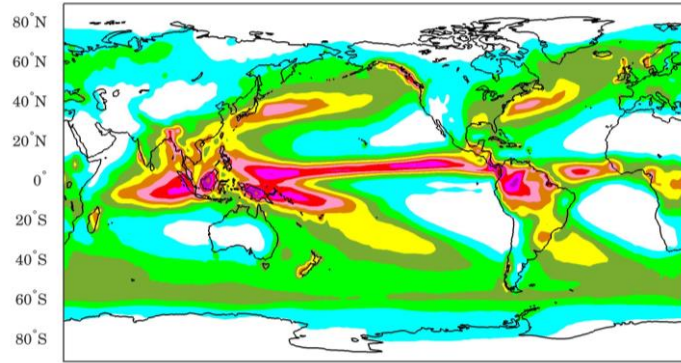
1
2 Figure 3 – Annual average time series for the global average (a) net of the radiation at
3 TOA (positive values indicates that the atmosphere is warming) and (b) net of the
4 ocean/atmosphere heat flux (positive values indicates that the ocean is warming),
5 simulated by the Historical run over the period 1850-2005 (156 years).

6
7

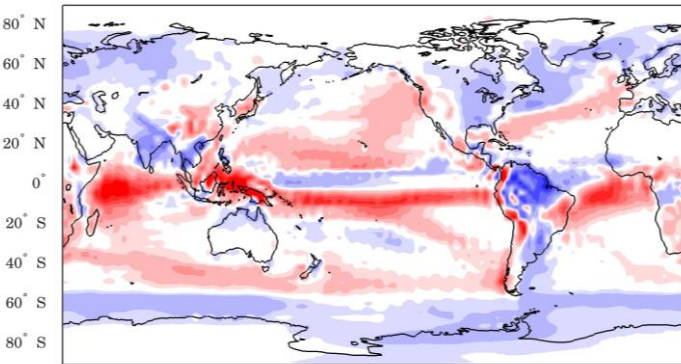
a) Annual mean precipitation (BESM-OA2.5)



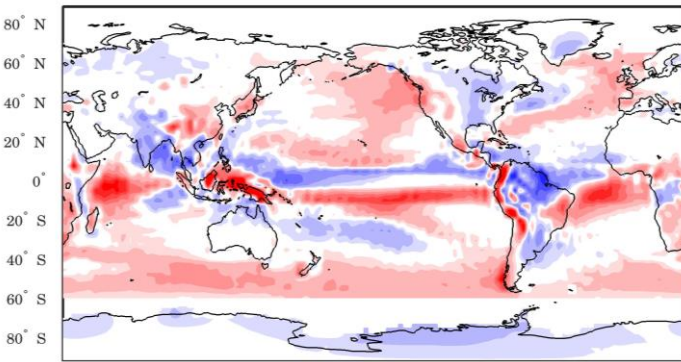
b) Annual mean precipitation (GPCP)



c) BESM-OA2.5 - GPCP mean: 0.3 mm/day rmse: 1.4 mm/day



d) BESM-OA2.5 - CMAP mean: 0.4 mm/day rmse: 1.5 mm/day



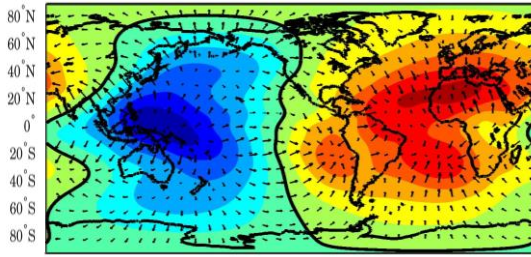
30°E 90°E 150°E 150°W 90°W 30°W 30°E

1 | Figure ~~43~~ – Spatial map of annual mean precipitation for (a) BESM-OA2.5, for (b)
2 | GPCP, (c) the bias of BESM-OA2.5 relative to GPCP and (d) the bias of BESM-OA2.5
3 | relative to CMAP. The averages values are computed over the periods 1971–2000 (for
4 | BESM-OA2.5) and 1979–2008; (for ~~BESM-OA2.5 and~~ GPCP and CMAP);
5 | ~~respectively~~. Units are in mm day⁻¹.

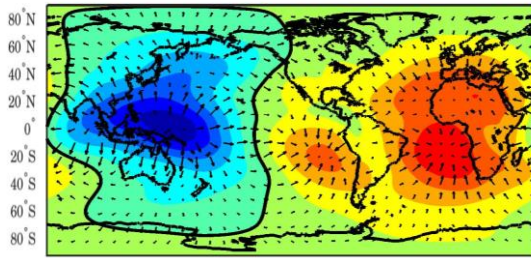
6 |

7 |

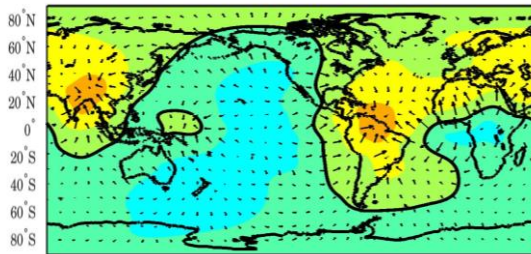
a) BESM-OA2.5 200 hPa Vel. Potential/Div. Wind



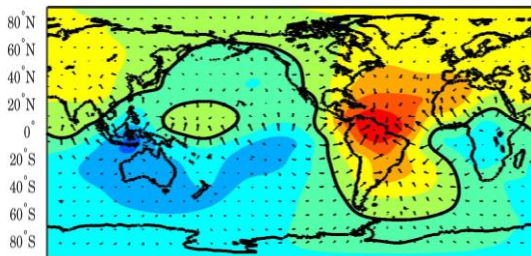
b) 20CRv2 200 hPa Vel. Potential/Div. Wind



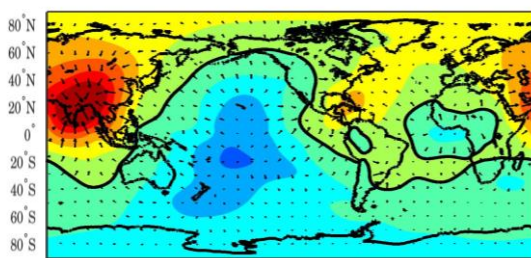
c) BESM-OA2.5 Bias 200 hPa Vel. Potential/Div. Wind



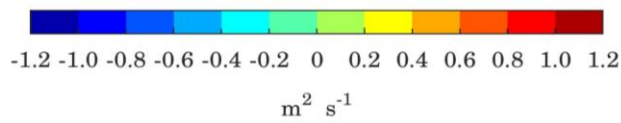
d) BESM-OA2.5 Bias 200 hPa Vel. Potential/Div. Wind MAM



e) BESM-OA2.5 Bias 200 hPa Vel. Potential/Div. Wind JJA



30°E 90°E 150°E 150°W 90°W 30°W 30°E



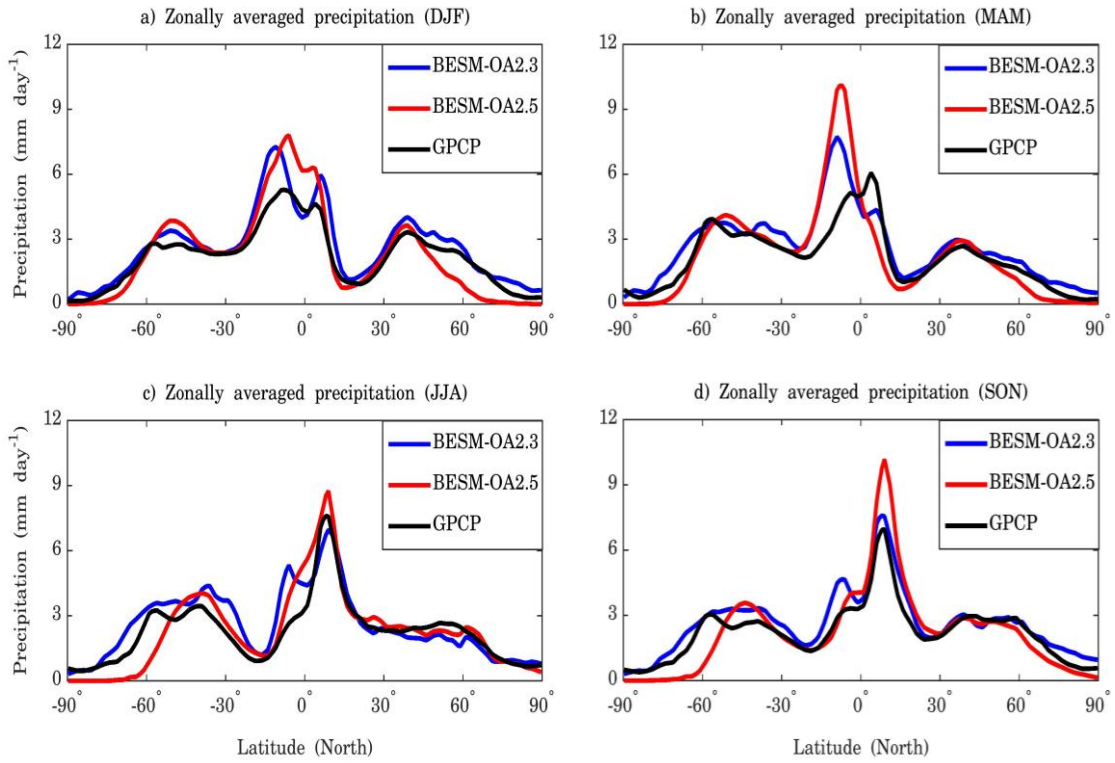
1

2 | Figure 54 – Spatial maps with averaged global anomalies of velocity potential and wind
3 | divergence at 200 hPa pressure level for (a) BESM-OA2.5 and (b) Reanalysis. (c) The
4 | bias of the model relative to the Reanalysis, (d) and (e) are the bias for MAM and JJA
5 | seasons, respectively. The averages are computed over the period 1950–2005. Units are
6 | in m s^{-1} .

7

1

2



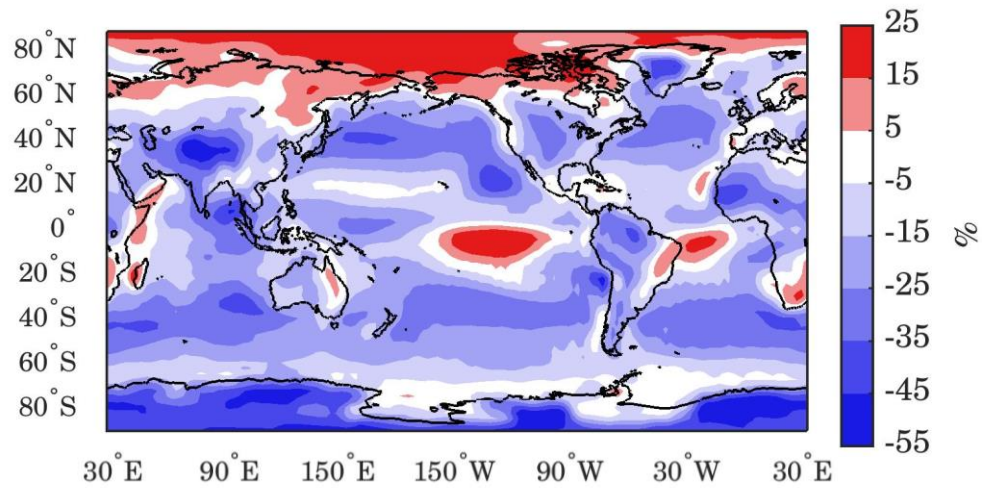
3

4 | Figure 65 – Zonally averaged annual mean precipitation for BESM-OA2.5, BESM-
5 | OA2.3 and GPCP dataset relative to the seasons DJF, MAM, JJA and SON. The zonally
6 | averages values are computed over the periods 1971–2000 and 1979–2008, for BESM-
7 | OA2.5 and GPCP, respectively. Units are in mm day⁻¹.

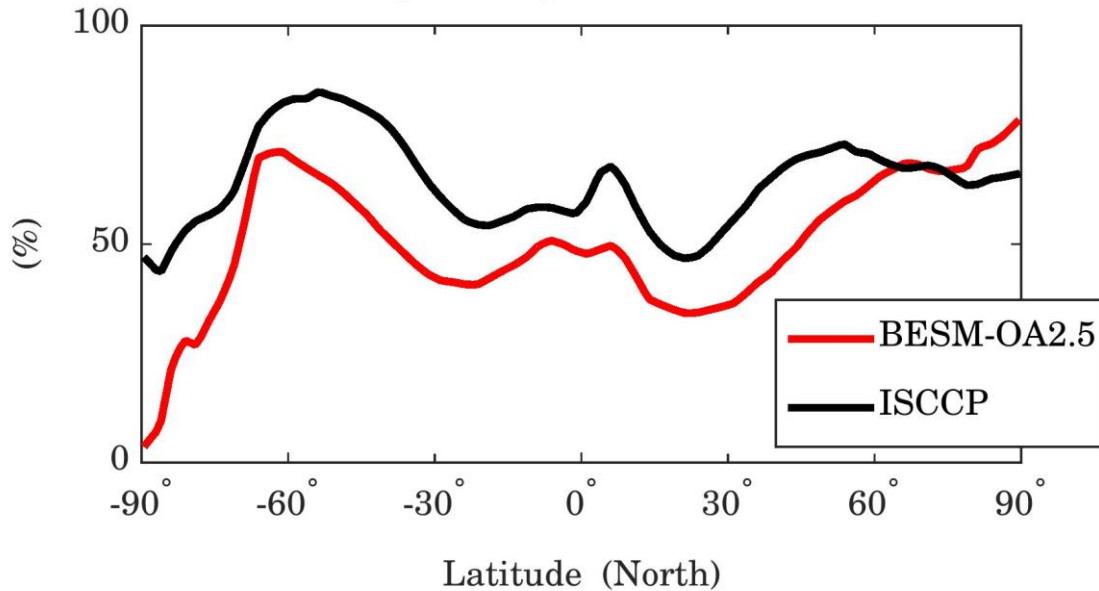
8

9

a) Total cloud fraction (BESM-OA2.5 - ISCCP)



b) Zonally averaged total cloud cover

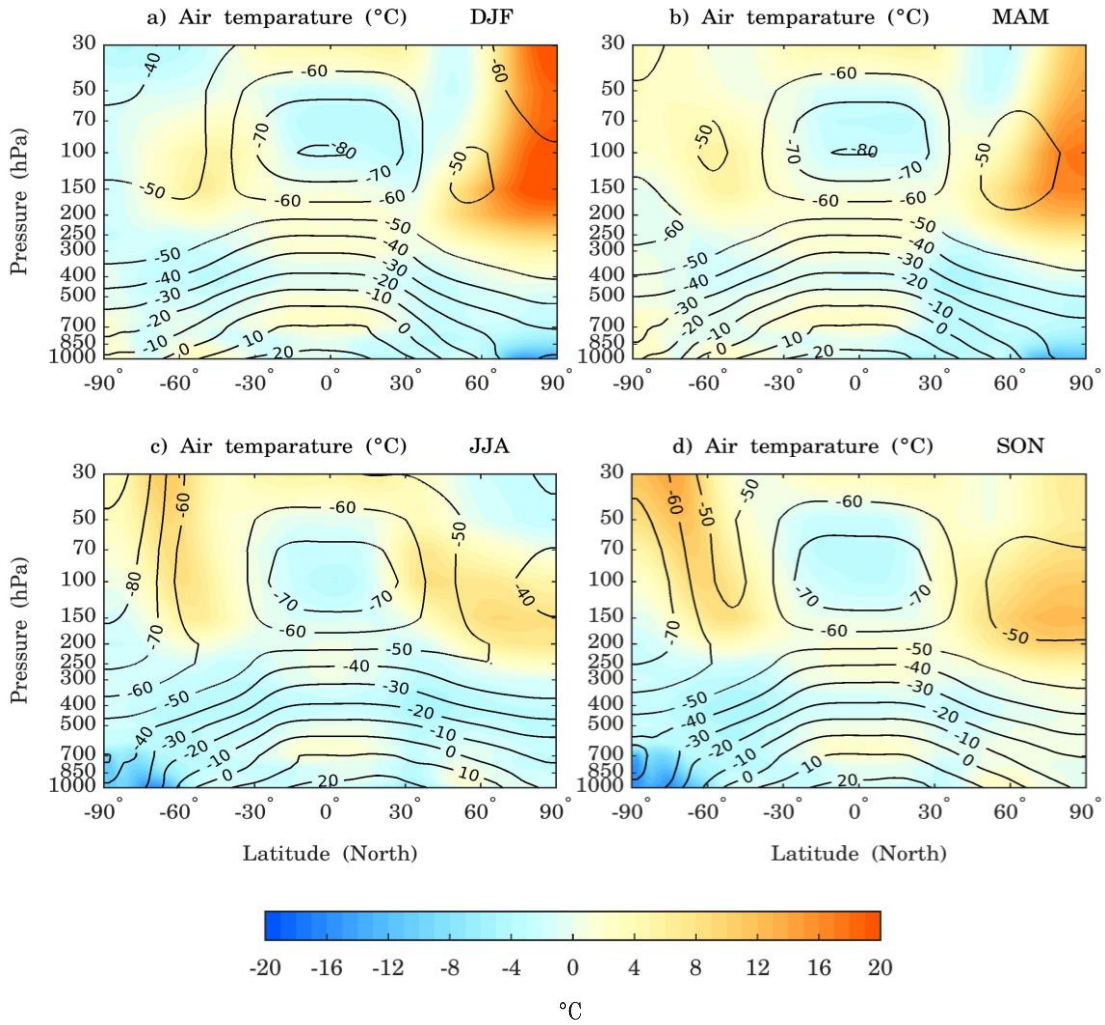


1

2 | Figure 76 – (a) Spatial map of annual mean total cloud fraction bias of BESM-OA2.5
 3 | relative to ISCCP. (b) Zonally averaged total cloud cover for BESM-OA2.5 and ISCCP
 4 | dataset. The periods used are 1971–2000 and 1984–2009 for BESM-OA2.5 and ISCCP,
 5 | respectively. Units are in percentage.

6 |

1



2

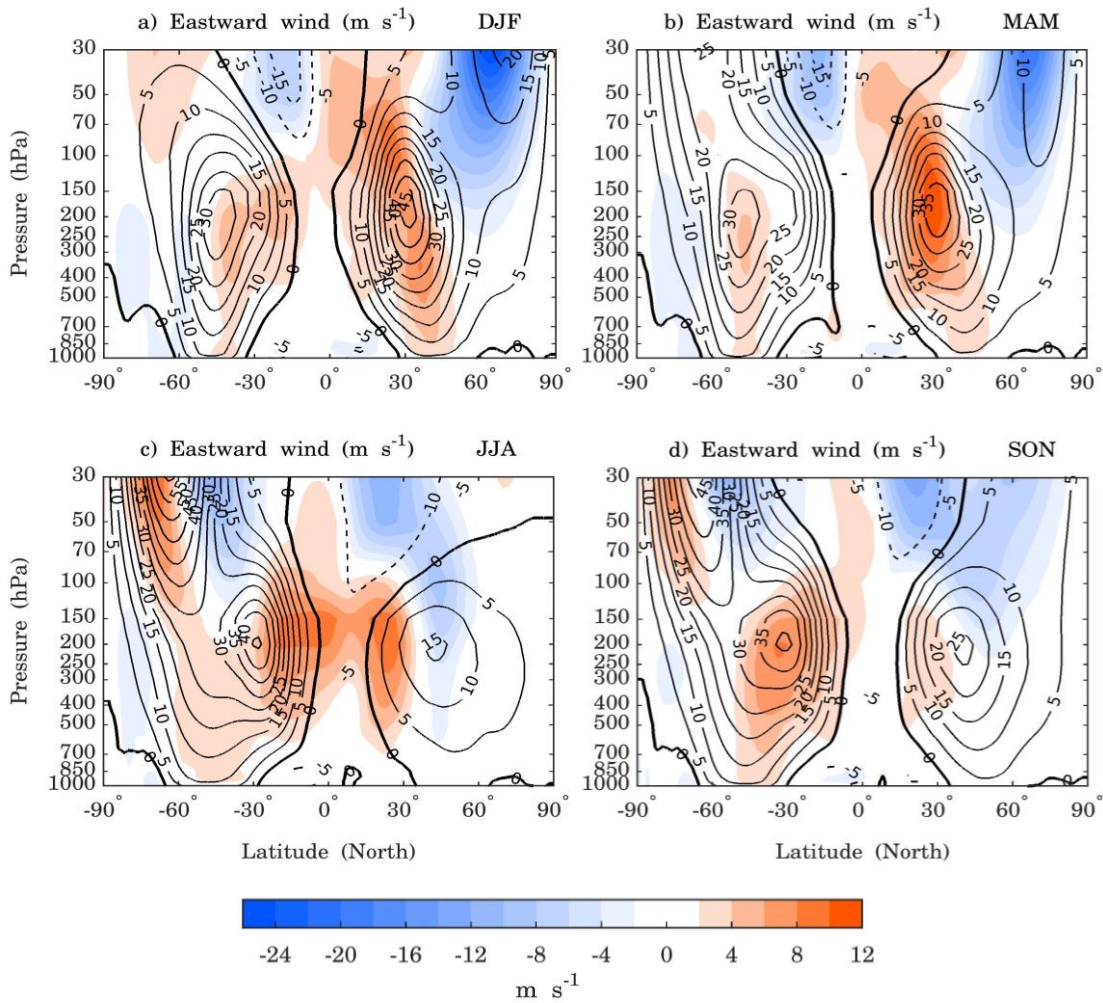
3

4 | Figure 87 – Contour lines are the zonally averaged vertical air temperature for BESM-
5 | OA2.5 and in shaded are the difference BESM-OA2.5 - 20CRv2 data set. Both are
6 | averaged over the period 1971–2000. The units are in °C and the contour interval is 10
7 | °C.

8

9

1



2

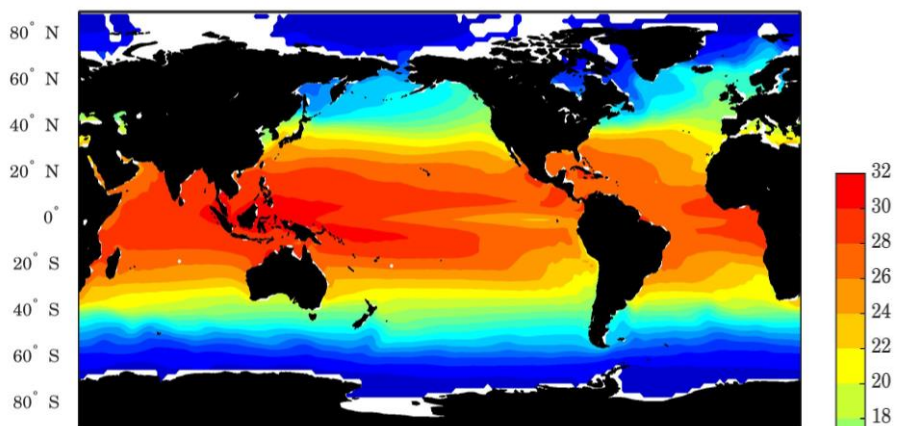
3

4 | Figure 98 – Contour lines are the zonally averaged zonal wind for BESM-OA2.5 and in
5 | shaded are the difference BESM-OA2.5 - 20CRv2 data set. Both are averaged over the
6 | period 1971–2000. The solid contour lines represent eastward zonal wind and the
7 | dashed contour lines represents westward zonal wind. The units are in meters per
8 | second and the Eastward contour interval is 5 m s^{-1} , with the contour line zero highlighted.

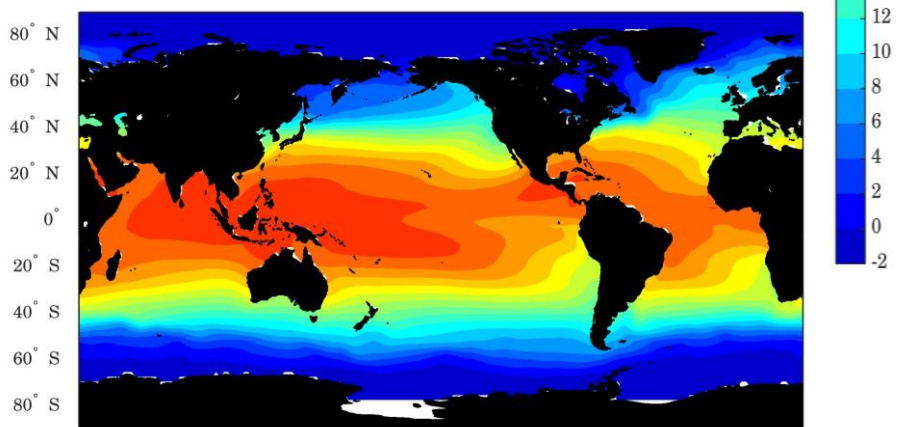
9

10

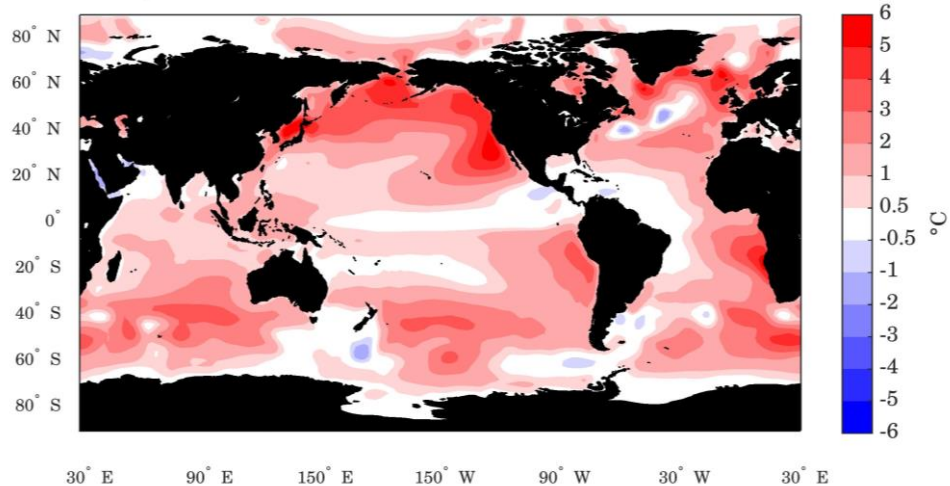
a) Annual mean SST (BESM-OA2.5)



b) Annual mean SST (ERSSTv4)



c) BESM-OA2.5 - ERSSTv4 mean: 1.5°C rmse: 1.9°C



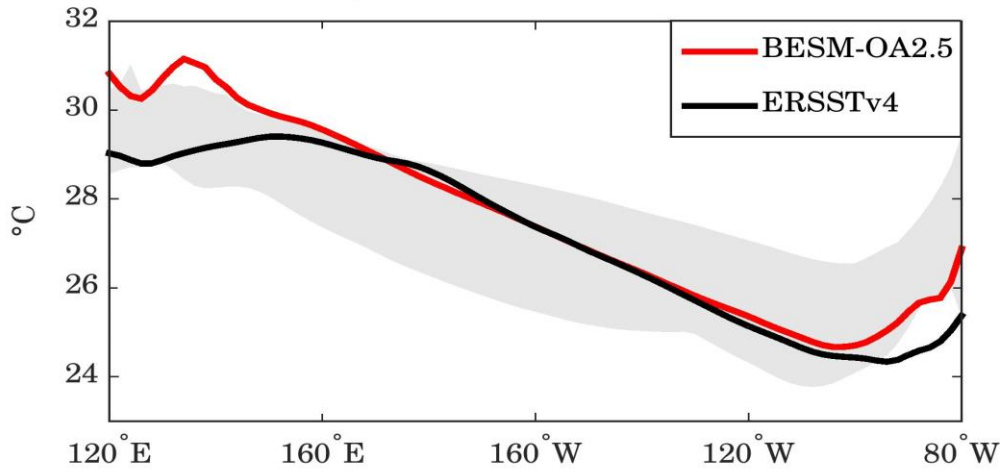
- 1
- 2
- 3

1 | Figure [109](#) – Spatial map of annual mean sea surface temperature [for \(a\) BESM-OA2.5,](#)
2 | [\(b\) ERSSTv4 and \(c\) the](#) bias of BESM-OA2.5 relative to ERSSTv4. The averages are
3 | computed over the period 1971–2000. Units are in °C.

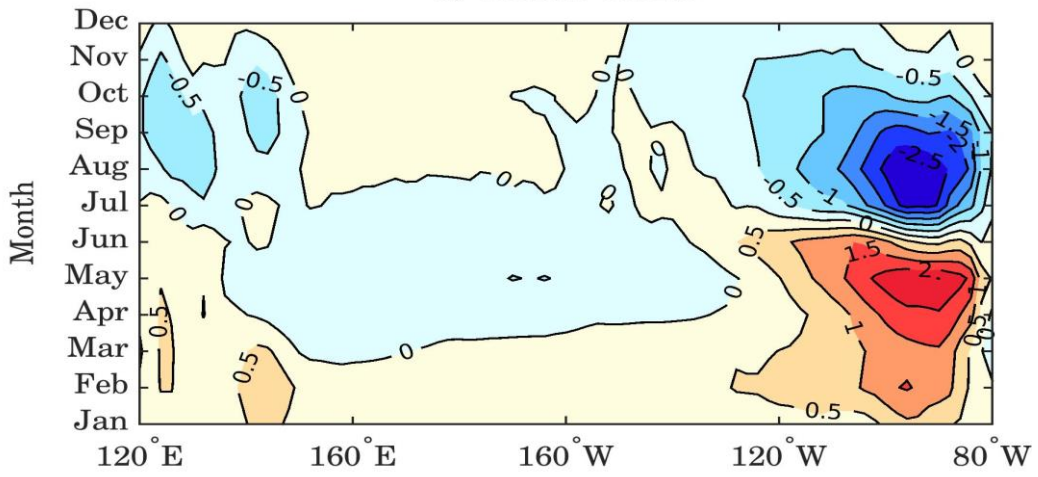
4

5 |

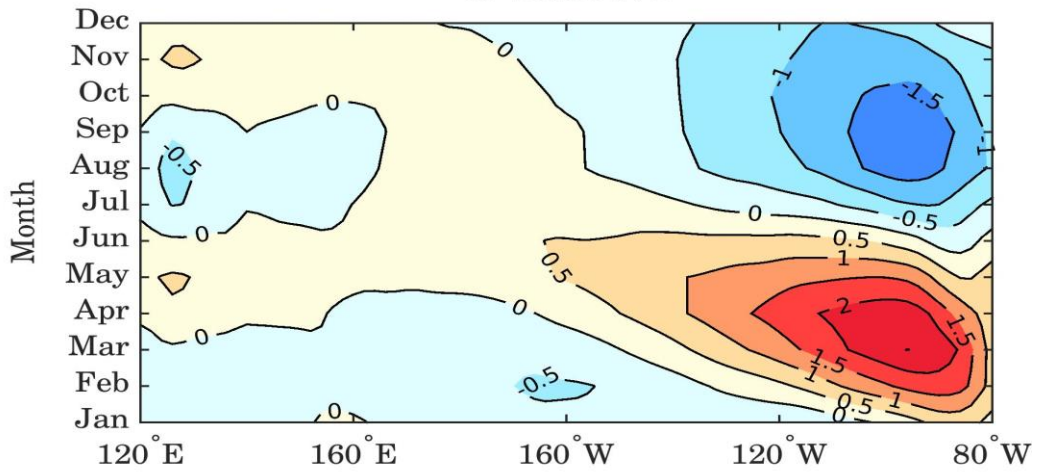
a) Equatorial Pacific Mean SST



b) BESM-OA2.5



c) ERSSTv4



1

2

1

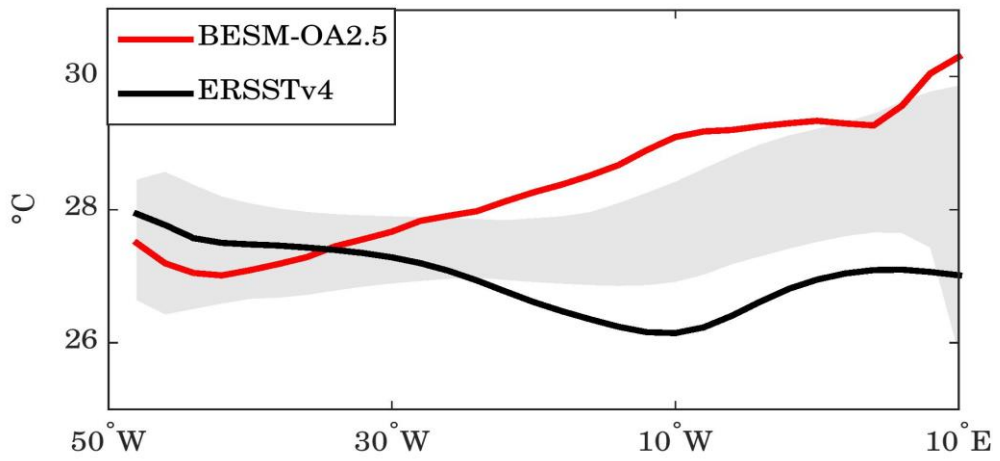
2 | Figure ~~11.10~~ – (a) Mean SST along the equator in the Pacific Ocean and annual cycle of
3 | the equatorial Pacific SST anomalies for (b) BESM-OA2.5 and (c) ERSSTv4.
4 | Equatorial region is defined by averaging over 2° S–2° N. BESM-OA2.5 and ERSSTv4
5 | are averaged over the period 1971–2000. In (a) the grey shadow represents the spread of
6 | 11 CMIP5 models, which are also averaged over the period 1971–2000. Units are in °C.

7

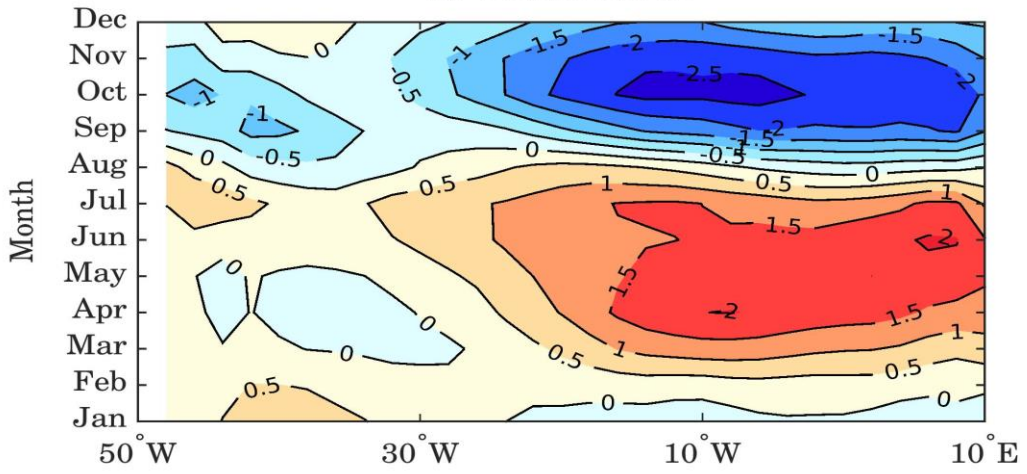
8

9

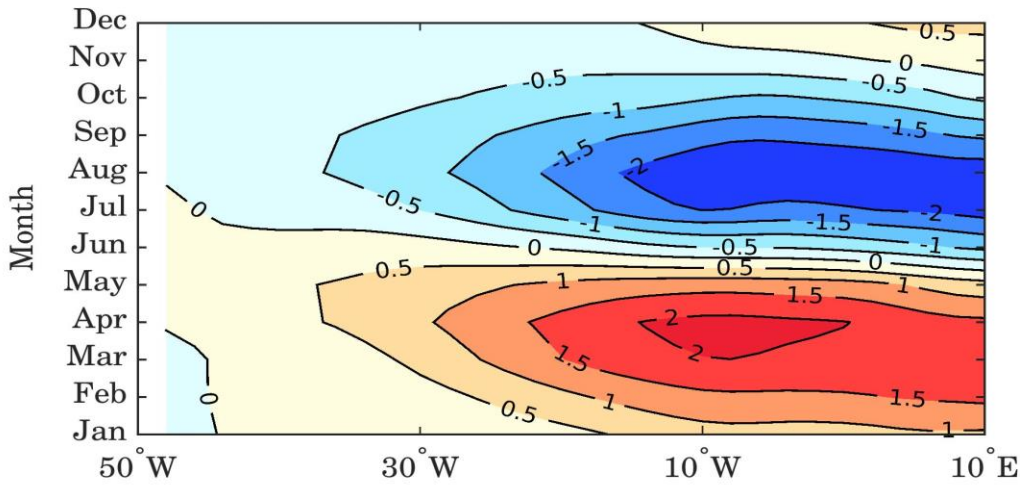
a) Equatorial Atlantic Mean SST



b) BESM-OA2.5



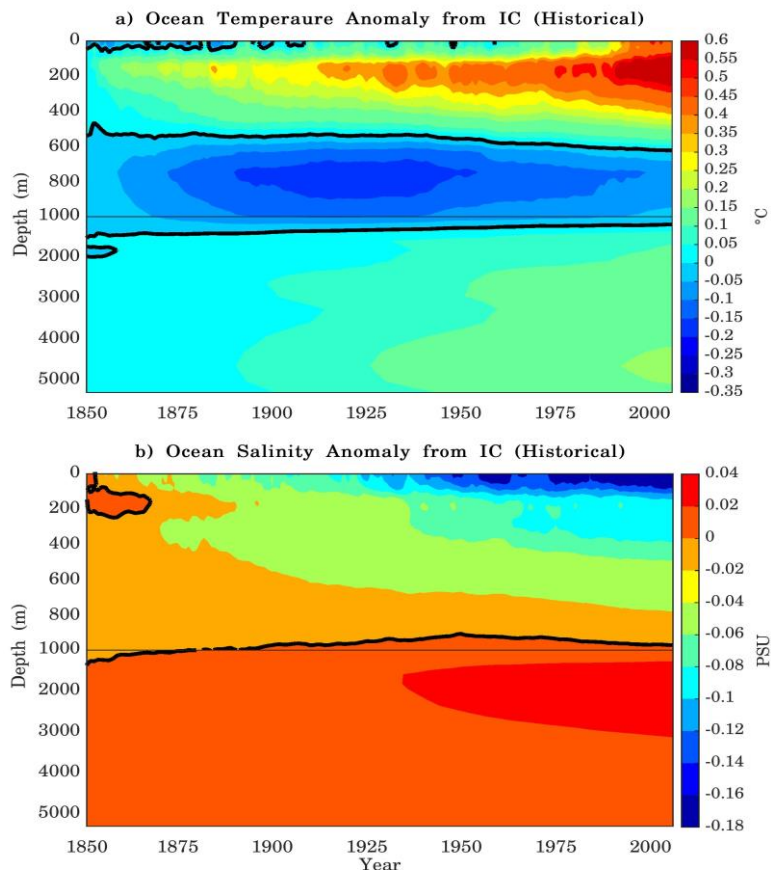
c) ERSSTv4



1

2

1 | Figure ~~1211~~ – As Fig. ~~1110~~ but for the Atlantic Ocean.

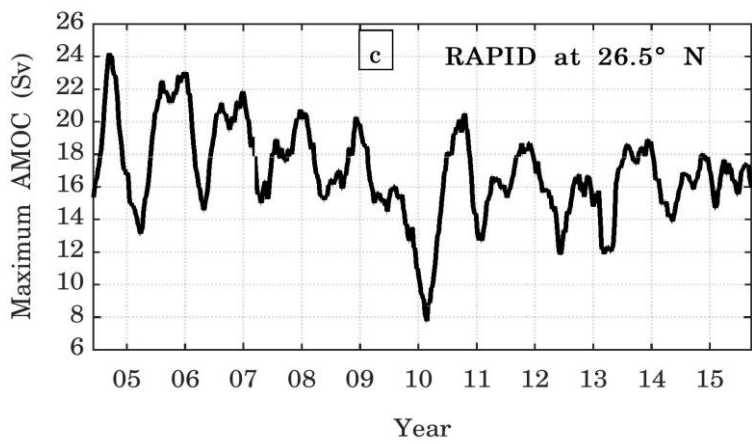
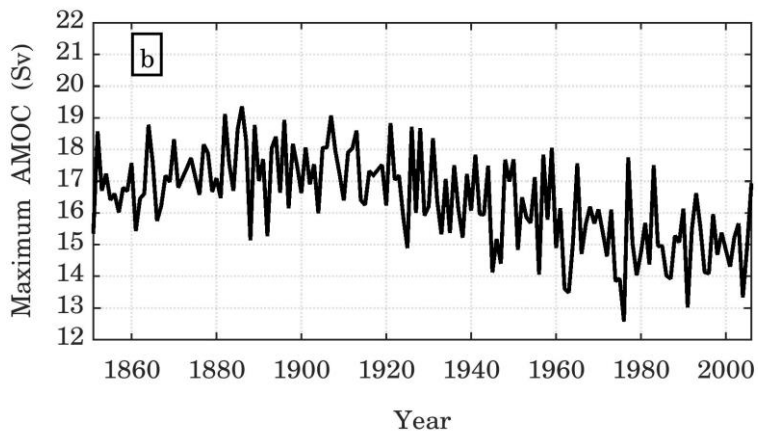
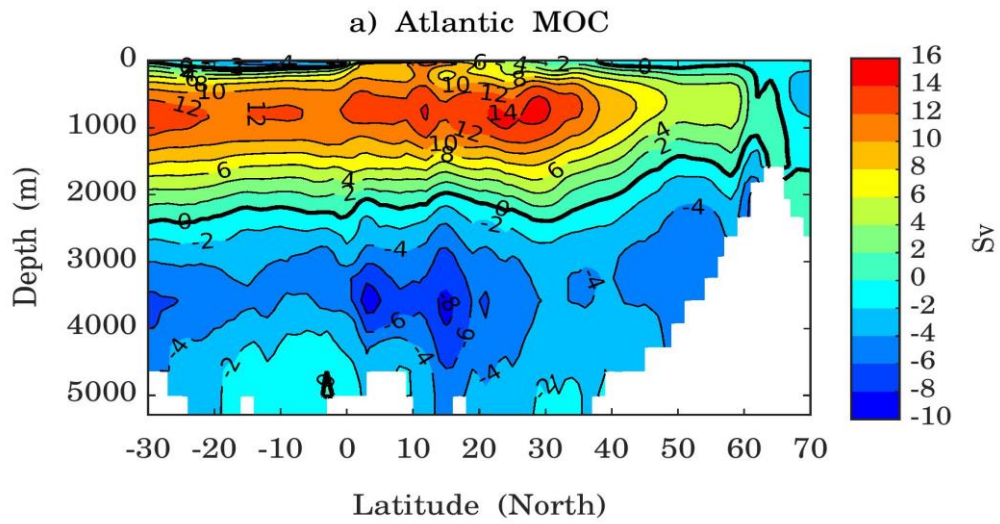


1

2 Figure 13 - Depth-time Hovmöller diagrams of global average ocean temperature and
 3 salinity anomalies from the respective initial conditions (IC). Here the initial conditions
 4 are taken from the 1th year. The diagrams are based on annual average time series
 5 simulated by the Historical simulation over the period 1850-2005 (156 years). The thick
 6 black line represents the zero contours. Note that the vertical scales are different above
 7 and below 1000 m.

8

9



1

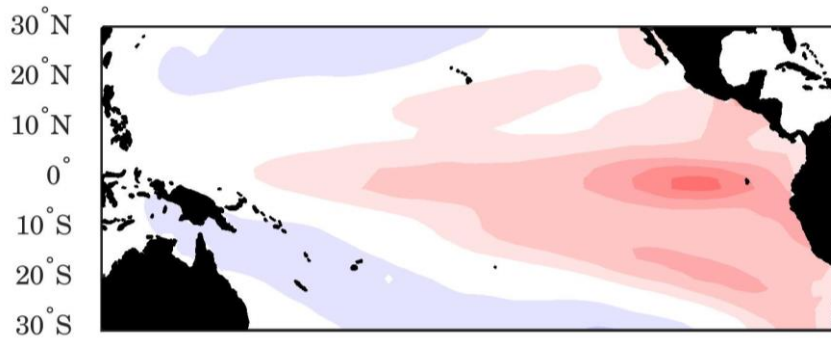
2

3

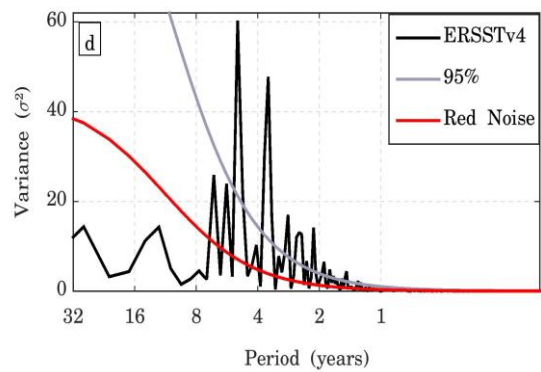
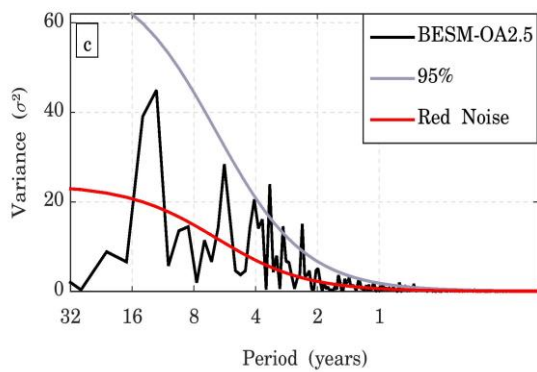
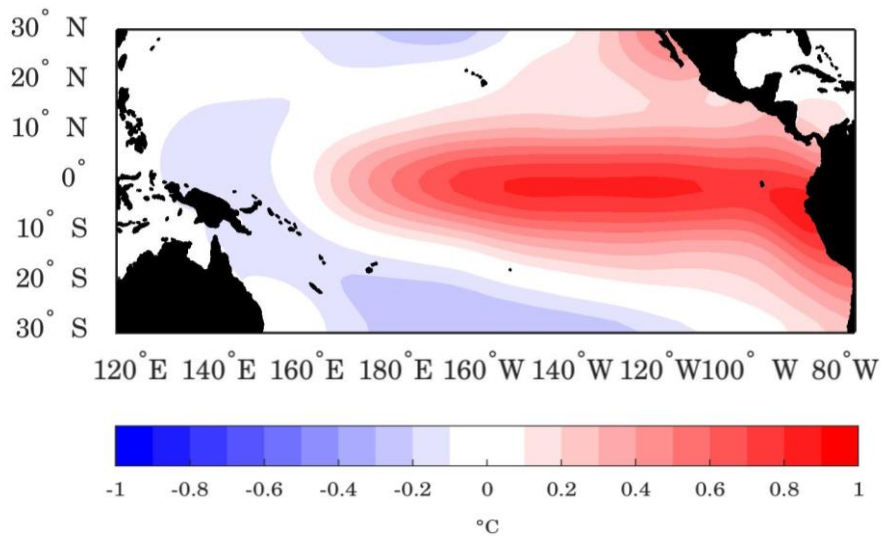
1 | Figure ~~1412~~ – (a) Atlantic Meridional Overturning Circulation averaged for the period
2 | 1971–2000 and (b) annual mean maximum AMOC strength time series at the latitude
3 | 30° N simulated by BESM-OA2.5 for historical simulation over the period 1850–2005.
4 | The smaller graph shows the AMOC time series measured by the project RAPID at
5 | 26.5° N over the period April/2004 to October/2015. The RAPID time series is
6 | smoothed by a 3-month running average. Units are in Sverdrup.

7 |

a) Pacific SST EOF1 (17.9%) BESM-OA2.5



b) Pacific SST EOF1 (45.0%) ERSSTv4

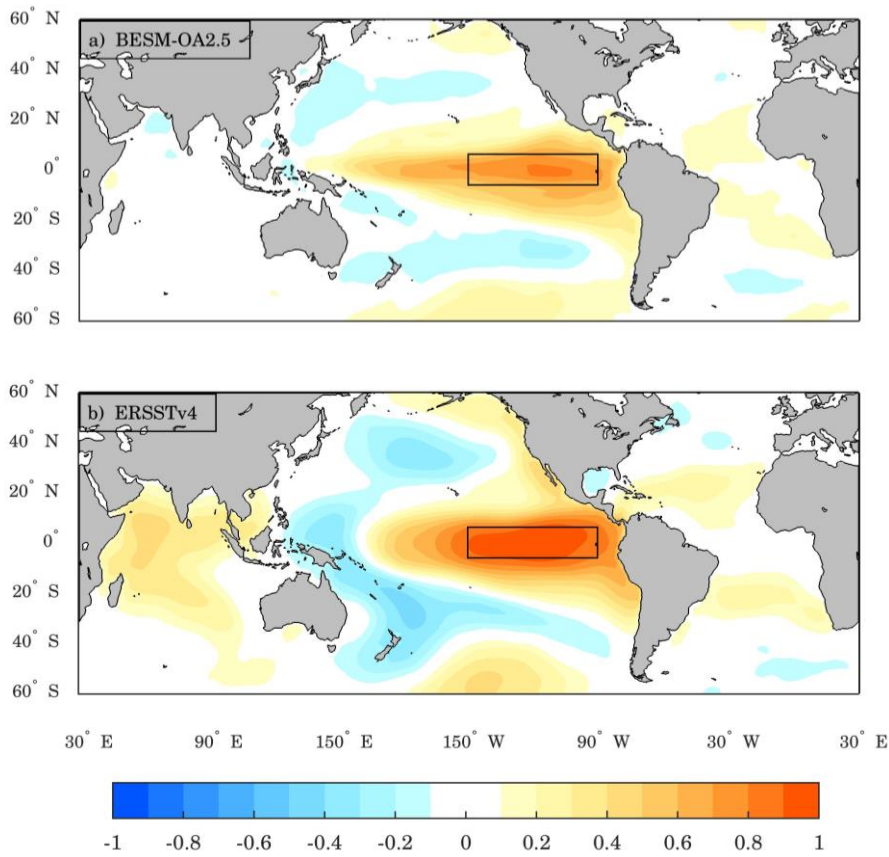


1 | Figure ~~15~~¹³ – The leading EOF modes of the detrended monthly SST anomalies over
2 | the Tropical Pacific region (30° S–30° N; 240°–70° W) for (a) BESM-OA2.5 and (b)
3 | ERSSTv4. The results are shown as the SST anomalies regressed onto the
4 | corresponding normalized PC time series (°C per standard deviation) over the period
5 | 1950–2005. The percentage of the variance explained by each EOF is indicated in the
6 | title of the figure. The contour interval is 0.1 °C. Figures (c) and (d) are the power
7 | spectrum of the leading joint PC time series of the pattern for BESM-OA2.5 and
8 | ERSSTv4, respectively. The solid red line represents the theoretical red noise spectrum
9 | and the gray line represents the 95 % confidence level.

10

11 |

1



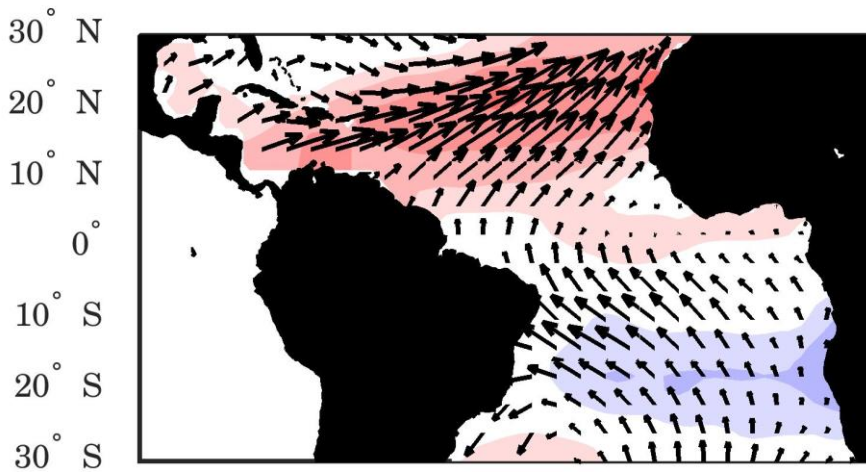
2

3

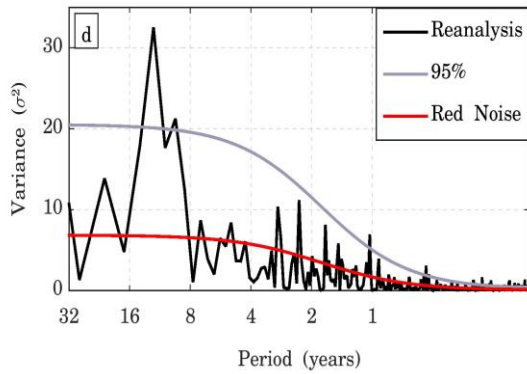
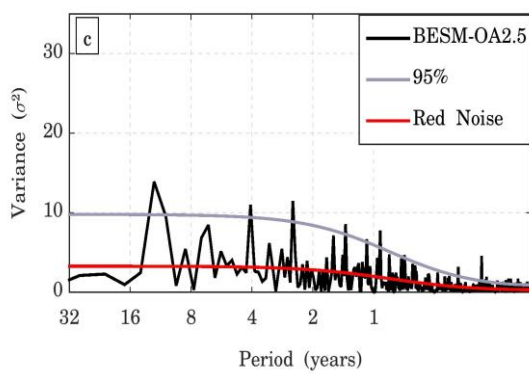
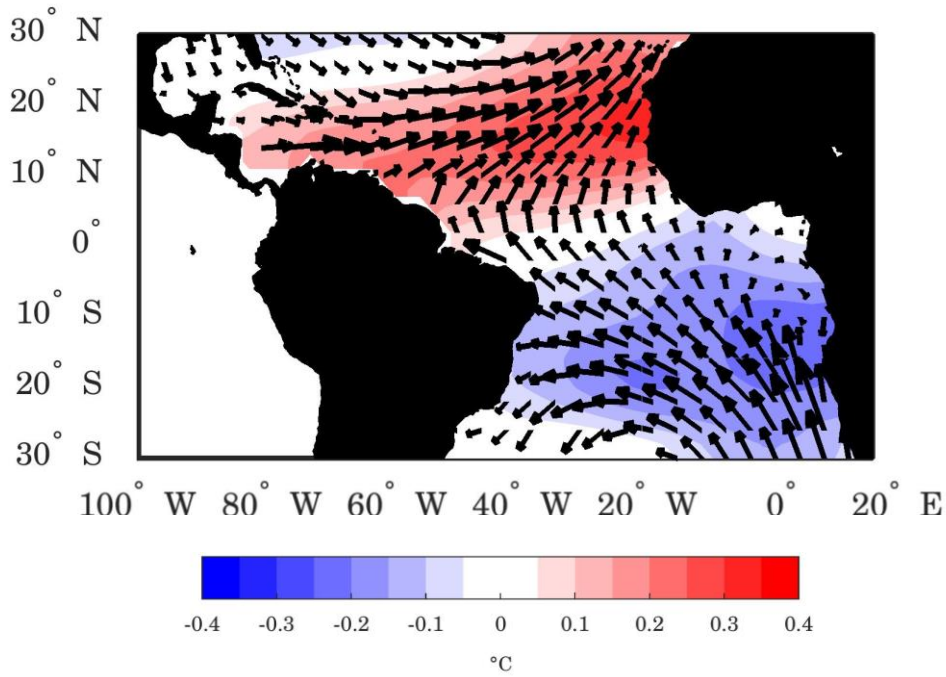
4 | Figure 16+4 – Spatial maps with the monthly correlation between Niño-3 index and
5 | global SST anomalies computed for (a) BESM-OA2.5 and (b) ERSSTv4 over the period
6 | 1900–2005. The anomalies are obtained by subtracting the monthly means for the whole
7 | detrended time series at each grid point. Black rectangles show the Niño-3 index region.
8 | Shaded areas are statistically significant at the 95 % confidence level (through two
9 | tailed t-student test).

10

a) AMM jEOF1 (10.7%) BESM-OA2.5



b) AMM jEOF1 (11.8%) ERSSTv4 (SST), 20CRv2 (Taux,Tauy)



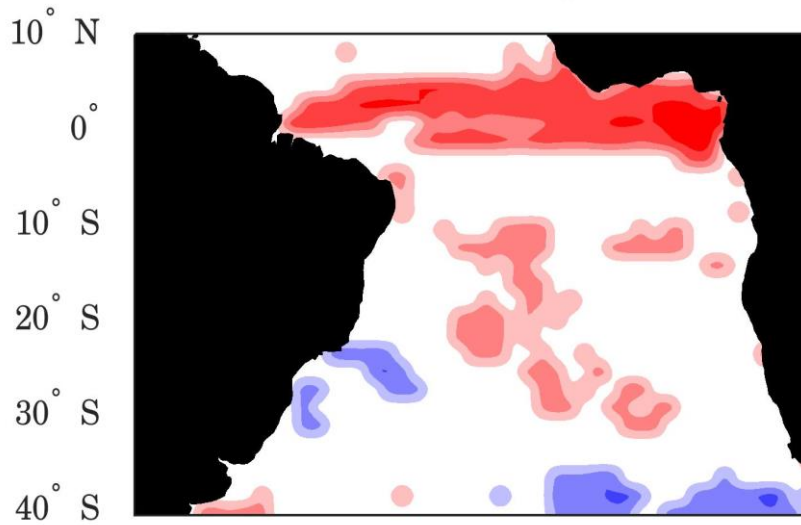
1 | Figure ~~17~~¹⁵ – The leading joint EOF modes of the detrended monthly SST and wind
2 | stress (Taux and Tauy) anomalies for the Tropical Atlantic region (30° S–30° N; 100°
3 | W–20° E) for (a) BESM-OA2.5 and (b) for observation (ERSSTv4 and 20CRv2
4 | Reanalysis). The results are shown as the SST anomalies regressed onto the
5 | corresponding normalized PC time series (°C per standard deviation) and wind stress
6 | anomalies regressed onto the corresponding normalized PC time series (ms⁻¹ per
7 | standard deviation) over the period 1950–2005. The percentage of the variance
8 | explained by each EOF is indicated in the title of the figure. The contour interval is 0.05
9 | °C. Figures (c) and (d) are the power spectrum of the leading joint PC time series of the
10 | AMM pattern for BESM-OA2.5 and observation, respectively. The solid red line
11 | represents the theoretical red noise spectrum and the gray line represents the 95 %
12 | confidence level.

13 |

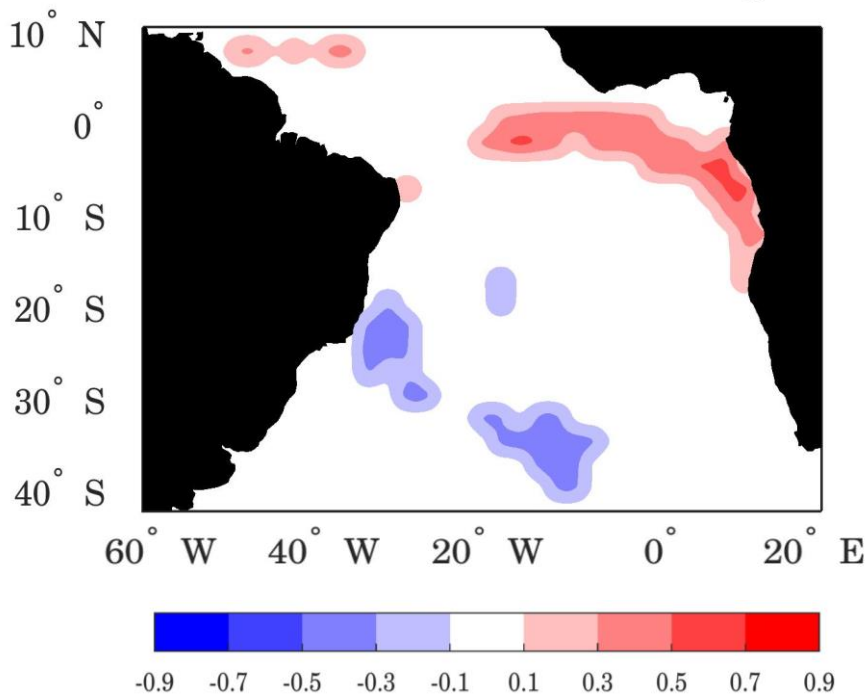
14 |

15 |

a) DJF Correlation SST vs Precipitation (BESM-OA2.5)



b) DJF Correlation SST (ERSSTv4) vs Precipitation (GPCP)

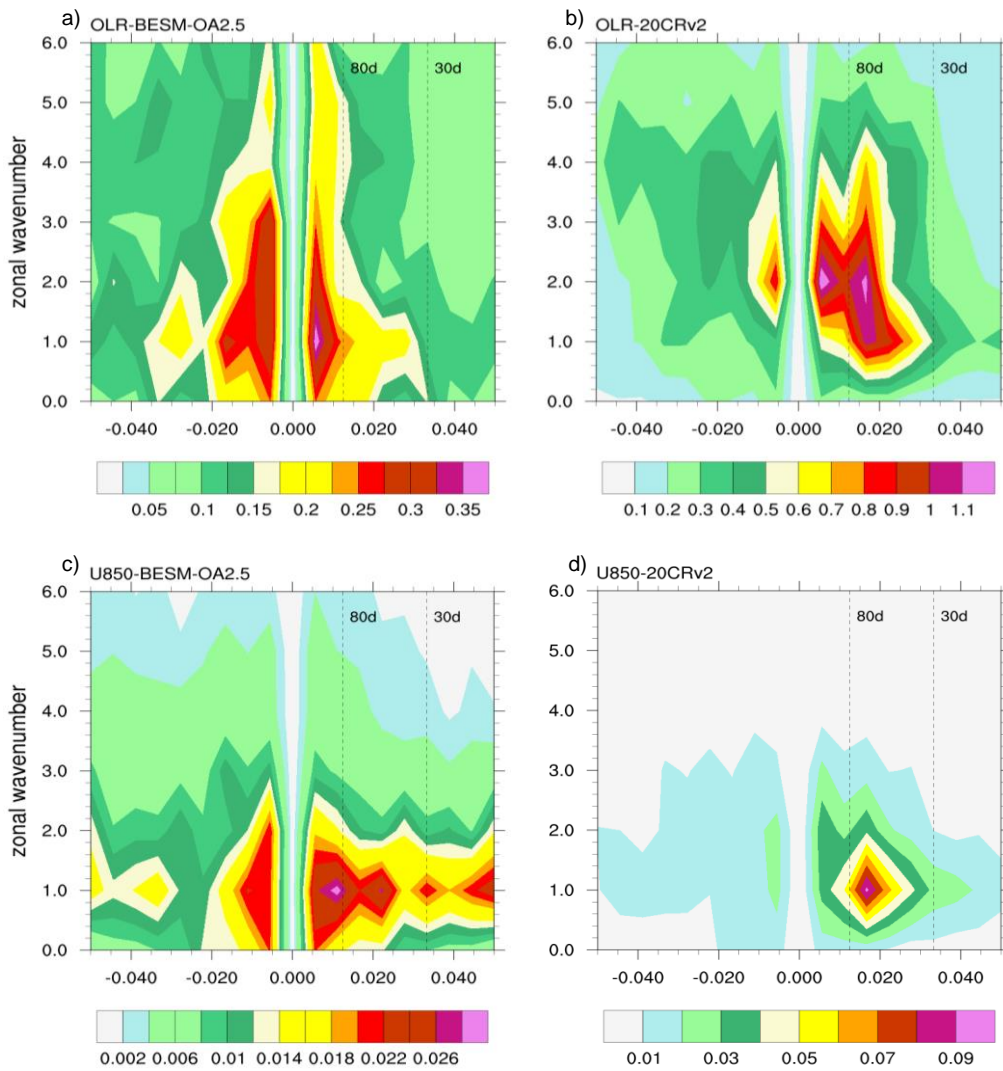


1

2 Figure 1846 – Spatial maps with the correlation between SST and precipitation
3 (seasonal average DJF) over the South Ocean (40° S–10° N; 70° W–20° E) computed
4 for (a) BESM-OA2.5 over the period 1971–2002 and (b) observations over the period
5 1979–2010. Shaded areas are statistically significant at the 95 % confidence level

1 | (through two tailed t-student test).
2 |

1

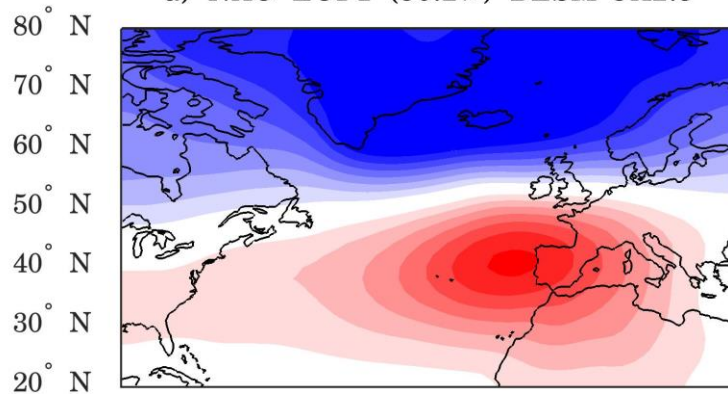


2

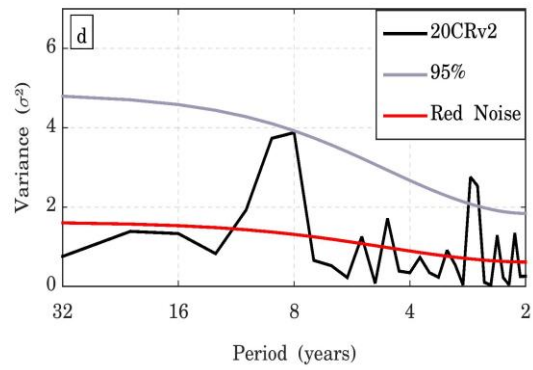
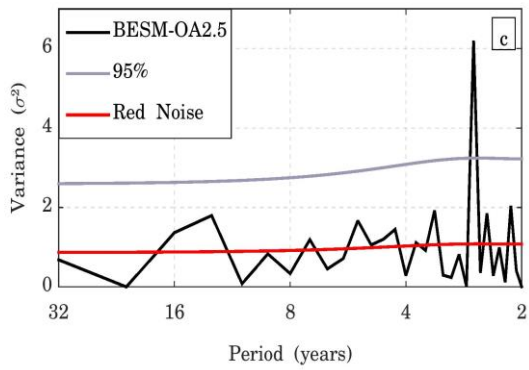
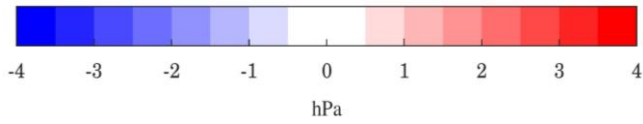
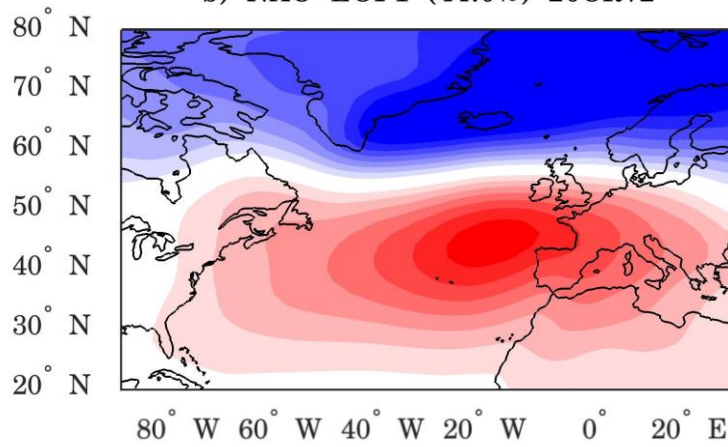
3 Figure 19 – Wavenumber-frequency power spectrum of tropical (10 °S–10 °N) averaged
4 daily outgoing long-wave radiation (OLR) for (a) BESM-OA2.5 and (b) 20CRv2,
5 respectively, and averaged daily zonal wind component at 850 hPa pressure level
6 (U850) for (c) BESM-OA2.5 and (d) 20CRv2, respectively. Data used are daily
7 anomalies for the boreal winter (Nov-Apr) over the period 1971–2000. Daily anomalies
8 are obtained by subtracting the climatological daily mean calculated over the period
9 1971–2000. Individual spectra were calculated for each boreal winter and then averaged

- 1 | over the time period used. Units for the zonal wind (OLR) are $\text{m}^{-2} \text{s}^{-2}$ ($\text{W m}^2 \text{s}^{-1}$) per
- 2 | frequency interval per wavenumber interval.

a) NAO EOF1 (50.2%) BESM-OA2.5



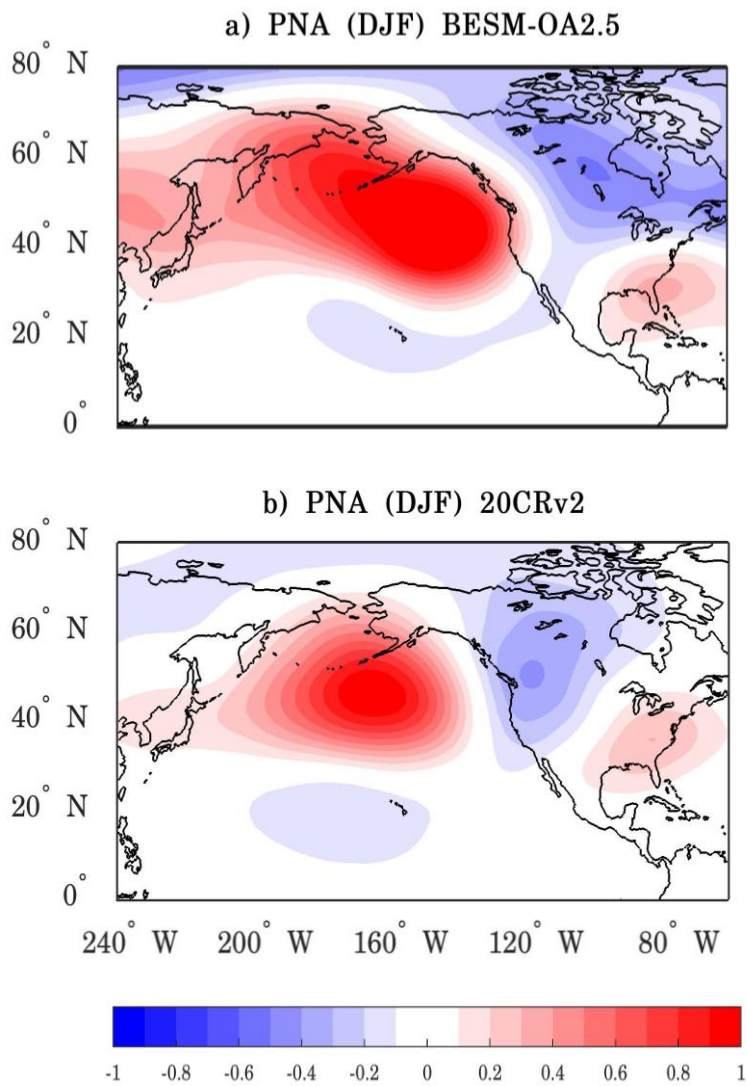
b) NAO EOF1 (44.0%) 20CRv2



1 | Figure ~~2017~~ – The leading EOF modes of the boreal winter (DJF) seasonal averaged
2 | SLP anomalies for the Euro-Atlantic region (20°–80° N; 100° W–30° E) for (a) BESM-
3 | OA2.5 and (b) 20CRv2. The results are shown as the SLP anomalies regressed onto the
4 | corresponding normalized PC time series (hPa per standard deviation) for the period
5 | 1950–2005. The percentage of the variance explained by each EOF is indicated at the
6 | title of the figure. The contour interval is 0.5 hPa. Figures (c) and (d) are the power
7 | spectrum of the leading PC time series of the NAO pattern for BESM-OA2.5 and
8 | 20CRv2, respectively. The solid red line represents the theoretical red noise spectrum
9 | and the gray line represents the 95 % confidence level.

10

11 |



1

2

3 | Figure 21+8 – One-point correlation map for (a) BESM-OA2.5 and (b) 20CRv2

4 | Reanalysis showing the correlation coefficient of 500 hPa geopotential level based at

5 | 45° N, 165° W and the other grid points. The time series used are boreal winter seasonal

6 | (DJF) averaged dataset for the period 1950–2005.

7

8 |

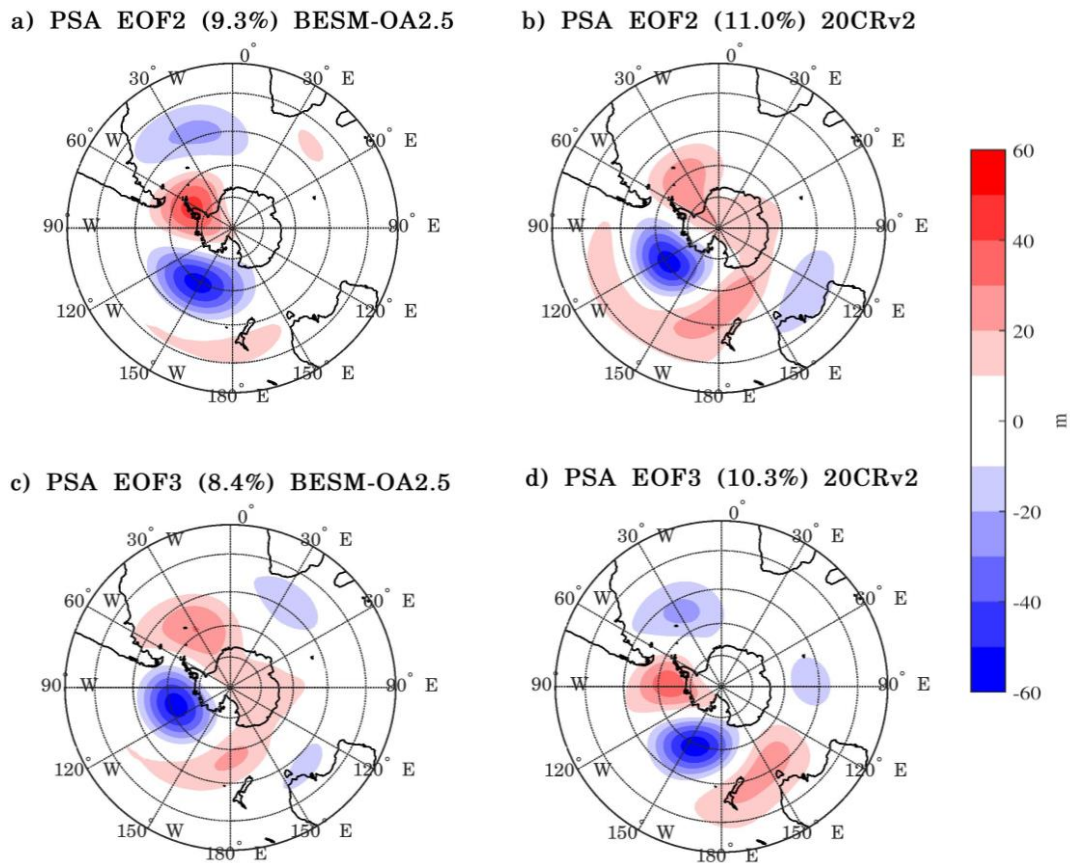
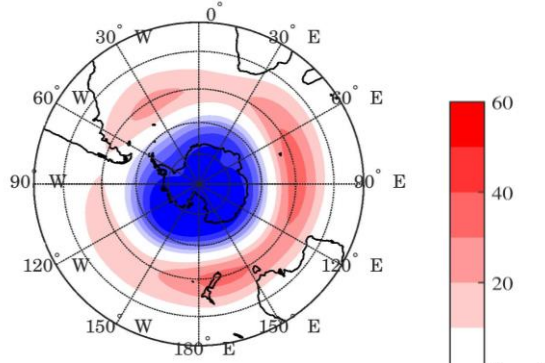
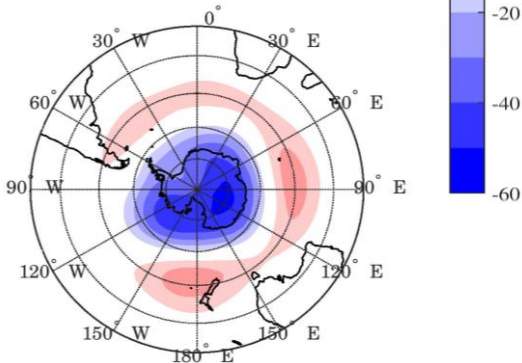


Figure 2219 – (a) The second and third EOF modes of the monthly mean 500 hPa geopotential height field for the Southern Hemisphere (20°–90° S) for BESM-OA2.5 (b) and for 20CRv2 Reanalysis. The results are shown as the 500 hPa geopotential height regressed onto the corresponding normalized PC time series (meters per standard deviation) over the period 1950–2005. The percentage of the variance explained by each EOF is indicated at the title of the figure. The contour interval is 10 m.

a) SAM EOF1 (34.1%) BESM-OA2.5

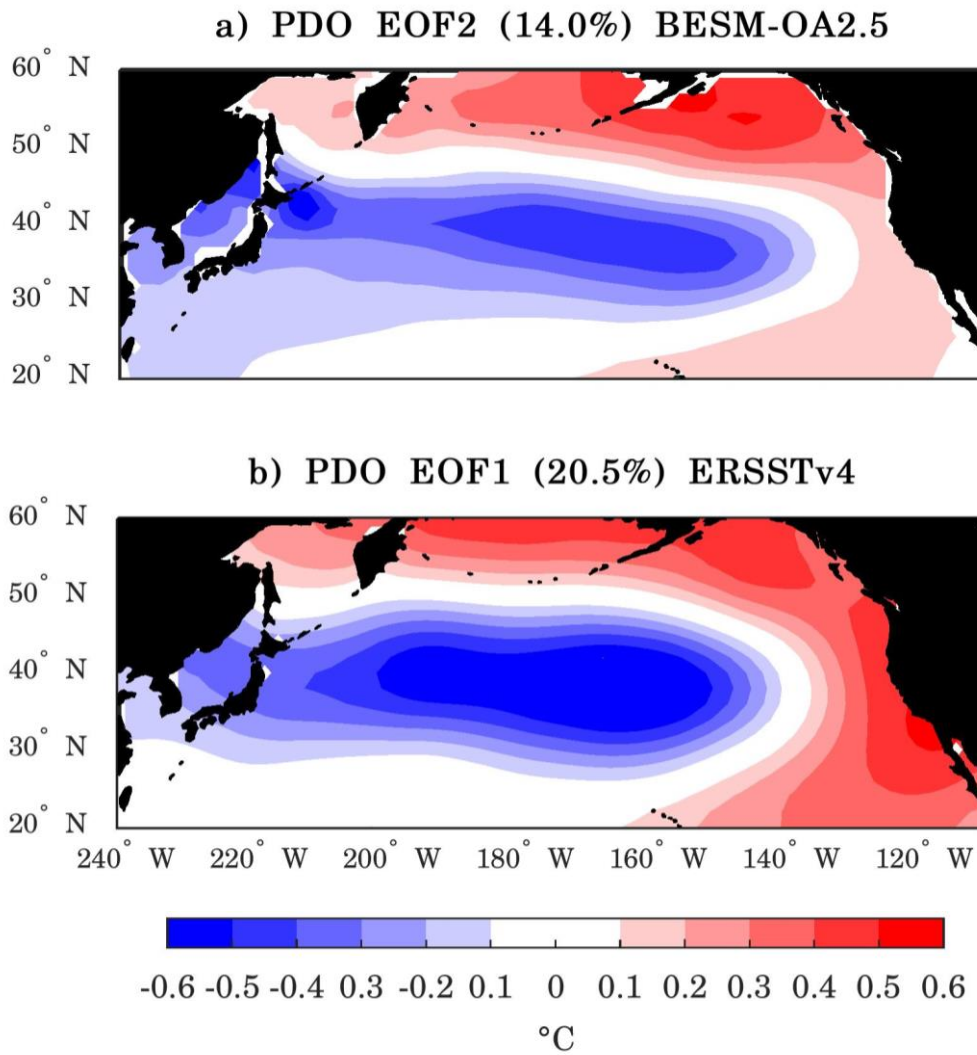


b) SAM EOF1 (21.0%) 20CRv2

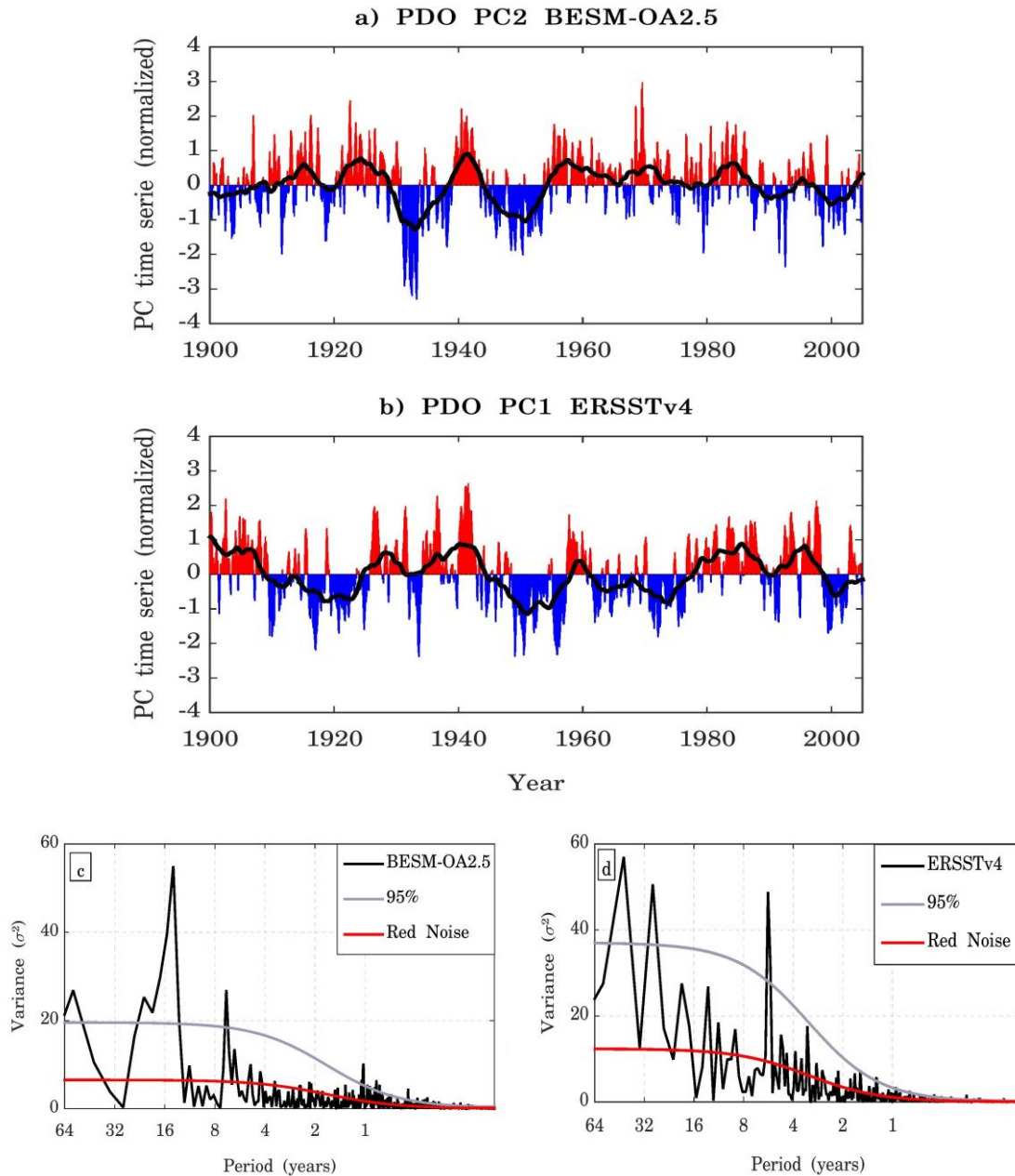


1
2
3
4
5
6
7
8
9
10

Figure 2320 – The leading EOF modes of the monthly mean 500 hPa geopotential height field for the Southern Hemisphere (20°–90° S) for (a) BESM-OA2.5 and (b) for 20CRv2 Reanalysis. The results are shown as the 500 hPa geopotential height regressed onto the corresponding normalized PC time series (meters per standard deviation) over the period 1950–2005. The percentage of the variance explained by each EOF is indicated at the title of the figure. The contour interval is 10 m.



1
2
3 Figure 2421 – (a) The second EOF mode of monthly SST anomalies of BESM-OA2.5
4 and (b) the leading EOF mode of monthly SST anomalies of ERSSTv4, both over North
5 Pacific Ocean (20°–60° N; 240°–110° W). The results are shown as the monthly SST
6 anomalies regressed onto the corresponding normalized PC time series (°C per standard
7 deviation) over the period 1900–2005. The percentage of the variance explained by
8 each EOF is indicated at the title of the figure. The contour interval is 0.1 °C.



1

2 | Figure 2522 – Normalized second PC time series for (a) BESM-OA2.5 and normalized
 3 | leading PC time series for (b) ERSSTv4 over the period 1900–2005. The solid black
 4 | lines are the 5-year running average. Figures (c) and (d) are the power spectrum of the
 5 | second PC time series for BESM-OA2.5 and for the leading PC time series for 20CRv2,
 6 | respectively. The solid red line represents the theoretical red noise spectrum and the
 7 | gray line represents the 95 % confidence level.

Institute	Model	Simulation	horizontal resolution (lat×lon)	
			Atmosphere	Ocean
Commonwealth Scientific and Industrial Research Organisation/Bureau of Meteorology (Australia)	ACCESS1.3	Historical GHG r3i1p1	1.25°×1.875°	300×360 (tripolar)
Canadian Centre for Climate Modelling and Analysis (Canada)	CanESM2	Historical GHG r1i1p1	2.7906°×2.8125°	0.9303°, 1.1407°×1.40625
National Center for Atmospheric Research (USA)	CCSM4	Historical GHG r1i1p1	0.9424°×1.25°	384×320 (tripolar)
Centre National de Recherches Météorologiques/Centre Européen de Recherche et de Formation Avancée en Calcul Scientifique (France)	CNRM-CM5	Historical GHG r1i1p1	1.4008°×1.40625°	292×362 (tripolar)
Geophysical Fluid Dynamics Laboratory (USA)	GFDL-ESM2M	Historical GHG r3i1p1	2.0225°×2.5°	0.3344°, 1°×1°
Goddard Institute for Space Studies (USA)	GISS-E2-H	Historical GHG r1i1p1	2°×2.5°	1°×1°
Met Office Hadley Centre (UK)	HadGEM2-ES	Historical GHG r1i1p1	1.25°×1.875°	0.3396°, 1°×1°
L'Institut Pierre-Simon Laplace (France)	IPSL-CM5A-MR	Historical GHG r1i1p2	1.2676°×2.5°	149×182 (tripolar)
Japan Agency for Marine-Earth Science and Technology, Atmosphere and Ocean Research Institute (The University of Tokyo), and National Institute for Environmental Studies (Japan)	MIROC-ESM	Historical GHG r1i1p1	2.7906°×2.8125°	0.5582°, 1.7111°×1.40625°
Meteorological Research Institute (Japan)	MRI-CGCM3	Historical GHG r1i1p1	1.12148°×1.125°	0.5°, 0.5°×1°
Bjerknes Centre for Climate Research and Norwegian Meteorological Institute (Norway)	NorESM1-M	Historical GHG r1i1p1	1.8947°×2.5°	384×320 (tripolar)

1

2 Table 1 - List of models from CMIP5 with historical GHG simulations used to compare
3 with BESM-OA2.5. Models with higher resolution in the tropical region and a

- 1 decreasing resolution towards the poles have two values for latitude in their respective
- 2 oceanic resolution column. Models with oceanic tripolar grid, the number of grid points
- 3 in each coordinate are presented.
- 4
- 5